FFI-rapport 2011/01445

# Investigation of conductive adhesive in harsh environment – the ReMi Fuze Case

Jakob Gakkestad

Norwegian Defence Research Establishment (FFI)

12 March 2012

FFI-rapport 2011/01445

1050

P: ISBN 978-82-464-2060-8
E: ISBN 978-82-464-2061-5

## Keywords

Ledende lim

Metallbelagte polymerkuler

Krevende miljø

Kontaktresistans

MEMS

## Approved by

| | |
|---|---|
| Hege Jødahl | Project Manager |
| Stein Grinaker | Director of Research |
| Johnny Bardal | Director |

## English summary

FFI and Nammo have participated in the project ”Fine Pitch Interconnect of Microelectronics and Microsystems for use in Rough Environments” (ReMi). The project has to a large extent been founded by the Norwegian Research Counsil (NFR). The purpose of the project was to develop interconnect technology based on Conparts metallized polymer spheres (MPS) and implement this for new applications. Partners in this project were Sintef, Vestfold University College (VUC), Conpart, Idex, Western Geco and FFI/Nammo. In the project each industrial partner had their own industry case. The FFI/Nammo case was denoted “Fuze”. This case exploited use of conductive adhesive based on Conparts MPS for interconnection of MEMS structures onto printed circuit boards (PCB) for use in medium caliber ammunition fuzes.

During this project, MEMS test devices have been designed at FFI and fabricated at Sintef. PCBs have been designed, and the MEMS test devices have been mounted onto these boards using conductive adhesive. After mounting, characterization of contact resistances has been done. The boards have been subjected to various types of temperature cycling tests and test firing in 30 mm ammunition as well.

The tests show that the conductive adhesive might be a viable method for mounting MEMS devices directly to PCBs in fuze applications. However, more investigation must be carried out to verify this.

The results from this project have been published internationally and have also become the basis for a proposed EDA project named ”Packaging 3D for Heterogeneous Rugged Electronics” (PERU). Norwegian partners in that project are FFI, Nammo, Conpart and Sintef.

# Sammendrag

FFI har, sammen med Nammo, deltatt i det NFR finansiert prosjektet ”Fine Pitch Interconnect of Microelectronics and Microsystems for use in Rough Environments” (ReMi). Formålet med prosjektet var å undersøke om ledende lim basert på Conparts metallbelagte polymerkuler kunne brukes i krevende miljø. Prosjektet ble ledet av Sintef. Andre deltagere var Høyskolen i Vestfold, Conpart, Nammo, Western Geco og Idex. Hver industripartner (Idex, Western Geco og Nammo/FFI) hadde sitt eget industri delprosjekt. Nammo/FFI skulle undersøke om ledende lim kunne brukes til å kontaktere MEMS-brikker direkte til kretskort (PCB) i brannrør, og dermed slippe et ekstra pakkenivå for MEMS-brikkene.

I dette prosjektet, som på FFI ble gjennomført som en del av prosjekt ”MEMS for bruk i ammunisjon”, ble det designet MEMS teststrukturer. Disse ble prosessert på Sintef. I tillegg ble det laget forskjellige kretskort slik at det kunne gjøres nødvendige tester. Disse testene besto av elektriske tester, temperaturtester og mekaniske tester, inkludert skytetester.

Forsøkene viste at ledende lim basert på Conparts teknologi kan være velegnet for å montere MEMS-kretser direkte på kretskort i brannrørselektronikk. Imidlertid så må det gjøres flere tester før dette blir endelig verifisert. Bruk av denne type ledende lim gir muligheter for både plass- og kostnadsbesparelser siden man dermed kan unngå et ekstra pakkenivå på MEMS-kretsen.

Resultatene fra dette arbeidet er blitt publisert internasjonalt, og det har også dannet grunnlaget for et mulig EDA-prosjekt kalt ” Packaging 3D for Heterogeneous Rugged Electronics”, forkortet PERU.

# Contents


| | | |
|---|---|---|
| **1** | **Introduction** | **7** |
| **2** | **Motivation and background for ReMi participation** | **7** |
| **3** | **Design and fabrication of the MEMS test structures** | **8** |
| **4** | **Design of the temperature test PCB** | **9** |
| **5** | **Description of the measurement system** | **11** |
| **6** | **Experiments using the temperature test PCB** | **13** |
| 6.1 | Types of conductive adhesive | 13 |
| 6.2 | Mounting test structures with ICA based on metallized polymer spheres | 14 |
| 6.2.1 | Mounting components using 10 µm gold coated spheres (ICA-10G) | 14 |
| 6.2.2 | Mounting components using 30 µm silver coated spheres (ICA-30S) | 16 |
| 6.2.3 | Mounting test structures at OSI using H20 conductive adhesive | 16 |
| 6.3 | Contact resistance and temperature cycling results | 17 |
| 6.4 | Preliminary conclusions after tests carried out using the temperature board | 23 |
| **7** | **Thermo mechanical calculations** | **23** |
| **8** | **Rheological properties of the adhesive** | **23** |
| **9** | **Design of the Remi firing board** | **27** |
| **10** | **Experiments using the Remi firing boards** | **28** |
| 10.1 | Mounting of components | 28 |
| 10.2 | Initial measurement results | 31 |
| 10.3 | Temperature cycling tests | 32 |
| 10.4 | Firing test | 35 |
| 10.5 | Vibration test | 39 |
| **11** | **Summary of test conditions and tests preformed using the Temp_board and the Remi_firing_board** | **40** |
| **12** | **Conclusions** | **41** |
| | **References** | **42** |
| | **Abbrevations** | **43** |
| **Appendix A** | **Information about the measurement and experimental setup** | **44** |

A.1 Cable connection scheme 44
A.2 Relationship between channel number and resistance measured on the Temp_board 46
A.3 Relationship between channel number and resistance measured on the Remi firing board 48
A.4 Overview of the experimental setup using the Remi firing board 49

**Appendix B Paper presented at Pan Pacific Microelectronic Symposium, 2009, Big Island of Hawaii 53**

**Appendix C Paper presented at the ESTC conference 2010 59**

**Appendix D Spie newsroom publication 66**

**Appendix E Spie Photonic West conference paper 69**

**Appendix F Publication in Journal of Micro/Nanolithography, MEMS and MOEMS 81**

# 1 Introduction

The NFR founded project ReMi – “Fine pitch Interconnect of Microelectronics and Microsystem for use in Rough Environment”, started in 2008. The purpose of the project was to develop interconnect technology based on Conparts metalized polymer spheres (MPS) and implement this for new applications. Partners in this project were Sintef, Vestfold University College (VUC), Conpart, Idex, Western Geco and FFI/Nammo. The project was lead by Sintef and the project founded one PhD student at VUC. In the project each industrial partner had their own industry case. The FFI/Nammo case was denoted “Fuze”. This case investigated use of conductive adhesive based on Conparts MPS for interconnection of MEMS structures onto PCB for use in medium caliber ammunitions fuzes.

The ReMi project lasted for four years, while the Fuze case ended in 2010. During the project, each industrial participant contributed with 100 000 kr/year. At FFI, this work was carried out in the project “MEMS for use in Ammunition”, project number 1050.

This report summarized the work that was carried out in the fuze industry case.

# 2 Motivation and background for ReMi participation

Multi functional programmable ammunition with functionality such as e.g. airburst and/or delayed impact requires electronic systems integrated into the ammunition. Normally, such systems are integrated into the fuze. Integrating electronic devices into fuzes involve several challenges. First of all, the space available for electronic systems is normally very limited. Besides that, the enviromental forces during firing and flight might also be very severe. E.g. in a 30 mm fuze, typically only 1 – 3 $cm^3$ is available for electronic components. In addition, the environmental forces are severe. During firing the setback acceleration exceeds 60 000 g. Due to the rotation of the projectile, the centripetal acceleration is approximately 9000 g/mm out of center.

Based on work in previous projects, we have developed MEMS sensors for registration of setback acceleration and spin during firing and flight of a 30 mm projectile. Unlike the integrated circuit (IC) industry, where a large variety of commercial IC packages exists, there are no standard MEMS packages available. Thus, encapsulation of the developed MEMS structure becomes an issue, both with respect to cost and testing. In addition, and this is important in our case, encapsulation of the MEMS device requires extra space on the PCB compared to mounting it directly to the PCB.

A method for mounting the MEMS devices directly to the PCB without additional encapsulation is shown in Figure 2.1.

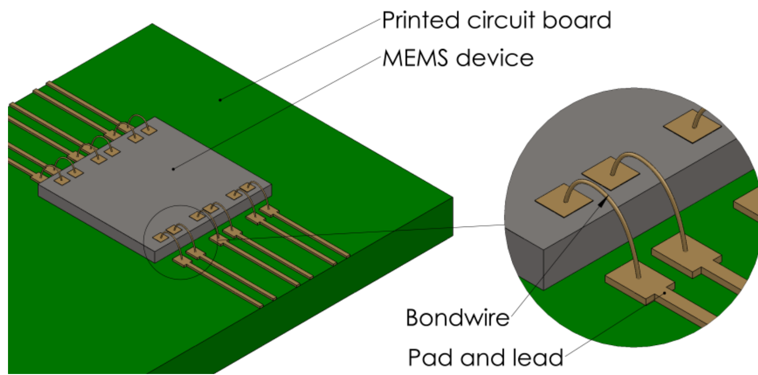


*Figure 2.1 Wire bonding of the MEMS device to the PCB. Drawing: Per Dalsjø.*

Using such a method requires that the movable parts in the MEMS device are protected. A disadvantage using this method is that the bond wires need protection. Protecting these bond wires may be complicated since the protection must withstand harsh environment and not destroy the bond wires.

An alternative, and better, way of connecting the MEMS device is shown in Figure 2.2.

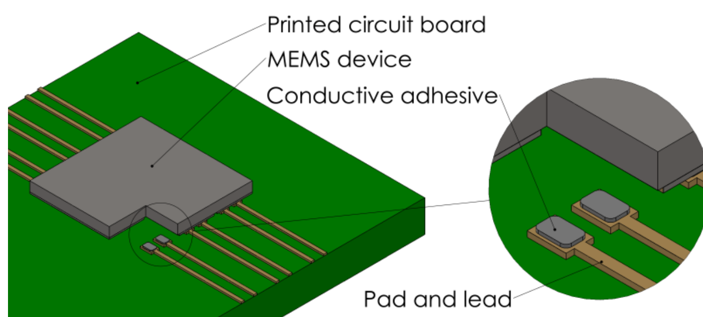


*Figure 2.2 Interconnection and attachment of the MEMS device to the PCB using conductive adhesive. Drawing: Per Dalsjø.*

The obvious advantage using this method is that it consumes less space and that the pads are protected by the MEMS device itself. As for the other method, the movable parts of the MEMS device must be protected.

# 3 Design and fabrication of the MEMS test structures

To test how the conductive adhesive performs in the harsh environment, four "dummy" MEMS test devices were designed with no moving parts. The layout of the four MEMS devices are shown in Figure 3.1.

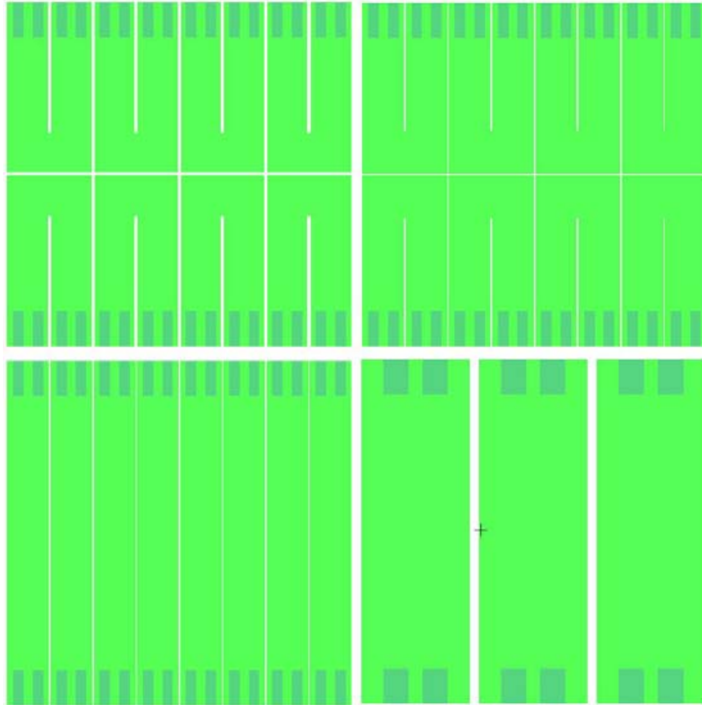

*Figure 3.1 Layout of the four MEMS test devices. Upper left: U-40, upper right: U-20, lower left: I-20 and lower right: I-100. The nomenclature describes the shape of the conductive paths, and the number describes the spaces between the conductive paths. The darker area represents the pads on the test devices.*

The test structures were fabricated at Sintef MiNaLab. The test devices were processed in a Silicon on Insulator (SOI) process using wafers with 43 µm thick device layer and a 2 µm thick buried oxide layer. A 300 – 500 nm thick layer of chrome, nickel and gold was sputtered onto the wafers to provide a conductive layer. A more detailed description of the fabrication process can be found in Appendix F. The size of each device is 3.5 X 3.5 mm. The pad size for the I-100 device is 250 X 350 µm and 100 X 350 µm for the other test devices. The pitch of the I-100 pads is 400 µm on the same conductive area, and 200 µm for the other test devices.

# 4 Design of the temperature test PCB

A PCB was designed in order to test the electrical properties of the conductive adhesive used for interconnection of the MEMS test devices. This board was primarily designed for temperature tests and was denoted Temp_board. On the board there were structures for measuring the contact resistance of the connection between the PCB and the MEMS device. A sketch of the measuring principle is shown in Figure 4.1.

*Figure 4.1 Principle for measuring contact resistance on the red pad.*

Knowing the current flowing through Iin and Iout, and by measuring the voltages between the Vout and Viout, the contact resistance can be calculated. This type of measurement is called a 4 wire measurement or a Kelvin measurement. The advantage of using a Kelvin measurement is that the resistances in wires, cables etc. are eliminated.

Figure 4.2 shows the layout of the Temp_board. The board has 4 layers and the dimensions are approximately 12 x 7.1 cm.

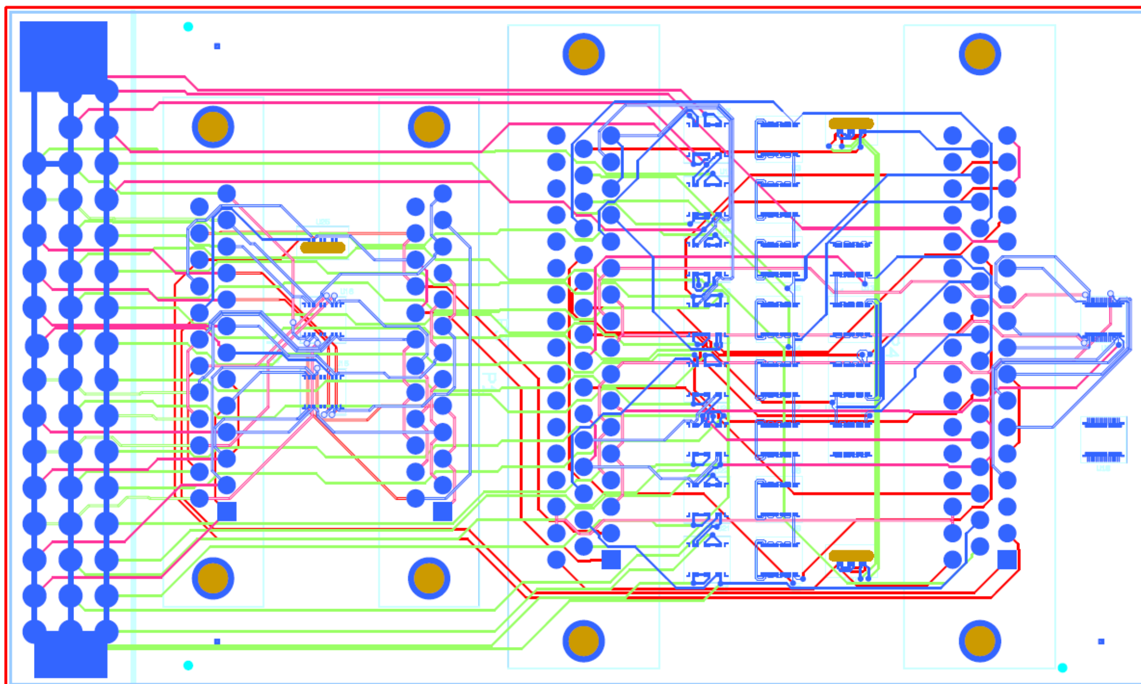

*Figure 4.2 Layout of the Temp_board.*

Figure 4.3 shows the component placement and associated component types.

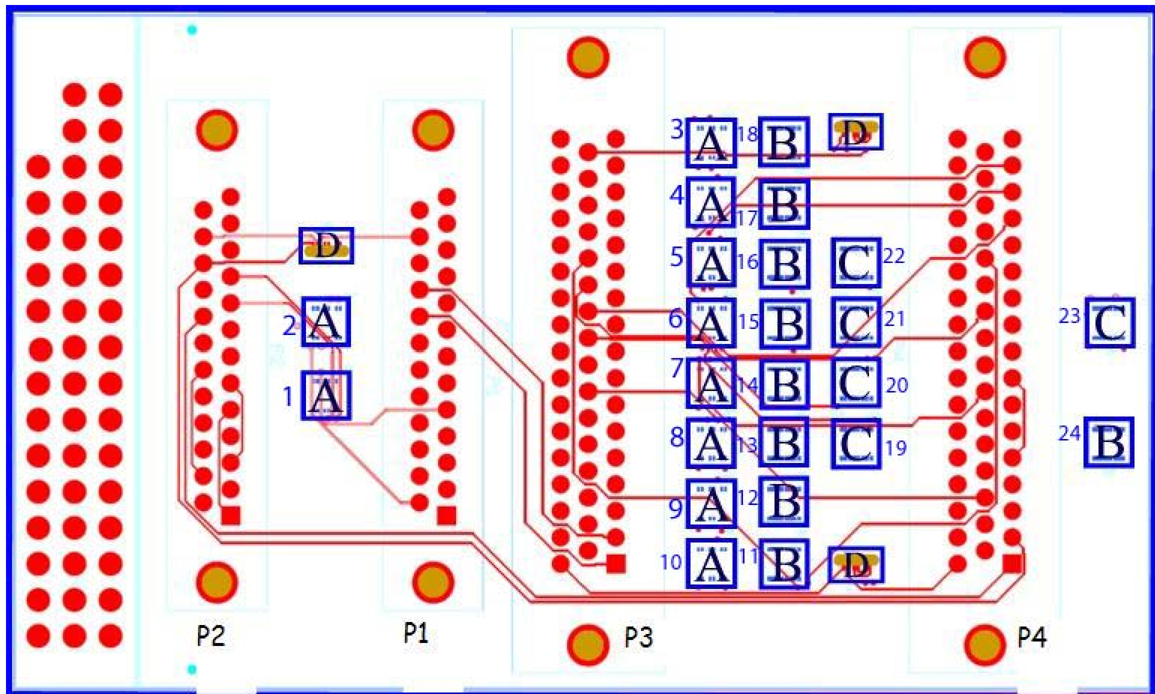


*Figure 4.3 Component placement on the Temp_board.*

Component A corresponds to the I-100 test device, components B and C correspond to the U-40 and I-20 test device respectively. Component D is the I-100 test device mounted vertically through the board, which was never tested.
Components no. 1 and 2 (see Figure 4.3) were used to measure contact resistance on the I-100 test devices. Components no. 3-6, and no. 7-10 consist of two daisy-chains each with 4 I-100 test devices. Components no. 11-18 makes a daisy-chain of 8 U-40 test devices while components no. 19-22 constitute a daisy-chain of 4 I-20 test devices. Components no. 23 and 24 were intended to measure potentially short circuits between signals in case the conductive adhesive was squeezed into the neighbor signals.

All resistances are measured using Kelvin measurements. 30 resistances can be measured on the Temp_board. The next chapter describes the test measurement system and the interface to the Temp_board.

## 5 Description of the measurement system

A Keithly Model 3706 System Switch/Multimeter [1] equipped with a Model 3720 dual 1X30 Multiplexer card was purchased in order to measure the contact resistances. Configured for Kelvin measurements, this equipment is capable of measuring 30 resistors with a resolution of 0,1 μΩ when measuring 1 Ω resistance.

The block diagram for the Model 3720 dual 1X30 Multiplexer card is shown in Figure 5.1. During Kelvin measurements, one bank (bank1) is used for setting up current, while the other bank (bank 2) is used for voltage reading. As an example, when performing the Kelvin

measurement channel no. 1 consits of channel 1 in bank 1 (signals 1Hi and 1Lo) and channel 31 in bank 2 (signals 31Hi and 31Lo), see Figure 5.1. The channels cannot be used independently, e.g. it is not possible to use channel 2 in bank 1 with e.g. channel 34 in bank 2 when doing Kelvin measurements.

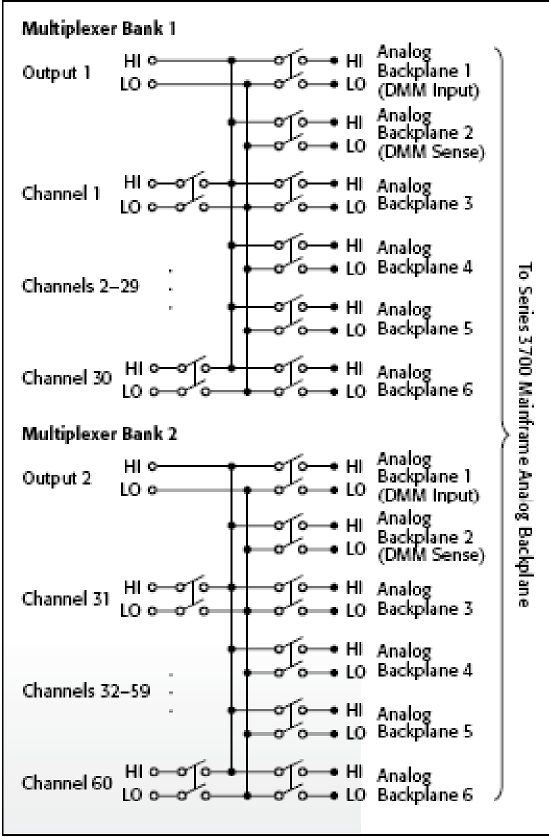


*Figure 5.1 Block scheme for the 3720 dual 1X30 multiplexer card*

The input to the multiplexer card is two 78 pins D-SUB contacts. The connection information for these contacts is shown in Figure 5.2.

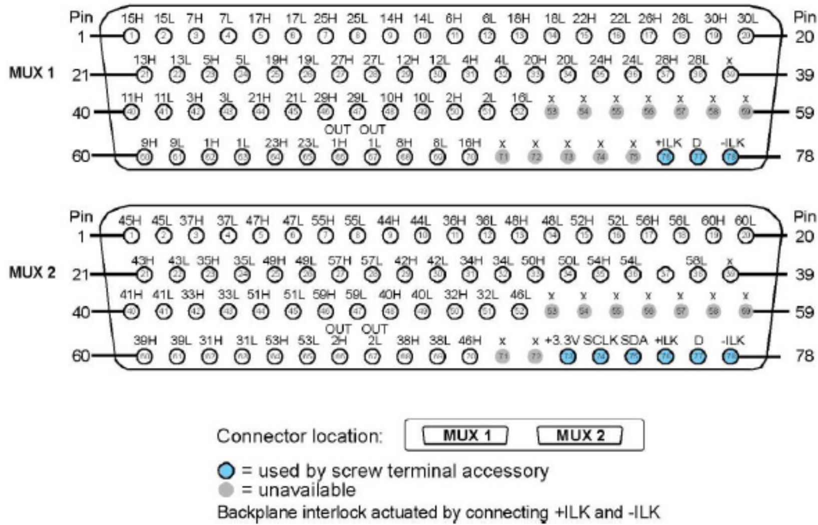


*Figure 5.2 D-SUB connection information for the 3720 multiplexer card*

A two meter long cable with one 25 pins D-SUB and one 50 pins D-SUB contact on the one end and a 78 pins D-SUB contact in the other end ensures interface between the PCB and the multiplexer. Hence, for measurements, two such cables are used. More information about the measurement system can be found in Appendix A.1 and A.2. All D-SUB contacts and cables are qualified for temperature ranges between -55°C and +125°C.

# 6 Experiments using the temperature test PCB

This section describes the various experiments that were carried out using the Temp_board.

## 6.1 Types of conductive adhesive

Electrically conductive adhesive (ECA) can be divided into two subgroups; isotropic and anisotropic [2].
Anisotropic conductive adhesive (ACA) provides conductivity vertically (along the z-axis). This directional conductivity is achieved by using a relatively low volume loading (vol%) of conductive particles (5-20 vol %). Figure 6.1 shows an IC mounted to a PCB using ACA. As can be seen from this figure, the loading of MPS is quite low.

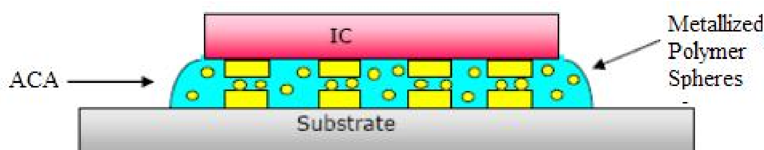


*Figure 6.1 IC mounted to PCB using ACA.*

Isotropic conductive adhesive (ICA) conduct current in all directions. This property is achieved by adding conductive particles (in our case MPS) to the adhesive matrix above the percolation

threshold [3]. When the vol% of the MPS is below the percolation threshold, the adhesive behaves as an insulator. When the vol% exceeds the threshold, the adhesive becomes conductive. The percolation threshold for MPS is in the range between 30 – 40 vol%[3].

## 6.2 Mounting test structures with ICA based on metallized polymer spheres

The conductive adhesive was deposited onto the Temp_board by stencil printing. This is same process which is typically used when solder paste is deposited onto a PCB. These experimets however, showed that the adhesive printing process was more complicated than expected, and that the process depends upon several factors such as:

- Rheological properties of the adhesive
- Quality of the stencil
- Pad opening and size of MPS
- Speed and pressure of the squeegee

We mounted components on the Temp_board at FFI using two types of ICA, one containing 10 μm gold coated spheres (ICA-10G) and one containing 30 μm silver coated spheres (ICA-30S).

### 6.2.1 Mounting components using 10 μm gold coated spheres (ICA-10G)

The first mounting of components was done Nov 18th 2008. In this experiment, the adhesive was prepared by Microjoining AB in Sweden. The adhesive was based on a commercially available epoxy with Au coated polymer spheres from Conpart with a diameter of 10 μm, hereafter denoted ICA-10G. The printing of the adhesive went quite well, as illustrated in the figures below.

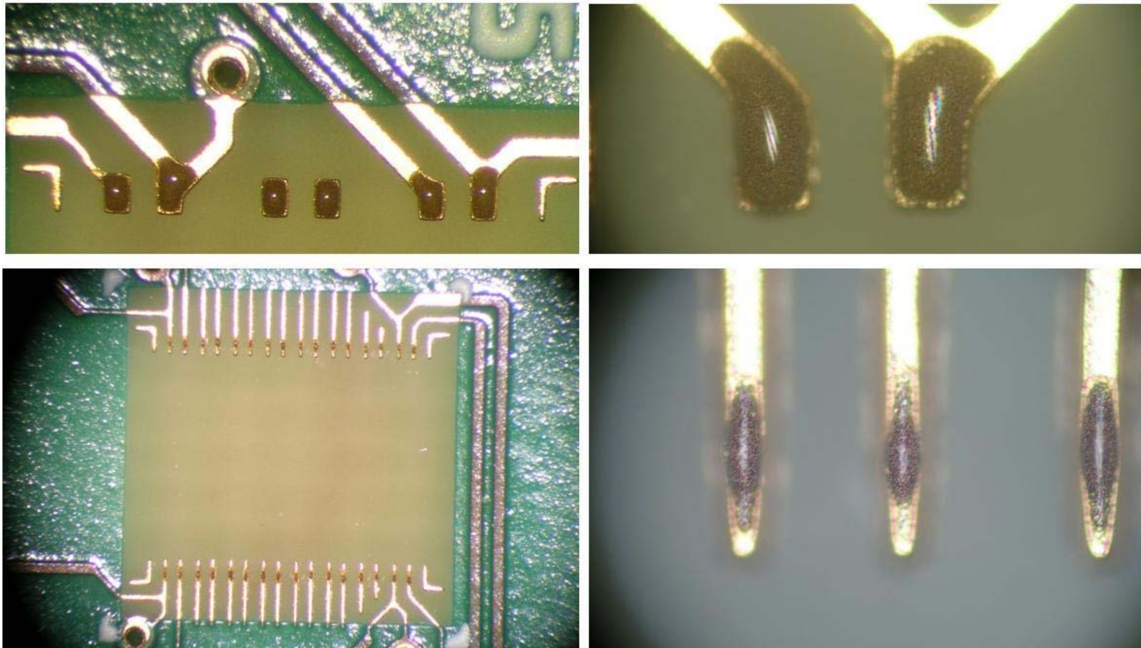

*Figure 6.2 Printing of ICA-10G. Upper row: Printing adhesive on large pads (250X350 μm). Lower row: Printing of adhesive on small pads (100X350 μm). Photo: Per Dalsjø.*

For mounting of the components on the board, the My 9 pick and place machine at FFI was used. Figure 6.3 shows a photograph of one of the Temp_board with components mounted on the board.

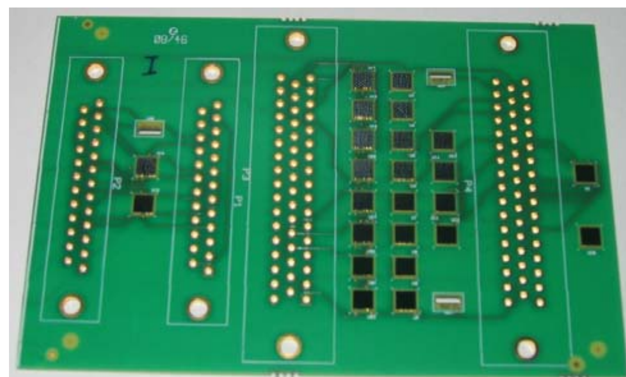

*Figure 6.3 Temp_board with mounted components. Photo: Per Dalsjø.*

When measuring the contact resistances, after mounting of the components and after curing, the resistances showed to be much higher than expected. The lowest contact resistance measured was 1.2 Ω and the highest measured contact resistance was 18.4 Ω! The resistances in the daisy-chains made of four 1-100 test devices were also unacceptable high, varying from 10 Ω to 25 Ω.

In order to investigate these disappointing results, cross sections were made on some of the mounted components. Figure 6.4 shows a cross section of one of the interconnections.

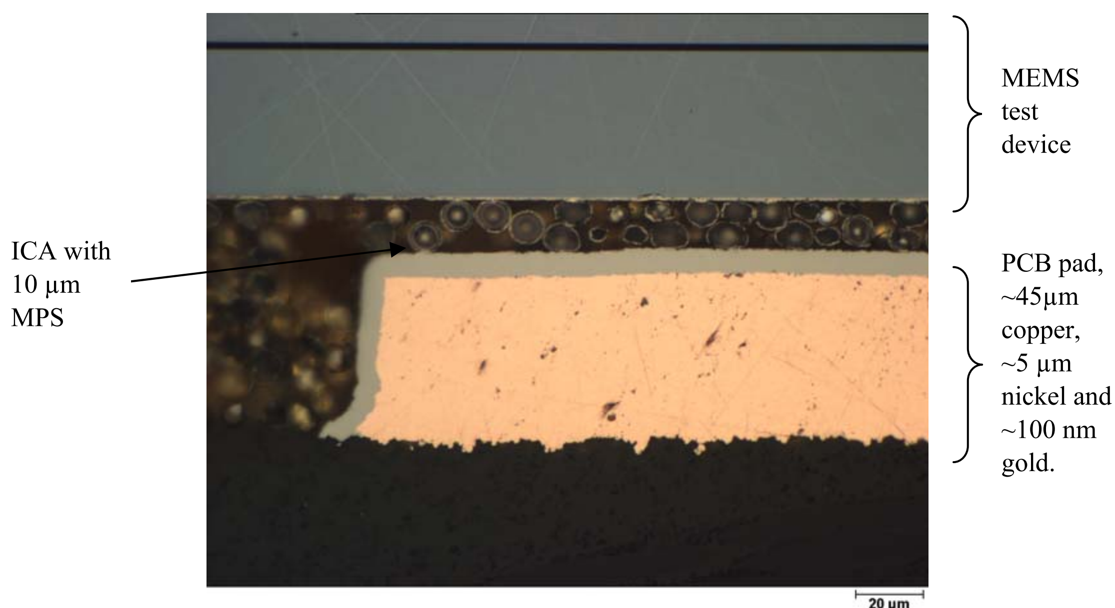


*Figure 6.4 Cross section picture of one of the interconnections between the PCB and the MEMS test structure. Note that the adhesive is also squeezed out to the side of the pad. A connection path formed by the spheres from the PCB pad to the MEMS test device is easily visible. Photo: Rolf Johannessen, Sintef.*

As can be seen from Figure 6.4, an electric path from the pad to the chip is easily visible. Therefore, the high contact resistance must be caused by some other effects. After some investigations, it was found that the MPS were covered with a surfactant causing the high contact resistance. The spheres were originally intended for use in anisotropic conductive adhesive, and the surfactant was added to avoid contact between spheres.

Shear test were performd on some of the test devices. These test revealed that the minimum bond strength was 2.1 kg, which is approximately more than 100% higher than specified in MIL_STD 883G method 2019.7 (see Appendix B).

A paper from this first experiment was presented at the Pan Pacific Microelectronic Symposium at Big Island of Hawaii in January 2009 [3]. The paper is presented in Appendix B.

### 6.2.2 Mounting components using 30 µm silver coated spheres (ICA-30S)

On Dec 10th, 2008, components were mounted using conductive adhesive with 30µm silver coated polymer spheres (hereafter denoted ICA-30S). The MPS were added to the epoxy at FFI, and the amount of MPS was adjusted to obtain a satisfactory contact resistance.

The printing process was more complicated than using the ICA-10G. One of the reasons was the larger diameter of the spheres. Pictures in Figure 6.5 show the printing of the adhesive.

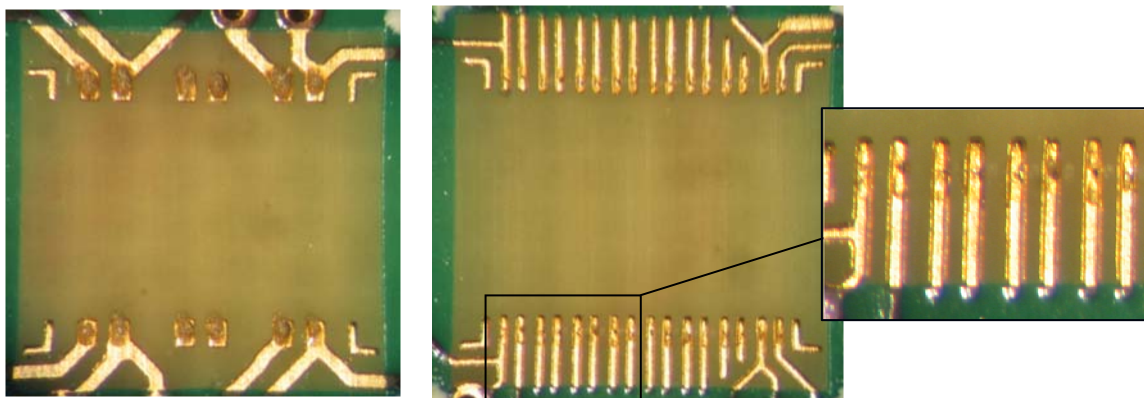

*Figure 6.5 Printing ICA-30S on large pads (left) and small pads (right).*

Clearly, the printing of the ICA-30S on the smaller pads are not acceptable. However, the printing was sufficient for the larger pads. As a result only the I-100 test devices were mounted onto the Temp_board.

### 6.2.3 Mounting test structures at OSI using H20 conductive adhesive

Test devices were mounted to the Temp_board at OSI Optoelectronics in Horten, using a commercially available CA, the H20 from Epotek (www.epotek.com). The adhesive uses silver particles as the conductive part. The particle size is equal or less than 45 µm. The adhesive was deposited at the board using a dispenser. Figure 6.6 - Figure 6.8 show the results of the

depositions. As can be seen, the deposition of the adhesive is very well controlled for the large pads, and relatively well controlled on the fine pitch pads. The test devices were mounted with a force of 100gram/die, and the curing temperature was 150 °C for two hours. No underfill was used. In total, four boards were mounted with test devices.

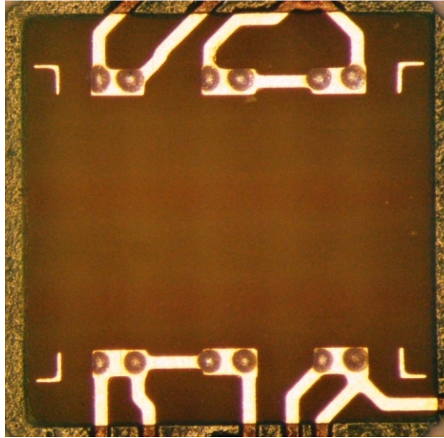

*Figure 6.6 ICA H20 dispensed at position for I-100 um (A).*

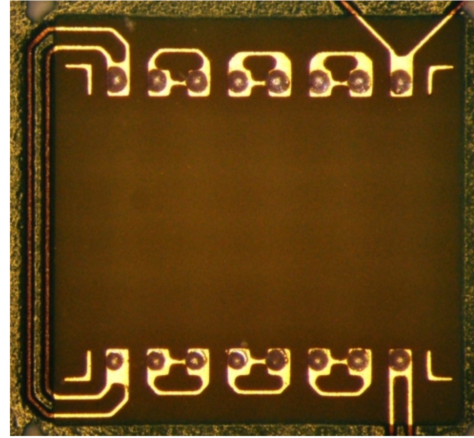

*Figure 6.7 ICA H20 dispensed at position for U-40 um (B).*

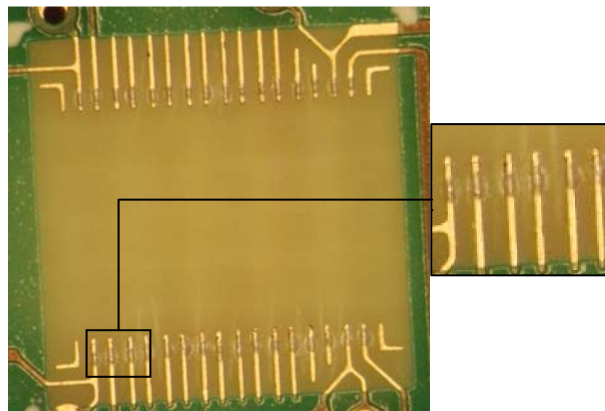

*Figure 6.8 ICA H20 dispensed at position for U-40 um (B) or I-20 um (C).*

One of the four boards with test devices mounted at OSI was destroyed at FFI when handling the board. The adhesion between the board and the test devices was extremely poor, and most of the test devices fell off the board. One theory about the cause of the poor adhesion was that the pads had some form of contamination/oxide on the surface, due to inadequate cleaning of the PCBs before adhesive deposition. On the other side, the boards mounted at FFI were not cleaned either.

### 6.3 Contact resistance and temperature cycling results

Measured contact resistances for test devices mounted with the ICA-30S and with the commercially available H20 CA, are shown in Table 6.1.

| | ICA-30S | H20 epoxy |
|---|---|---|
| Average contact resistance (Ω) | 0,549 | 0,055 |
| Standard deviation (Ω) | 0,413 | 0,013 |
| Max contact resistance (Ω) | 1,393 | 0,098 |
| Min contact resistance (Ω) | 0,182 | 0,044 |
| No of measured resistances | 8 | 16 |

*Table 6.1 Initial contact resistance for components mounted with ICA containing 30 µm silver coated spheres and H20 epoxy.*

As can be seen from this table, the H20 epoxy gives significantly lower contact resistance and the variation in contact resistance is also lower.

The contact resistances using ICA-30S were higher than expected. Therefore, cross sectioning of the board was carried out at Sintef in order to find a possible cause for the high contact resistance.

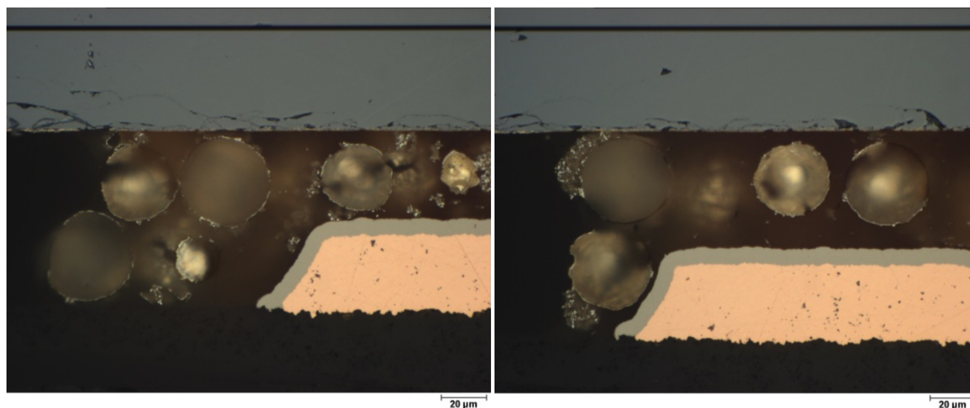


*Figure 6.9 Cross section picture of the interconnections between the PCB and the MEMS test devices. It can be clearly seen that the silver coating has delaminated from the polymer shere. Photo: Rolf Johannessen, Sintef.*

Figure 6.9 shows that the silver coating has delaminated from the polymer shere. This is the cause of the higher than expected contact resistance. The delamination was caused by insufficient adhesion between the polymer sphere and the silver metal.

The boards were temperature cycled between -46 °C and + 70 °C. Two boards with test structures mounted with ICA-30S were tested, denoted ICA board 2-3 and ICA board 2-4 respectively. Three boards, denoted OSI board 1, 2 and 3, with test structure mounted with H20 epoxy were also tested. Fail criteria for the contact resistances was set to infinite resistance (no contact). The following figures show the test results.

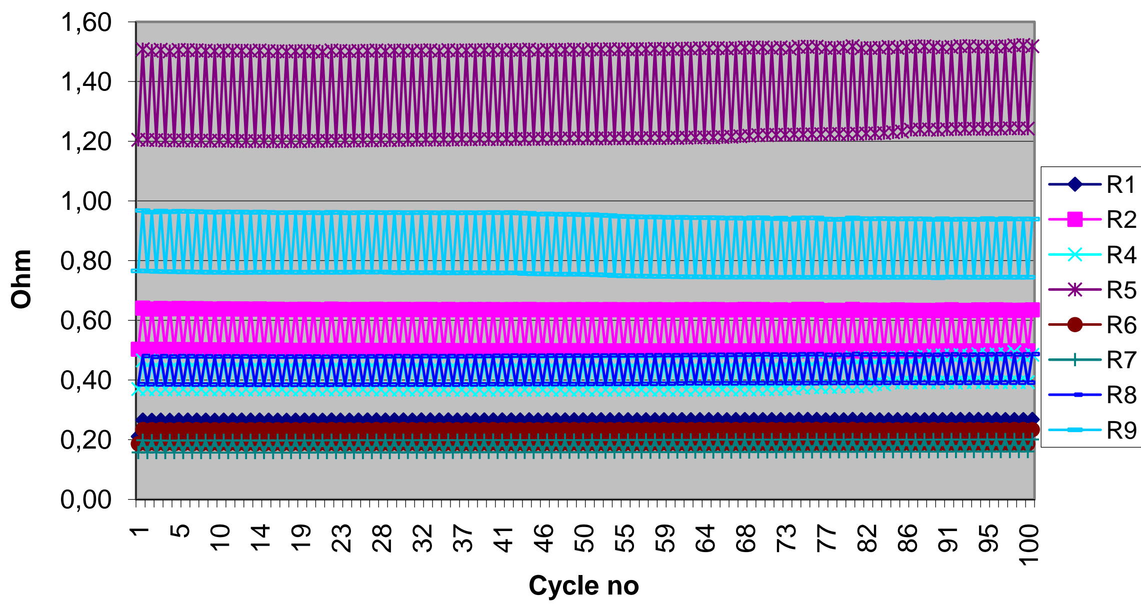


*Figure 6.10 Changes in contact resistances as a function of number of temperature cycles between -46 °C and 70 °C for ICA board 2-3. Note that resistance values are almost constant (for same temperature) independent of number of cycles.*

All contact resistances on ICA board 2-3 survived 100 temperature cycles.

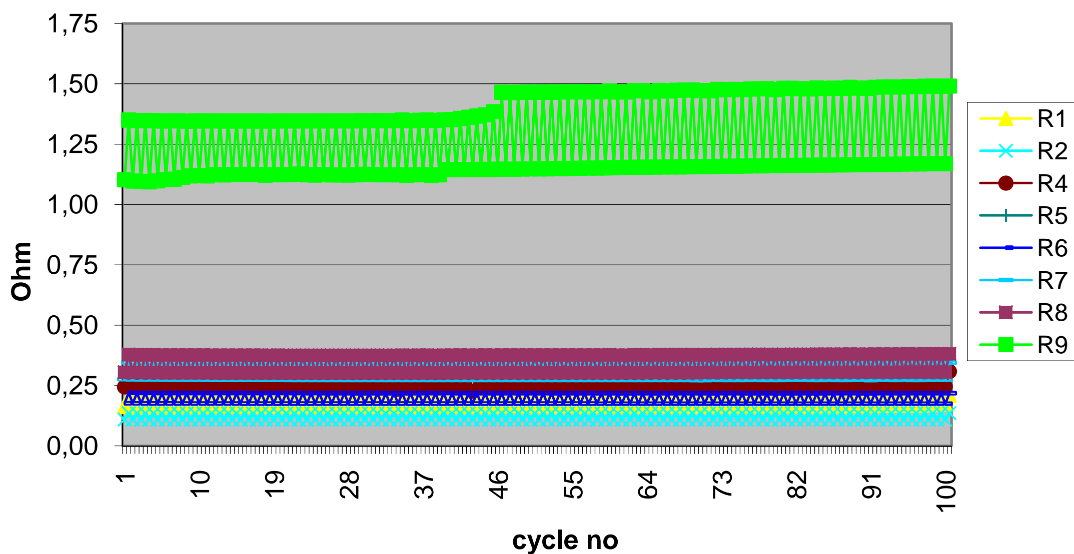


*Figure 6.11 Changes in contact resistances as a function of number of temperature cycles between -46 °C and 70 °C for ICA board 2-4. Note that resistance values are almost constant (for same temperature) independent of number of cycles.*

All contact resistances on the ICA board 2-4 survived 100 temperature cycles. The board was exposed to more than 760 cycles. All the contact resistances survived 274 cycles. The next figure shows the variation of the contact resistances during this number of cycles.

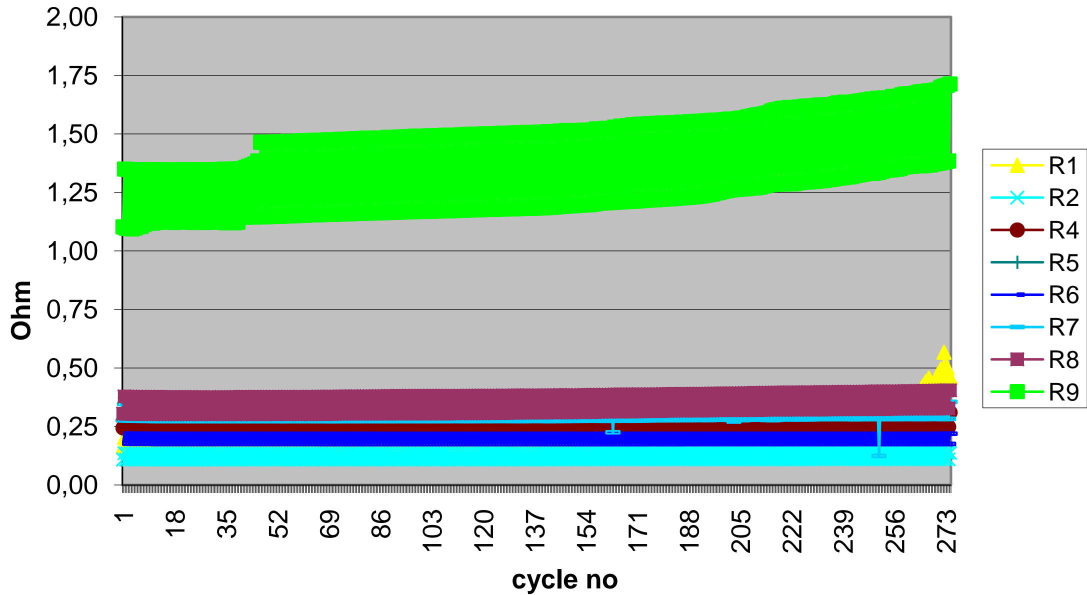


*Figure 6.12 Changes in contact resistances during 274 cycles for the ICA board 2-4.*

Two contact resistances survived 766 temperature cycles. The next figure shows how the resistances vary during the number of cycles.

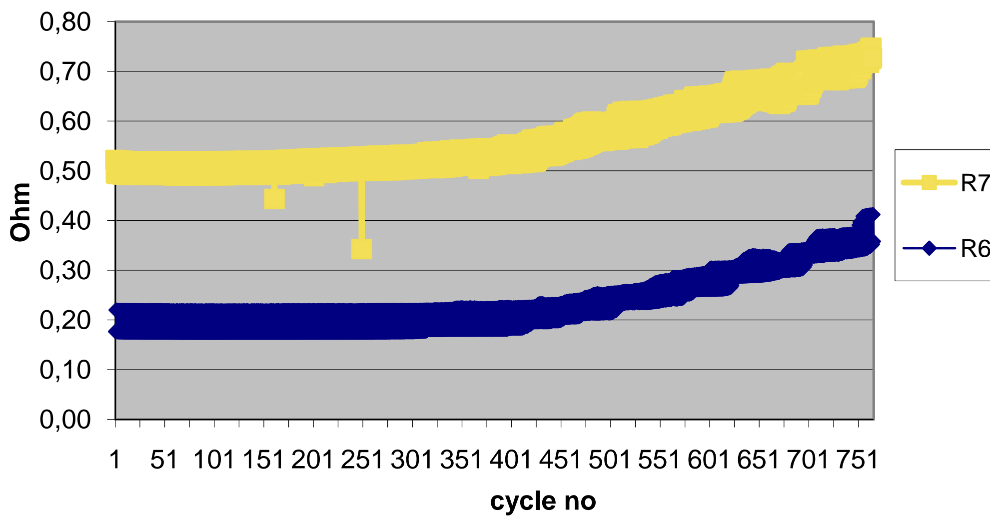


*Figure 6.13 Contact resistance changes for R6 and R7 during 766 temperature cycles.*

Except for two “outlier” values for the R7 resistance, it is noteworthy that the resistances start to increase in value after approximately 400 temperature cycles.

The OSI boards had a poorer performance in the temperature cycle tests. The figure below shows the result from the OSI board no 1.

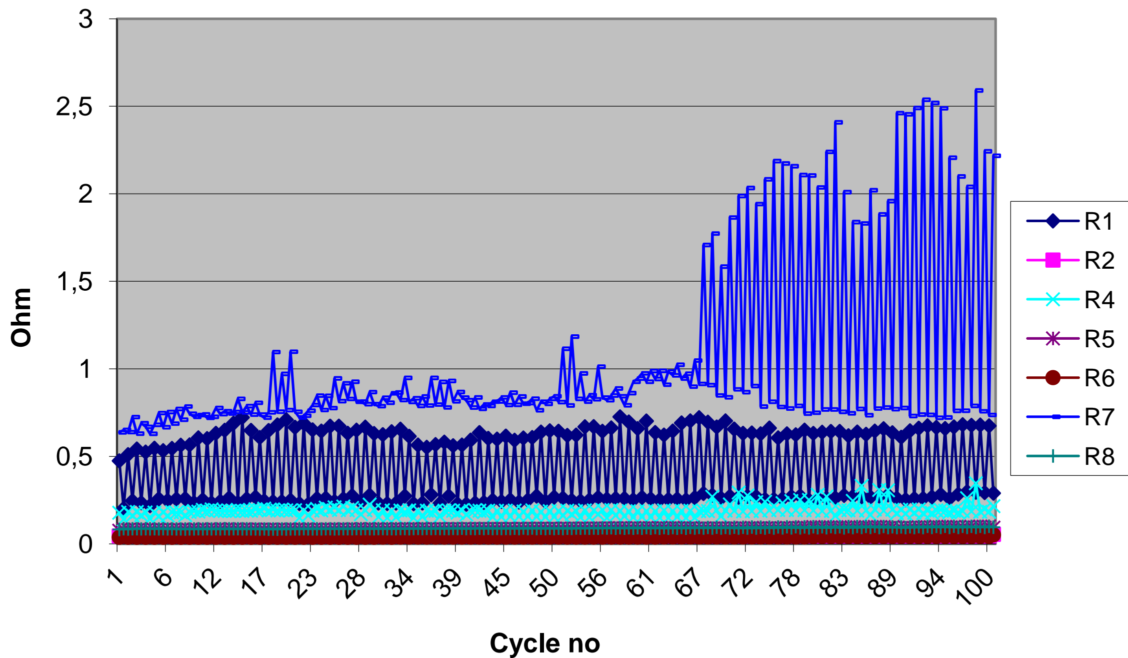


*Figure 6.14 Variation in contact resistance during 100 temperature cycles between -46 °C and 70 °C on the OSI board no 1.*

One resistor (R9) failed (no contact) after 82 cycles, and is not shown in this figure. It is notable that the R7 resistor starts to get large variations between high and low temperatures after 67 cycles. This might indicate that the contact resistance is going to increase and eventually fail within relatively few temperature cycles.

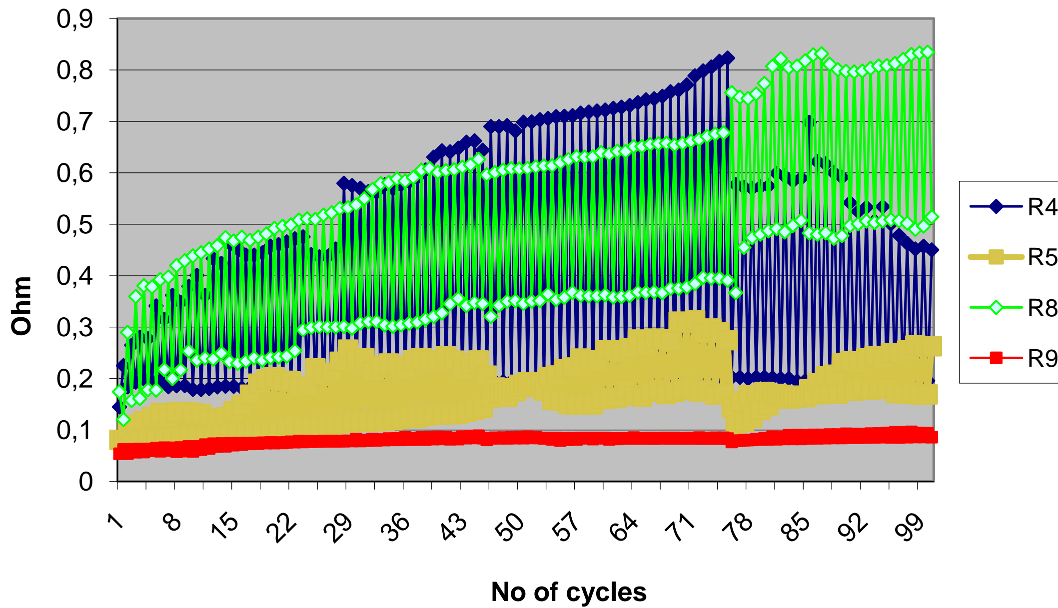


*Figure 6.15 Variation in contact resistance during 100 temperature cycles between -46 °C and 70 °C on the OSI board no 2. The test devices are mounted onto the board with H20 adhesive.*

On OSI board no 2, four contact resistances (R1, R2, R6 and R7) failed during the test.

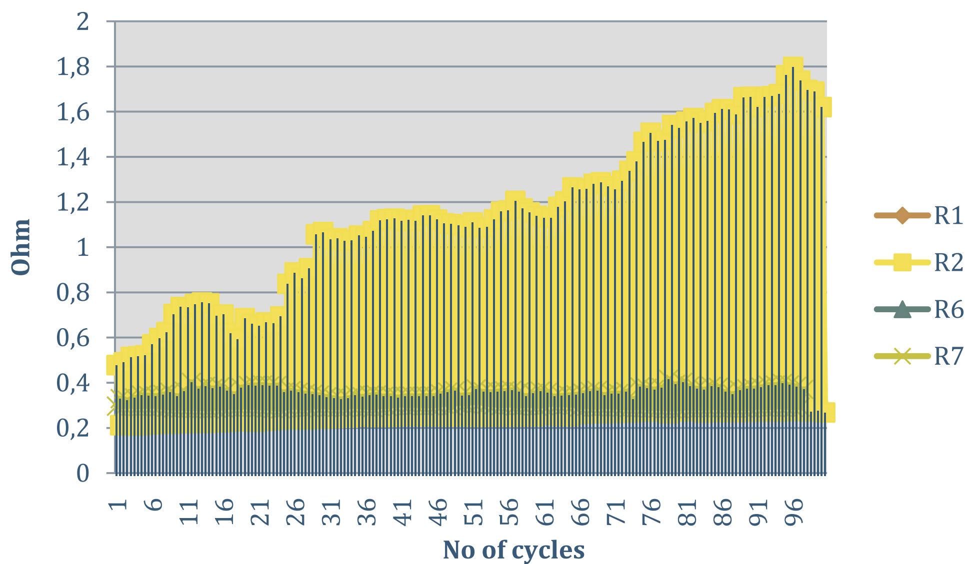


*Figure 6.16 Variation in contact resistance during 100 temperature cycles between -46 °C and 70 °C on the OSI board no 3. The test devices are mounted onto the board with H20 adhesive.*

On OSI board no 3, three contact resistances failed during test. One contact resistance was initially defect. Figure 6.16 also shows that the R2 resistance has a very large change in values between hot and cold temperatures.

### 6.4 Preliminary conclusions after tests carried out using the temperature board

The temperature test shows that the ICA-30S has very good properties regarding thermal cycling compared to the commercially available H20 epoxy. However, the H20 has much lower contact resistance. The high contact resistance when using the ICA-30S adhesive was caused by a delamination of the silver coating from the polymer sheres. Solving this problem should give a lower contact resistance for the ICA-30S. The thermal properties of the H20 adhesive might be influenced by the low adhesion between the components and the PCB. In order to verify this, more tests have to be performed.

The main challenge using ICA with MPS is the process of printing the adhesive onto the PCB. This process therefore has to be refined in order to be able repeatably print adhesive on small pads.

## 7 Thermo mechanical calculations

A thorough discussion about the thermo-mechanical analysis of the MEMS to PCB interconnections is presented in a FFI memo[4]. This memo describes how the interconnections are exposed to forces during temperature cycling. Since the curing temperature is in the range 100 – 200 °C, the largest forces occurs at the lowest temperature. Depending on the test conditions, the lowest temperature may be as low as – 55 °C.

The analysis show that the shear stresses and normal stresses will be above acceptable levels for the adhesive and its interfaces when ICA is used without underfill.

## 8 Rheological properties of the adhesive

The printing process of the ICA containing MPS is very dependent upon the rheological (flow) properties of the adhesive. One of the factors influencing the printing process is the volume fraction of spheres relatively to the volume of the adhesive matrix. The volume fraction will also strongly influence the viscosity of the adhesive matrix. Therefore, we measured the viscosity of the adhesive with various vol% of spheres. The experiments described in this section were carried out together with Hoang-Vu Nguyen, a PhD student from Vestfold University College (VUC) working on the Remi project.

The viscosity was measured using the PAAR Physica UDS 200 instrument at FFI. The temperature during measurements was 25°C and the gap between the spindle and the plate was 0.5 mm. The frequency used was 1 Hz. Viscosity measurements were carried out with vol% ranging from 3.5 to 55vol%.

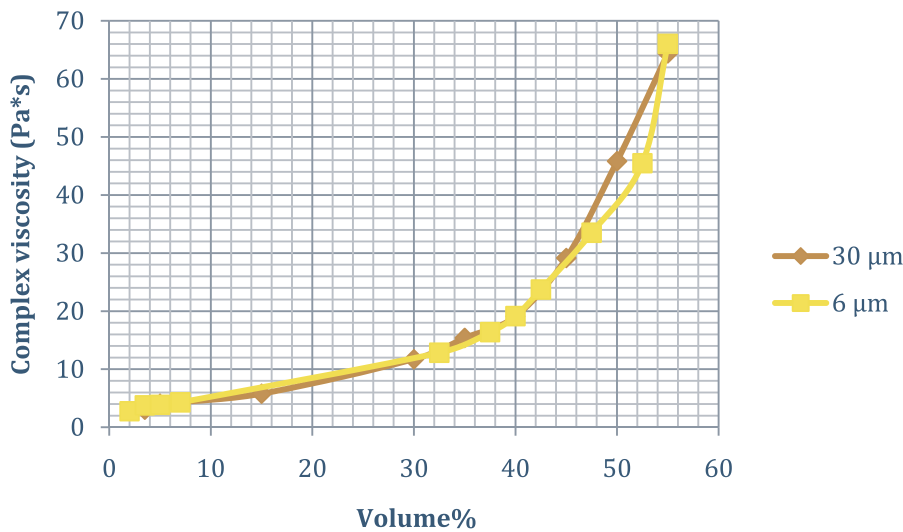


*Figure 8.1 Complex viscosity for different polymer sphere sizes as a function of the volume fraction of polymer spheres.*

The spheres had no metal coating in order to reduce the cost, and no resin was added to the epoxy. From Figure 8.1, we see that the viscosity is rapidly changing when the vol% exceeds 40%.

We also carried out printing experiments with various vol% of the spheres. Also in this experiment, the spheres had no metal coating. We printed the adhesive on a copper plate without any pattern. The stencile used was made for the Remi firing board (see chapter 9). Using such a plate simplified the printing process since we did not have to align the stencil to a PCB layout. The large pads have a size of 600X650 µm, and are used for mounting 0402 resistors. The small pads have a size of 100X350 µm. The following pictures show some of the printing results.

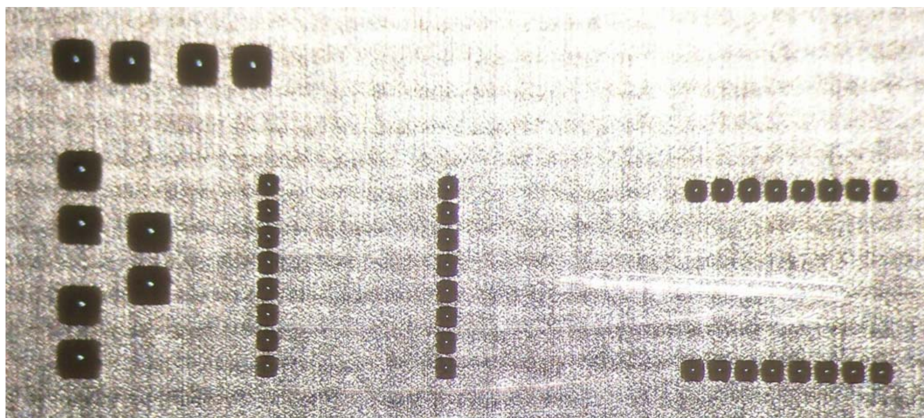

*Figure 8.2 Printing of adhesive with 45vol% 6µm spheres. The small pad sizes are floating together, making it look like 8 larger pad in one row when it in fact it should be 16 smaller pads on each row. The largest pads are shown to the left in this picture.*

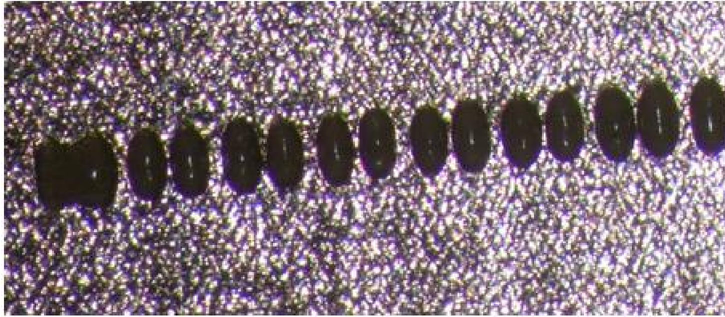

*Figure 8.3 Printing adhesive with 50 vol% 6μm spheres. The small pads are now clearly visible.*

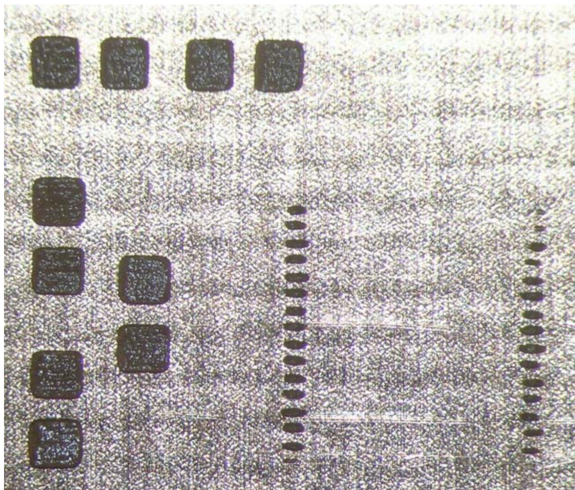

*Figure 8.4 Printing adhesive with 55 vol% 6μm spheres. The small pads are now clearly visible, but the printing is insufficient at some pads.*

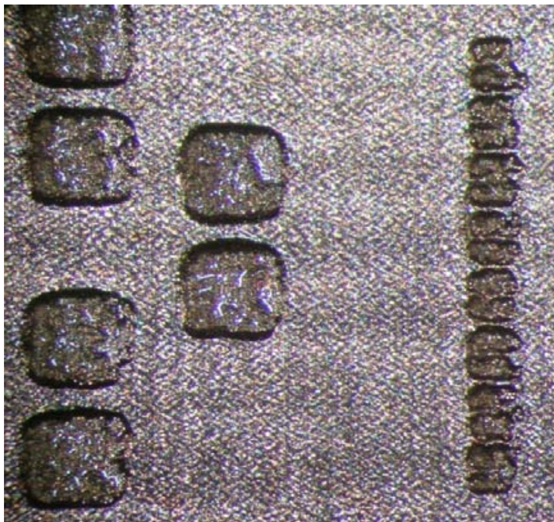

*Figure 8.5 Printing adhesive with 45 vol% 30μm spheres. The small pads are visible, but some of the pads are close to floating together.*

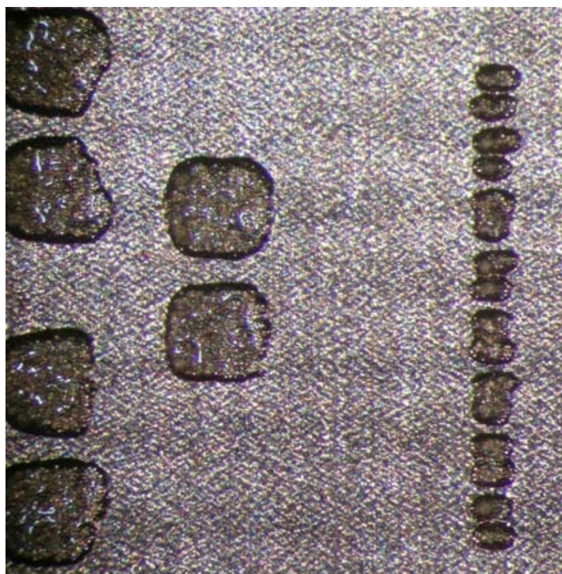

*Figure 8.6 Printing adhesive with 50 vol% 30µm spheres. Four of the small pads have good printing. For the other small pads, the adhesive is floating together.*

*Figure 8.7 Printing adhesive with 55 vol% 30 µm spheres. As can be clearly seen, the printing of the small pads is insufficient.*

Figure 8.2 - Figure 8.7 show that a vol% of 45 – 50 gives the best results for adhesive printing. This corresponds to a complex viscosity in the range of 30 – 47 Pa*s. If the vol% gets too high (>55%), the printing becomes insufficient and if it becomes too low, the adhesive floats together. It is important to be aware of, that the printing process is not solely dependent upon the viscosity, but also factors as e.g. shear thinning property. The shear thinning property determines how well the adhesive will flow when exposed to shear force.

Results from this work were presented on the ESTC conference in 2010 [5]. The paper is presented in Appendix C.

# 9 Design of the Remi firing board

It was of great interest to measure changes in contact resistances before and after test firings. If the contact resistances survived the test firings, this could imply that the ICA based on Conpart technology could be used for mounting components directly to PCB in ammunition applications. Due to limited available space inside 30 mm projectile, a special board was designed for this purpose, denoted Remi firing board.

The size of the board was designed to be 9 X 16 mm, and a sketch of the board is shown in Figure 9.1. Choosing this dimension, it is possible to mount the board vertically or to rotate it 90° inside the projectile. The front side of the board contains two U-40 MEMS test devices and four resistors (size 0402), while the backside contains two I-100 MEMS test devices and four resistors.

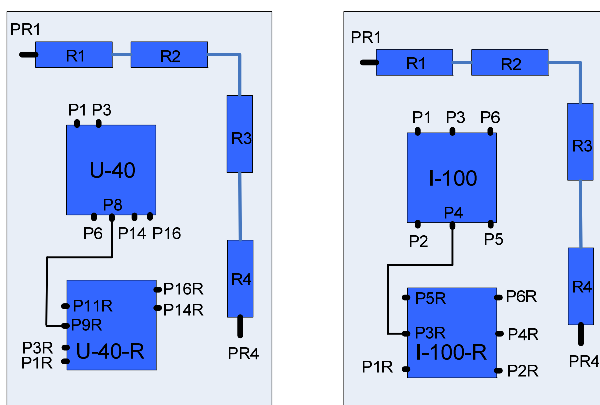


*Figure 9.1 Sketch of the Remi firing board with MEMS test devices. Front side to the left. The pin numbering indicates at which pin the resistances are measured.*

In order to investigate if pad orientation with respect to rotation/firing direction influenced the measured results, one of the components on each side was rotated 90° compared to the other.

Due to the size of the board, the contact resistances have to be measured using probes after firing. This is very inconvenient, at least when measuring resistances after mounting of components and e.g. temperature cycling. Therefore, the board was designed as shown in Figure 9.2. with four rows with test pins. A photograph of the board is shown in Figure 9.3.

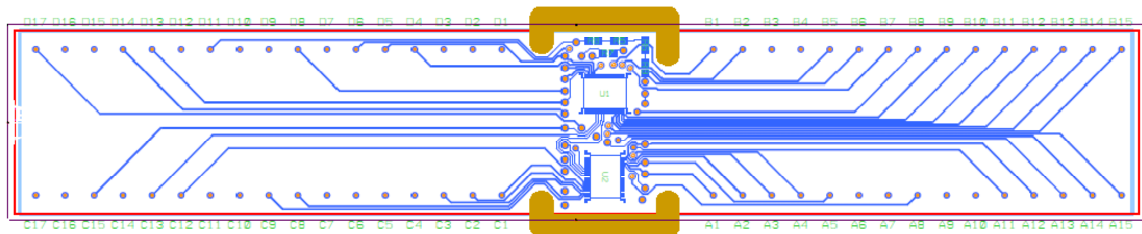

*Figure 9.2 Layout of the front side of the Remi firing board.*

*Figure 9.3 Photograph of the Remi firing board. Left side shows the board with mounted components and test pins. Left side shows the part of the board suited for mounting inside a 30 mm projectile.*

The four rows of test pins are denoted A, B, C and D. Row A is bottom right, B is located top right, C is bottom left and D is top left. The numbering of the test pins starts nearest the test devices. These test pins are for measuring contact resistance on the mounted test devices. A motherboard with so-called zero insertion force sockets were designed to interface the the Remi firing board using the test pins. This motherboard was connected to the Keithly 3706 instrument when measuring the contact resistances. Before the board was mounted in the 30 mm projectile, the board is cut along the notches as shown to the left in Figure 9.3, and the resulting board is shown to the right in Figure 9.3. Table A.3 in Appendix A.3 gives the relationship between channel number for the Keithly 3706 instrument, measured resistance and test pin number.

# 10 Experiments using the Remi firing boards

Several experiments were carried out in order to test the properties of the conductive adhesive. Two types of adhesives were used, one with 30 µm silver coated spheres (ICA-30S) and one with 4 µm gold coated spheres (ICA-4G). The experiments included a temperature cycling test, a shear test and a firing test. Contact resistances were measured after mounting of components, after the temperature cycling test and after the firing test.

For these experiments, 8 boards with I-100 test devices, 13 boards with U-40 test devices and 5 boards for the shear test were prepared. These boards were denoted I1-I8, U1-U13 and S1-S8 respectively. On the I and the U boards there were either one or two test devices mounted onto the boards, while the S boards contained five test devices each. Table A.4 - Table A.6 in Appendix A.4 give an overview of the experimental setup. These tables were used as “living” documents during the experiments which lasted for about two months.

## 10.1 Mounting of components

Even though we had achieved experience and more knowledge about the printing process of the adhesive, it was still challenging to achieve good printing results.

The printing of adhesive onto the I1-I8 boards went reasonably well. Figure 10.1 shows the printing results using both types of adhesive.

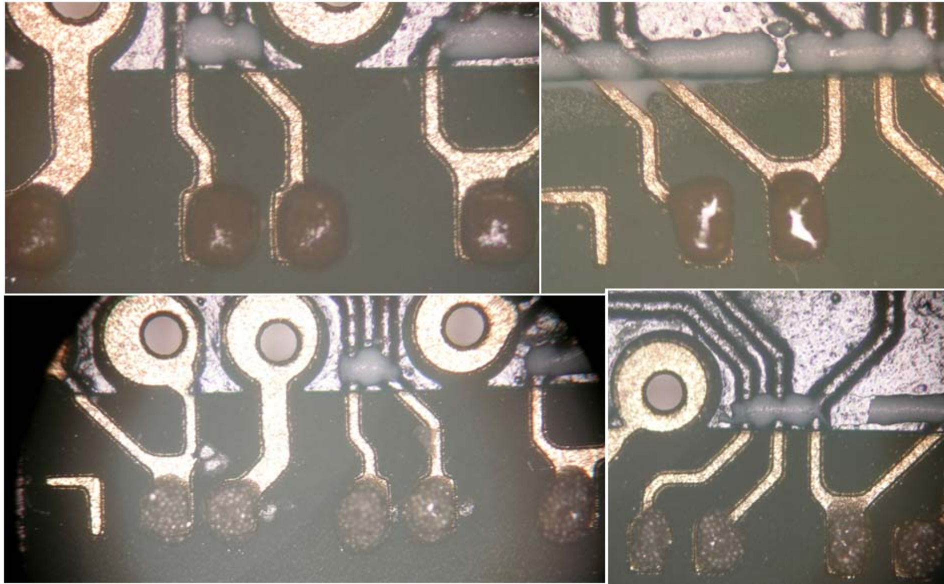

*Figure 10.1 Stencil printing of ICA-4G (upper) and ICA-30S (lower). The 30 µm spheres are easily visible in this picture.*

It was originally planned to mount five boards with the U-40 test device using ICA-30S (U1-2, U7-9, see Table A.5). Due to the small pad size (100x350 µm) of the U-40 test device and the "large" spheres in the ICA-30S resulted in inadequate printing of the adhesive. Therefore no test devices were mounted on these boards.

The printing of ICA-4G on the small pads was also a challenging task, and several tests were carried out. Figure 10.2 shows the insufficient printing on such a board. No components were mounted on this board.

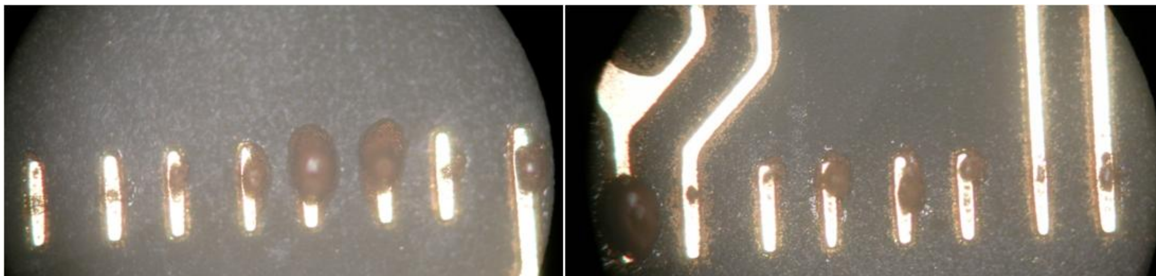

*Figure 10.2 Insufficient printing of ICA-4G on small pads.*

However, some of the trials were successful, and Figure 10.3 shows an example where the printing was sufficient.

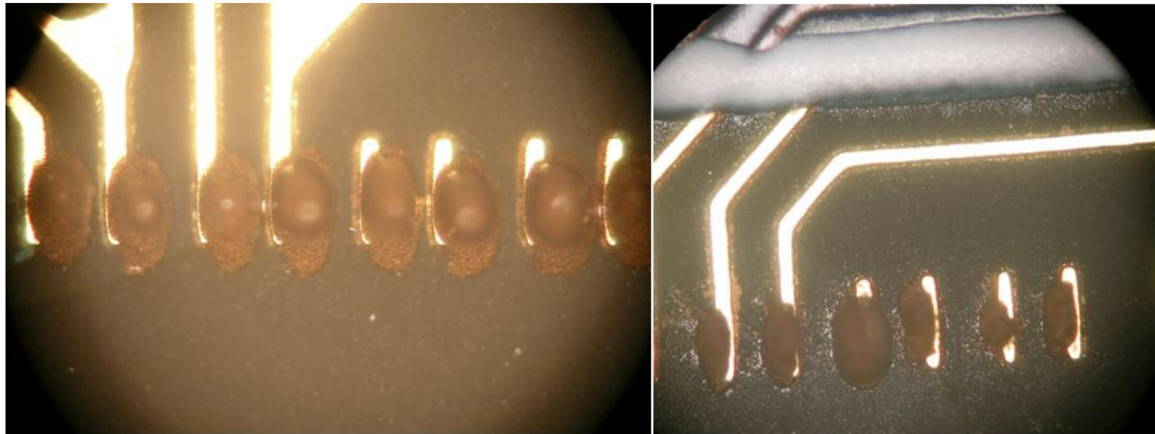

*Figure 10.3 Sufficient printing results for ICA-4G on small pads. Note that some pads are unconnected.*

As seen from Figure 10.3, there is a potential risk for a short-circuit between pads when the MEMS test device is mounted onto the board. The adhesive might be squeezed out to the next pad during mounting. This will naturally affect the measurement result, but we did not investigate this further during the project.

The Temp_board (see chapter 4) was used for the shear tests. Since the number of I-100 test structures were limited, the I-20 test structure was used instead (see Figure 3.1). The I-20 test devices were rotated 90 degrees so the pads on the board are along the conductive path of the test device. Since no electrical test was going to be performed on these boards, the rotated I-20 test devices should have the same performance during shear tests as the I-100 test devices. Figure 10.4 shows some of the printing results for this test.

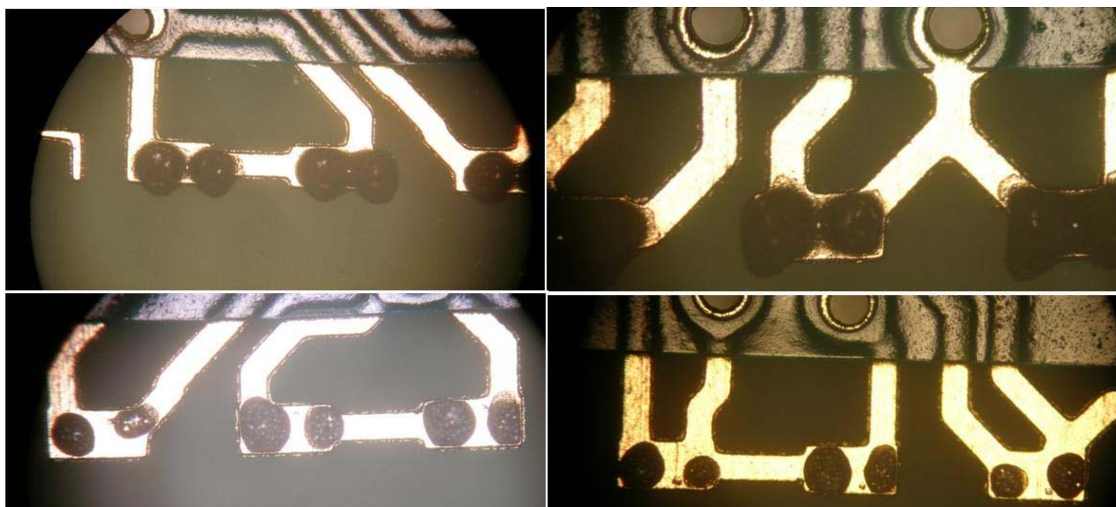

*Figure 10.4 Printing of adhesive for the shear test boards. Upper: ICA-4G. Lower part: ICA-30S.*

It is easily seen from these pictures, that the amount of adhesive is not equal from pad to pad. This will of course affect the shear test results. The shear test results are presented in Appendix F.

F. The shear force is presented in gf (gram-force). The conversion to Newton is given by multiplying the gf with a factor of 0,00981.

### 10.2 Initial measurement results

After mounting of the test devices, the initial resistance values were measured. Table 10.1 summarizes the measured results for the I boards.

| Resistance name | Average contact resistance using ICA-30S (Ω) | Average contact resistance using ICA-4G (Ω). |
|---|---|---|
| R1 | 0,428 | 0,081 |
| R2 | 0,243 | 0,09 |
| R5 | 0,304 | 0,126 |
| R6 | 0,185 | 0,099 |
| R1R | 0,293 | 0,124 |
| R2R | 0,495 | 0,113 |
| R5R | 0,258 | 0,11 |
| R6R | 0,44 | 0,102 |
| RI-100D | 1,035 | 0,894 |
| RPR | 5,759 | 1,993 |

*Table 10.1 Average contact resistance value for the I-100 test devices mounted with conductive adhesive.*

The RI-100D is a daisy-chain resistor between pin 3 on I-100 and pin 4 on I-100R (see Figure 9.1) and the RPR is a daisy-chain resistance consisting of four 0 Ω resistances. For the contact resistances, it is notable that the adhesive using silver coated spheres has approximately three times the resistances as for the one mounted with adhesive containing gold coated spheres.

Corresponding measurements were done on the U boards. The table below gives the average resistances measured for these boards.

| Resistance name | Average contact resistance using ICA-4G (Ω) |
| --- | --- |
| R1 | 0,436 |
| R3 | 0,443 |
| R14 | 0,448 |
| R16 | 1,039 |
| R1R | 0,391 |
| R3R | 0,479 |
| R14R | 0,301 |
| R16R | 2,059 |
| RU-40D | 1,814 |
| RPRU | 6,062 |

*Table 10.2 Average contact resistance value for the U-40 test devices mounted with ICA-4G.*

It is notable that these contact resistances are significantly higher than for the I boards mounted with the same type of adhesive. The ratio in pad size between pads on the I and the U boards is 250µm/100µm = 2.5. Since the contact resistance R~1/A where A is the pad area, the ratio between contact resistances mounted on the U and I board with ICA-4G should be 2.5. Comparing the measured results in Table 10.1 and Table 10.2, it can be seen that the ratio is varying from 2,7 up to 5,3 when disregarding the outliers R16 and R16R. Given the uneven adhesive printing results an exact match between the theoretical ratio and calculated ratio is not expected.

## 10.3 Temperature cycling tests

Some of the boards (see Table A.4 - Table A.6) were exposed to 10 or 100 temperature cycles between -55 °C and + 125 °C according to MIL-STD 883 G method 1010.8 test condition B.

Figure 10.5 shows how one of the resistances on the I-3 board performed during 100 temperature cycles.

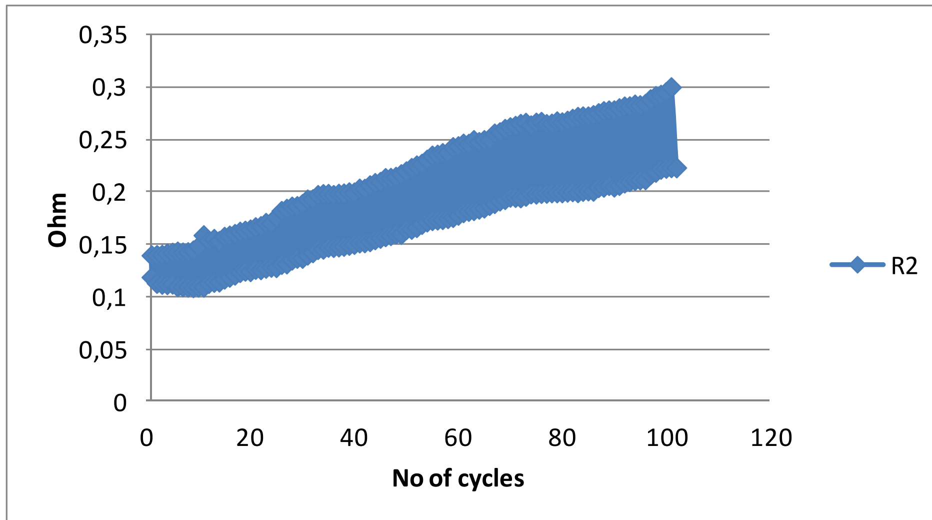


*Figure 10.5 Contact resistance during 100 temperature cycles between -55 °C and + 125 °C.*

Table 10.3 gives the contact resistances on two boards before and after temperature cycling.

| | Board I-1 (ICA-30S) | | | Board I-3 (ICA-4G) | | |
|---|---|---|---|---|---|---|
| | After mounting | After 100 cycles | | After mounting | After 100 cycles | |
| Resistance | Mean value (Ω) | Mean value (Ω) | % change | Mean value (Ω) | Mean value (Ω) | % change |
| R1 | 0,404 | 1,101 | 172,772 | 0,081 | 0,109 | 34,675 |
| R2 | 0,284 | 0,376 | 32,216 | 0,070 | 0,258 | 267,966 |
| R5 | 0,515 | 0,866 | 68,325 | 0,134 | 0,181 | 34,549 |
| R6 | 0,335 | 0,811 | 142,066 | 0,093 | 0,241 | 160,270 |
| R1R | 0,263 | 0,416 | 58,473 | 0,123 | 0,131 | 6,734 |
| R2R | 0,441 | 0,709 | 60,765 | 0,139 | 0,291 | 110,413 |
| R5R | 0,327 | 0,515 | 57,412 | 0,151 | 0,355 | 135,780 |
| R6R | 0,316 | 0,605 | 91,333 | 0,110 | 0,166 | 51,526 |
| RI-100D | 1,058 | 1,241 | 17,289 | 0,891 | 1,043 | 17,101 |
| RPR | 4,177 | 5,515 | 32,036 | 1,741 | 3,096 | 77,847 |

*Table 10.3 Contact resistance value before and after 100 temperature cycles between -55 °C and + 125 °C. Test devices on board I-1 are mounted with ICA-30S and test devices on board I-3 are mounted using ICA-4G.*

As can be seen from this table, the increase in contact resistance varies a lot from resistance to resistance. There might be several explanations for this behavior. One might be that some of the resistances are close to failure; hence the resistance value is increasing rapidly. Another explanation may be that the difference is caused by uneven adhesive printing. Also, the observant reader would note the difference of the contact resistance presented for the R2 resistance in Figure 10.5 and Table 10.3. In Figure 10.5, the resistance is higher than 0.1 Ω at low and high temperatures, while the initial measured value was 0,070 Ω. It should be expected that the resistance should be less than 0,07 Ω at low temperatures and higher than 0,07 Ω at the high

temperature. This behavior is also observed at some of the other resistances as well. It is difficult to find a good explanation for this behavior. One reason might be that some “post” curing has occurd in the time between the initial measurements were performed to the temperature cycling experiments started, and that the “post” curing process has resulted in a higher initial contact resistance than shown in Table 10.3. The time elapsed between the two measurements was approximately two weeks.

Cross sections were made on some of the boards. When cross section was done after 10 temperature cycles on board I-8, it was revealed that the silver coating had partly delaminated (see also Figure 6.9). This is easily seen on Figure 10.6. The delamination occurs most probably during the printing process when the MPS are subjected to external forces when the adhesive is squeezed through the stencile and onto the pads. It might also have occurred during mixing of the adhesive, but this is more unlikely since the MPS are subjected to much smaller forces during mixing then under the printing process. Figure 6.9 also shows that the delamination occurs before temperature cycling. This supports our above hypothesis Delamination is therefore regarded as one of the causes for the difference in contact resistance between the silver coated spheres and the gold coated spheres. Another cause may be that, since they are smaller, the gold coated spheres form numerous paths between the pads on the PCB to the pads on the test device, thus giving a lower contact resistance.

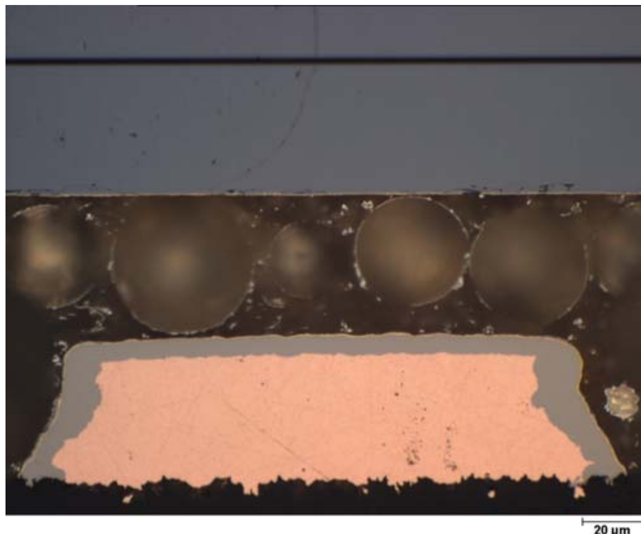


*Figure 10.6 Cross section picture on I-8 board after 10 temperature cycles. Delamination of silver is easily visible.*

For the U board, the resistances vary a lot after 10 cycles, as shown in Table 10.4. It is noteworthy that some of the resistances in fact decreases after temperature cycling and that two resistor fail during testing. The reason why the resistace decreases during temperature cycling is explained in [6], see also Appendix F. Otherwise, the uneven printing of the adhesive is probably the cause for the large variations in the resistor changes during the temperature cycle test.

| | Board U-10 (ICA-4G) | | |
|---|---|---|---|
| | | After 10 cycles | |
| Resistance | Mean value (Ω) | Mean value (Ω) | % change |
| R1 | 0,756 | 1,644 | 117,629 |
| R3 | 0,390 | 1,020 | 161,431 |
| R14 | 0,862 | 0,754 | -12,613 |
| R16 | 1,011 | 1,603 | 58,537 |
| R1R | 0,143 | Failed | |
| R3R | 0,093 | 4,767 | 5012,787 |
| R14R | 0,147 | 0,135 | -8,451 |
| R16R | 0,268 | 0,234 | -12,612 |
| RU-40D | Failed | Failed | |
| RPRU | 6,497 | 9,675 | 48,919 |

*Table 10.4 Contact resistances before and after 10 temperature cycles between -55 °C and +125 °C for U-10 board.*

Based on the results from the temperature cycling tests, the thermo-mechanical analysis described in chapter 7 was too pessimistic. This can be caused by the fact that the heights of the pads are larger than assumed in the analysis, a larger number of pads, and that the property parameters for the PCB and the adhesive might be insufficient.

## 10.4 Firing test

The firing tests were performed on December 1, 2009. Boards I1 – I4, S6 and U3 and U10 were put into projectiles and fired. Before firing, but after temperature cycling, underfill was added on one of each of the test devices on the I-1 – I-4 boards. A picture of a test device with underfill is shown in Figure 10.7.

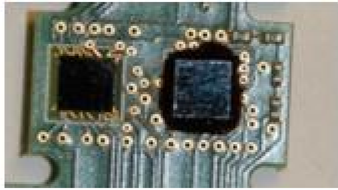

*Figure 10.7  Test device (to the right) with underfill before firing.*

The boards were put into two projectiles, and glass beeds were used as potting material. Figure 10.8 shows some of the boards after test firing.

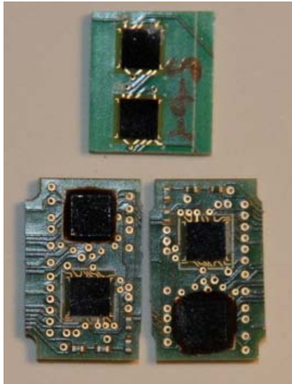

*Figure 10.8  Test boards after firing. The upper board contains test devices used for shear tests.*

Measuring contact resistances after test firing was quite time consuming. The Kelvin measurements had to be done manually using a probe station and the HP 34420A micro ohm meter. Probing had to be done on boards like the ones shown in the lower part of Figure 10.8.

Table 10.5 - Table 10.6 show how the contact resistances changes from the initial values after mounting of the test devices, after 100 temperature cycles and finally after firing test.

| Board I-1 (ICA-30S) | | | | | | |
|---|---|---|---|---|---|---|
| | | After 100 cycles | | After firing | | |
| | Mean value (Ω) | Mean value (Ω) | % change | Measured value (Ω) | % change wrt initial value | % change wrt temp test |
| R1 | 0,404 | 1,101 | 172,772 | 1,228 | 204,309 | 11,562 |
| R2 | 0,284 | 0,376 | 32,216 | 0,396 | 39,397 | 5,431 |
| R5 | 0,515 | 0,866 | 68,325 | 1,135 | 120,511 | 31,003 |
| R6 | 0,335 | 0,811 | 142,066 | 0,934 | 178,786 | 15,169 |
| R1R* | 0,263 | 0,416 | 58,473 | 0,374 | 42,461 | -10,104 |
| R2R* | 0,441 | 0,709 | 60,765 | 0,66 | 49,637 | -6,922 |
| R5R* | 0,327 | 0,515 | 57,412 | 0,509 | 55,433 | -1,257 |
| R6R* | 0,316 | 0,605 | 91,333 | 0,631 | 99,529 | 4,283 |
| RI-100D | 1,058 | 1,241 | 17,289 | 553 | | |
| RPR | 4,177 | 5,515 | 32,036 | 6,72 | | |

*Table 10.5 Measured contact resistances on the I-1 board after mounting of the test devices, after 100 temperature cycles and after firing test. The test devices are mounted using ICA-30G. The I-100 R (see Figure 9.1) has underfill and are marked with *. Two wire measurement is used measuring resistors RI-100D and RPR after firing.*

| Board I-3 (ICA-4G) | | | | | | |
|---|---|---|---|---|---|---|
| | | After 100 cycles | | After firing | | |
| | Mean value (Ω) | Mean value (Ω) | % change | Measured value (Ω) | % change wrt initial value | % change wrt temp test |
| R1* | 0,081 | 0,109 | 34,675 | 0,141 | 74,635 | 29,671 |
| R2* | 0,070 | 0,258 | 267,966 | 0,253 | 260,943 | -1,909 |
| R5* | 0,134 | 0,181 | 34,549 | 0,195 | 45,160 | 7,886 |
| R6* | 0,093 | 0,241 | 160,270 | 0,249 | 168,616 | 3,207 |
| R1R | 0,123 | 0,131 | 6,734 | 0,164 | 33,726 | 25,289 |
| R2R | 0,139 | 0,291 | 110,413 | 0,34 | 145,480 | 16,666 |
| R5R | 0,151 | 0,355 | 135,780 | 0,466 | 209,269 | 31,169 |
| R6R | 0,110 | 0,166 | 51,526 | 0,251 | 129,195 | 51,258 |
| RI-100D | 0,891 | 1,043 | 17,101 | 9,36 | | |
| RPR | 1,741 | 3,096 | 77,847 | 5,9 | | |

*Table 10.6 Measured contact resistances on the I-3 board after mounting of the test devices, after 100 temperature cycles and after firing test. The test devices are mounted using ICA-4G. The U-40 test device (see Figure 9.1) marked with * has underfill. Two wire measurement is used measuring resistors RI-100D and RPR after firing.*

As can be seen from Table 10.5 and Table 10.6, the test device with underfill has lower or even negative change in contact resistance after firing compared to the values after temperature cycling.

Table 10.7 shows the result of using underfill in firing tests. Based on the limted number of samples available in the experiments and the examinations carried out after the firing, it is very difficult to find plausible explanations why the contact resistances using ICA-30S decreased while the contact resistances increased using ICA-4G when underfill was used. Table 10.7 shows that underfill has a pronounced effect on how much the contact resistances varies after firing test. The effect of using underfill may be explained by the fact the mechanical forces during firing is distributed over a larger contact area (the area of the test device) hence reducing the mechanical stress at the contact pads.

| ICA | Board no. | No. of temp cycles | Underfill | $R_{average}$ after temp cycling (Ω) | $R_{average}$ after firing (Ω) | % change |
|---|---|---|---|---|---|---|
| 30µm | I1 | 100 | yes | 0,561 | 0,544 | -3,0 |
| 30 µm | I1 | 100 | no | 0,788 | 0,923 | 17,1 |
| 4 µm | I3 | 100 | yes | 0,197 | 0,21 | 6,6 |
| 4 µm | I3 | 100 | no | 0,236 | 0,305 | 29,2 |

*Table 10.7 Measured average contact resistance before and after firing for test devices with and without underfill.*

Two devices without underfill cracked in the test firing. A SEM picture of one of the cracked devices is shown in Figure 10.9.

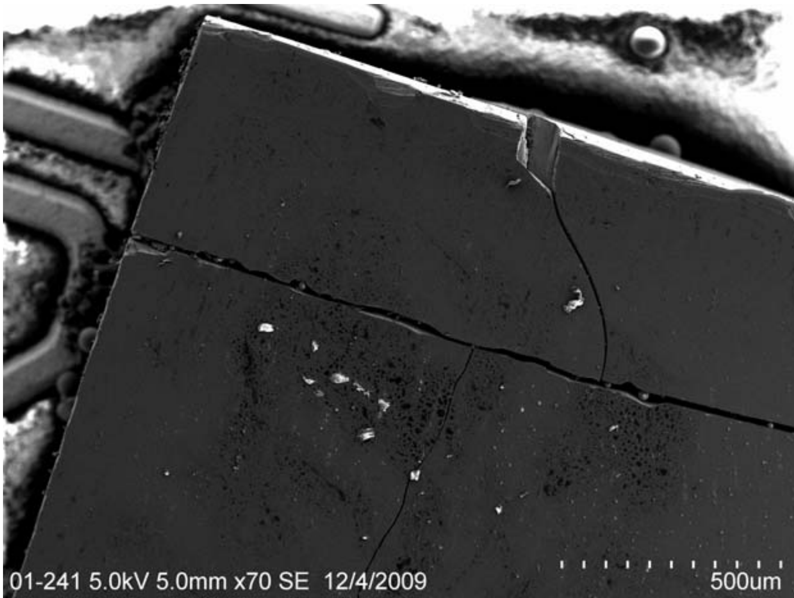


*Figure 10.9 SEM photo of a cracked I-2 test device after firing. Note that the cracked parts of the device are still attached to the PCB.*

The work described in this section was presented at the SPIE Photonic West conference in 2010. We were asked to write an “appetizer” before the conference which was published early January 2010 in the SPIE Newsroom [7]. This article is also given in Appendix D. The SPIE Photonic West conference paper is shown in Appendix E [8].

When the conference paper was accepted, we were also asked if we would submit an article to the Journal of Micro/Nanolithography, MEMS and MOEMS on the work we had done. This peer reviewed article was published late December 2010 [6]. During the work with this article, we got very good comments from the reviewers. Implementing the suggesting changes from the reviewers into the article improved the quality of the paper significantly. The journal paper is shown in Appendix F.

### 10.5 Vibration test

Vibration tests were performed on the I-7 and the U-5 boards. Acceleration spectral density for the CV 90 vehicle was used. The acceleration spectral density is shown in Figure 10.10.

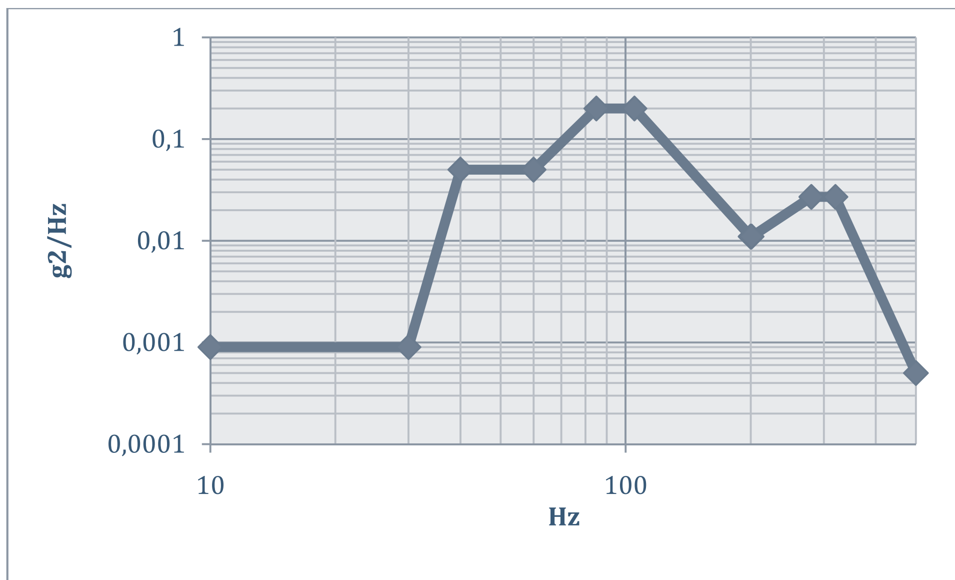


*Figure 10.10 Acceleration spectral density for the CV 90 vehicle.*

The boards were tested one hour in each direction. The results are presented in theTable 10.8.

| U-5 board (ICA-4G) | | | | I-7 board (ICA-30S) | | | |
|---|---|---|---|---|---|---|---|
| Resistance no | Contact resistance before shaking (Ω) | Contact resistance after shaking (Ω) | % change | Resistance no | Contact resistance before shaking (Ω) | Contact resistance after shaking (Ω) | % change |
| R1 | 0,002 | 0,002 | -5,789 | R1 | 0,279 | 0,278 | -0,36 |
| R3 | 1,253 | 1,259 | 0,471 | R2 | 0,215 | 0,215 | 0,00 |
| R14 | 0,109 | 0,147 | 35,561 | R5 | 0,162 | 0,165 | 1,85 |
| R16 | 1,028 | 1,129 | 9,810 | R6 | 0,116 | 0,116 | 0,00 |

*Table 10.8 Changes in contact resistance after vibration test.*

The I-7 and the U-5 boards have been exposed to 10 and 9.5 temperature cycles before vibration test respectively. As can be seen from Table 10.8, the contact resistances on the I-7 board do not change much. However, the changes are much more pronounced for the U-5 board. Again, this is probably due to the bad printing result of the adhesive for the test devices on this type of board.

A presentation of the results achieved in the Remi project including the viberation tests was given at the Fuze conference in May 2010 [9].

# 11 Summary of test conditions and tests preformed using the Temp_board and the Remi_firing_board

Table 11.1 summarizes the test conditions and the tests performed using the two PCBs designed in the ReMi project.

| | Temp_board | Remi_firing_board |
|---|---|---|
| Type of adhesive tested | ICA-10G, ICA-30S, H20 | ICA-30S, ICA-4G |
| Temperature range test | -46 - +70 | -55 - +125 |
| No of temperature cycles | Up to ~760 cycles | 10 and 100 |
| Shear tests | Yes | Yes |
| Vibration test | No | Yes |
| Firing tests | No (*) | Yes |

*Table 11.1 Summarizing of test conditions and test performed on Temp_board and Remi_firing_board.*

The temp_board was mainly used for long temperature cycling test. All PCBs were exposed to more than 100 temperature cycles. However, the temperature range was mainly set by the capability of the temperature chamber used in these tests.
(*) The Temp_board was not used for firing test, except as described in chapter 10.1.

## 12 Conclusions

The work carried out in the Remi Fuze case showed that a conductive adhesive based on Conparts technology with metallized polymer spheres may be used to mount MEMS devices directly to a PCB in very demanding environments such as an ammunition fuze. However, there are still some issues that must be improved/investigated further. Some of these issues are:

- The properties of the adhesive must be improved so that the printing process becomes much easier.
- Adhesion between polymer sphere and silver must be improved so that delamination is avoided.
- How the conductive adhesive performs during long time storage must be investigated. Currently, we have no information about this.
- Reduce the contact resistance when using silver coated spheres.

Participating in a project such as the Remi project has been very valuable. During this project we have established very good contact with our main cooperators Conpart and Sintef. We have also achieved good contact with Vestfold University College and the other industry partners in the project.

## References

[1] Keithley. [Online]. http://www.keithley.com/products/data/datalogger/?mn=3706A

[2] Daniel Lu and C.P Wong, *Materials for Advanced Packaging*.: Springer, 2009, ch. 11.

[3] H. Kristiansen et al., "Development of Low Modulus Conductive Adhesives for MEMS interconnects.," in *Pan Pasific Microelectronics Symposium*, Big Island of Hawaii, USA, February 10-12, 2009.

[4] P Dalsjø, "Thermo-mechanical analysis of MEMS to PCB interconnect," FFI-memo 2008/01626, 2008.

[5] H.V. Nguyen et al., "Spherical Polymer Particles in Isotropic Conductive Adhesives, - A Study on Rheology and Mechanical Aspects," in *Electronic System-Integration Technology Conference (ESTC)*, Berlin, Germany, Sept 13-16, 2010.

[6] J. Gakkestad, P. Dalsjø, H. Kristiansen, R. Johannessen, and M.M.V. Taklo, "Use of Conductive Adhesive for MEMS Interconnection in Ammunition Fuze Applications," *J. Micro/Nanolith., MEMS and MOEMS (JM3)*, p. 041108, Oct-Dec 2010.

[7] J Gakkestad, P Dalsjø, H Kristiansen, R Johannessen, and M M.V. Taklo. (2010, Januar) Spie newsroom. [Online]. http://spie.org/x38621.xml?pf=true&ArticleID=x38621

[8] J. Gakkestad, P. Dalsjø, H. Kristiansen, R. Johannessen, and M.M.V. Taklo, "Use of Conductive Adhesive for MEMS Interconnection in Military Fuze Applications.," in *Proc. Spie Photonic West Conference*, San Francisco, California, USA, January 23-28, 2010.

[9] J. Gakkestad, P. Dalsjø, H. Kristiansen, R. Johannessen, and M.M.V. Taklo, "Use of Conductive Adhesive in Fuze Applications," in *54th annual Fuze Conference*, Kansas City, Mo, USA, May 11-13,2010.

## Abbrevations

| | |
|---|---|
| ACA | Anisotropic conductive adhesive. |
| CA | Conductive adhesive. |
| ECA | Eletrically conductive adhesive. |
| IC | Integrated circuit. |
| ICA | Isotropic conductive adhesive. |
| ICA-10G | Isotropic conductive adhesive with 10 µm gold coated polymer spheres. |
| ICA-30S | Isotropic conductive adhesive with 30 µm silver coated polymer spheres. |
| ICA-4G | Isotropic conductive adhesive with 4 µm gold coated polymer spheres. |
| MEMS | Microslectroechanical system. |
| MPS | Metallized polymer spheres. |
| PCB | Printed circuit board. |
| ReMi | Fine pitch interconnect of Microelectronics and Microsystems for use in rough environment |
| SOI | Silicon on insulator. |

# Appendix A Information about the measurement and experimental setup

This appendix gives information about the measurement system used for the experiments carried out using the Temp_board and the Remi firing board.

## A.1 Cable connection scheme

Table A.1 gives the relationship between the 78 D-SUB contact on the Keithly instrument and the 50 and 25 pins D-SUB contacts.

| 25 pins D-SUB contact | 78 pins D-SUB contact | Channel no | 50 pins D-SUB contact | 78 pins D-SUB contact | Channel no |
|---|---|---|---|---|---|
| Pin no | Pin no | | Pin no | Pin no | |
| 1 | 62 | 1H | 1 | 21 | 13H |
| 2 | 63 | 1L | 2 | 22 | 13L |
| 3 | 50 | 2H | 3 | 9 | 14H |
| 4 | 51 | 2L | 4 | 10 | 14L |
| 5 | 42 | 3H | 5 | 1 | 15H |
| 6 | 43 | 3L | 6 | 2 | 15L |
| 7 | 31 | 4H | 7 | 70 | 16H |
| 8 | 32 | 4L | 8 | 52 | 16L |
| 9 | 23 | 5H | 9 | 5 | 17H |
| 10 | 24 | 5L | 10 | 6 | 17L |
| 11 | 11 | 6H | 11 | 13 | 18H |
| 12 | 12 | 6L | 12 | 14 | 18L |
| 13 | 3 | 7H | 13 | 25 | 19H |
| 14 | 4 | 7L | 14 | 26 | 19L |
| 15 | 68 | 8H | 15 | 33 | 20H |
| 16 | 69 | 8L | 16 | 34 | 20L |
| 17 | 60 | 9H | 17 | 44 | 21H |
| 18 | 61 | 9L | 18 | 45 | 21L |
| 19 | 48 | 10H | 19 | 15 | 22H |
| 20 | 49 | 10L | 20 | 16 | 22L |
| 21 | 40 | 11H | 21 | 64 | 23H |
| 22 | 41 | 11L | 22 | 65 | 23L |
| 23 | 29 | 12H | 23 | 35 | 24H |
| 24 | 30 | 12L | 24 | 36 | 24L |
| 25 | NC | | 25 | 7 | 25H |
| | | | 26 | 8 | 25L |
| | | | 27 | 17 | 26H |
| | | | 28 | 18 | 26L |
| | | | 29 | 27 | 27H |
| | | | 30 | 28 | 27L |
| | | | 31 | 37 | 28H |
| | | | 32 | 38 | 28L |
| | | | 33 | 46 | 29H |
| | | | 34 | 47 | 29L |
| | | | 35 | 19 | 30H |
| | | | 36 | 20 | 30L |
| | | | 37-50 | NC | |

*Table A.1 Connection scheme for the 25 and 50 D-SUB contact to the 78 pins D-SUB contact, and the associated channel number to the Keithley multiplexer card.*

The cables were fabricated by Mectro AS in Horten.

## A.2 Relationship between channel number and resistance measured on the Temp_board

Table A.2 gives the correspondence between the channel numbers in the Keithly 3706 instrument and the measured resistance when doing Kelvin measurements. Channels 1 – 12 are connected to contacts P1 and P2 (see Figure 4.3) and the remaining channels are connected to contacts P3 and P4. For numbering of the components and how they are placed on the board, see Figure 4.3.

| Channel no | Resistance | 3720 channels no | Resistance |
|---|---|---|---|
| 1 | R1 | 1H,1L, 31H,31L | Contact resistance on I-100, pin no 1 on component no. 1 |
| 2 | R2 | 2H, 2L, 32H, 32L | Contact resistance on I-100, pin no 2 on component no. 1 |
| 3 | R3 | 3H, 3L, 33H, 33L | Resistance between pin 1 and pin 2 on I-100 Measure internal resistance on the chip (one row). |
| 4 | R4 | 4H, 4L, 34H, 34L | Contact resistance on I-100, pin no 5 on component no. 1 |
| 5 | R5 | 5H, 5L, 35H, 35L | Contact resistance on I-100, pin no 6 on component no. 1 |
| 6 | R6 | 6H, 6L, 36H, 36L | Contact resistance on I-100, pin no 1 on component no. 2 |
| 7 | R7 | 7H, 7L, 37H, 37L | Contact resistance on I-100, pin no 2 on component no. 2 |
| 8 | R8 | 8H, 8L, 38H, 38L | Contact resistance on I-100, pin no 5 on component no. 2 |
| 9 | R9 | 9H, 9L, 39H, 39L | Contact resistance on I-100, pin no 6 on component no. 2 |
| 10 | R10 | 10H, 10L, 40H, 40L | Resistance between pin 5 and pin 6 on I-100. Measure internal resistance in the chip (one row). |
| 11 | R11 | 11H, 11L, 41H, 41L | Contact resistance on pin no 1 on I-100_v90 (circuit mounted through the board, located above chip no 2) |
| 12 | R12 | 12H, 12L, 42H, 42L | Contact resistance on pin no 2 on I-100_v90 (circuit mounted through the board, located above chip no 2) |
| 13 | R13 | 13H, 13L, 43H, 43L | Resistance between pin no 1 and 2 on I-100_v90 (circuit mounted through the board, located above chip no 2) |
| 14 | R14 | 14H, 14L, 44H, 44L | Contact resistance on I-20, pin no 1 on component no. 23 (note this is on the right side of the component) |
| 15 | R15 | 15H, 15L, 45H, 45L | Contact resistance on I-20, pin no 2 on component no. 23 (note this is on the right side of the component) |
| 16 | R16 | 16H, 16L, 46H, 46L | Resistance between pin 1 and 2 on component no 23 |

| Channel no | Resistance | 3720 channels no | Resistance |
|---|---|---|---|
| 17 | R17 | 17H, 17L, 47H, 47L | Contact resistance on I-20, pin no 15 on component no. 23 (note this is on the left side of the component) |
| 18 | R18 | 18H, 18L, 48H, 48L | Contact resistance on I-20, pin no 16 on component no. 23 (note this is on the left side of the component) |
| 19 | R19 | 19H, 19L, 49H, 49L | Measures the resistance in a daisy-chain between pin 1 on component 3 and pin 6 on component 6. The measured resistance consists of 24 contact resistances and the internal resistances of the four chips in the daisy-chain (components 3-6) |
| 20 | R20 | 20H, 20L, 50H, 50L | Measures the resistance between pin 1 and 6 on component no 5. The measured resistance consists of 6 contact resistances + the internal resistances on the chip. |
| 21 | R21 | 21H, 21L, 51H, 51L | Measures the resistance between pin 1 and pin 2 on component 5. The measured resistance consists of 2 contact resistances + the internal resistance of one row of the chip. |
| 22 | R22 | 22H, 22L, 52H, 52L | Measures the resistance in a daisy-chain between pin 1 on component 7 and pin 6 on component 10. The measured resistance consists of 24 contact resistances and the internal resistances of the four chips in the daisy-chain (components 7-10) |
| 23 | R23 | 23H, 23L, 53H, 53L | Measures the resistance between pin 1 and 6 on component no 8. The measured resistance consists of 6 contact resistances + the internal resistances on the chip (3 rows). |
| 24 | R24 | 24H, 24L, 54H, 54L | Measures the resistance between pin 1 and pin 2 on component 8. The measured resistance consists of 2 contact resistances + the internal resistance of one row of the chip. |
| 25 | R25 | 25H, 25L, 55H, 55L | Measures the resistance in a daisy-chain between pin 1 on component 22 (located at lower right corner of the chip) and pin 15 on component 19 (located at the upper right corner). The measured resistance consists of 64 contact resistances and the internal resistances of the four chips in the daisy-chain (components 19-22) |
| 26 | R26 | 26H, 26L, 56H, 56L | Measures the resistance between pin 1 (upper right corner) and 16 (lower left corner) on component no 20. The measured resistance consists of 16 contact resistances + the internal resistances on the chip (8 rows). |

| Channel no | Resistance | 3720 channels no | Resistance |
|---|---|---|---|
| 27 | R27 | 27H, 27L, 57H, 57L | Measures the resistance in a daisy-chain between pin 1 (located lower right corner) on component 11 and pin 2 (located upper right corner) on component 18. The measured resistance consists of 128 contact resistances and the internal resistances of the eight chips in the daisy-chain (components 11-18) |
| 28 | R28 | 28H, 28L, 58H, 58L | Measure the resistance between pin1 and pin 2 on component no 15 (on the right side of the component). The measured resistance consist of 16 contact resistances + internal resistance on the chip |
| 29 | R29 | 29H, 29L, 59H, 59L | Measure the contact resistance of 2 components mounted through the board. These are currently not been mounted yet. |
| 30 | R30 | 30H, 30L, 30H, 30L | Measure a dummy resistance on the board. The "resistance" is just a wire on the board. |

*Table A.2 Table showing the relationship between channel number and the corresponding measured resistance on the Temp_board.*

### A.3 Relationship between channel number and resistance measured on the Remi firing board

| Res. no./ Channel no. | 25 pins D-SUB Input | | Test pin | 25 pins DSUB Sense | | Test pin | Resistance - explanation |
|---|---|---|---|---|---|---|---|
| | Pin no | Signal | | Pin no. | Signal | | |
| 1 | 1 | I1 | D1 | 1 | VI1 | D3 | Contact resistance on pin 1 on U-20 component |
| | 2 | I3 | D7 | 2 | V1 | D13 | |
| 2 | 3 | I1 | D1 | 3 | VI3 | D5 | Contact resistance on pin 3 on U-20 component |
| | 4 | I3 | D7 | 4 | V3 | D4 | |
| 3 | 5 | I14 | B12 | 5 | VI14 | B13 | Contact resistance on pin 14 on U-20 component |
| | 6 | I16 | B10 | 6 | V14 | B14 | |
| 4 | 7 | I14 | B12 | 7 | VI16 | B9 | Contact resistance on pin 16 on U-20 component |
| | 8 | I16 | B10 | 8 | V16 | B11 | |
| 5 | 9 | 2I1 | C8 | 9 | 2VI1 | C3 | Contact resistance on pin 1 on U-20R component |
| | 10 | 2I3 | C12 | 10 | 2V1 | C9 | |
| 6 | 11 | 2I1 | C8 | 11 | 2VI3 | C1 | Contact resistance on pin 3 on U-20R component |
| | 12 | 2I3 | C12 | 12 | 2V3 | C2 | |
| 7 | 13 | 2I14 | A1 | 13 | 2VI14 | A5 | Contact resistance on pin 14 on U-20R component |
| | 14 | 2I16 | A3 | 14 | 2V14 | A7 | |
| Res. no./ Channel | 50 pins D-SUB Input | | Test pin | 50 pins DSUB Sense | | Test pin | Resistance - explanation |
| | Pin | Signal | | Pin | Signal | | |

| no. | no |  |  | no. |  |  |  |
|---|---|---|---|---|---|---|---|
| 8 | 15 | 2I14 | A1 | 15 | 2VI16 | A12 | Contact resistance on pin 16 on U-20R component |
|  | 16 | 2I16 | A3 | 16 | 2V16 | A2 |  |
| 9 | 17 | I6 | C13 | 17 | V6 | C15 | Daisy-chain resistance between pin 6 on U-20 and pin 11 on U-20R |
|  | 18 | 2I11 | C16 | 18 | 2V11 | C14 |  |
| 10 | 19 | RI1 | D9 | 19 | RV1 | D11 | Daisy-chain resistance of the 4 resistances of the front side of the board |
|  | 20 | RI2 | B6 | 20 | RV2 | B5 |  |
| 11 | 21 | BI1 | D15 | 21 | BVI1 | D17 | Contact resistance on pin 1 on I-100 component |
|  | 22 | BI2 | D2 | 22 | BV1 | D14 |  |
| 12 | 23 | BI1 | D15 | 23 | BVI2 | D8 | Contact resistance on pin 2 on I-100 component |
|  | 24 | BI2 | D2 | 24 | BV2 | D10 |  |
|  | 25 | NC |  | 25 | NC |  |  |
| 13 | 1 | BI5 | B8 | 1 | BVI5 | B15 | Contact resistance on pin 5 on I-100 component |
|  | 2 | BI6 | B7 | 2 | BV5 | A14 |  |
| 14 | 3 | BI5 | B8 | 3 | BVI6 | B2 | Contact resistance on pin 6 on I-100 component |
|  | 4 | BI6 | B7 | 4 | BV6 | B1 |  |
| 15 | 5 | B2I1 | A6 | 5 | B2VI1 | A9 | Contact resistance on pin 1 on I-100R component |
|  | 6 | B2I2 | C5 | 6 | B2V1 | A10 |  |
| 16 | 7 | B2I1 | A6 | 7 | B2VI2 | C6 | Contact resistance on pin 2 on I-100R component |
|  | 8 | B2I2 | C5 | 8 | B2V2 | C7 |  |
| 17 | 9 | B2I5 | A11 | 9 | B2VI5 | A4 | Contact resistance on pin 5 on I-100R component |
|  | 10 | B2I6 | D16 | 10 | B2V5 | A8 |  |
| 18 | 11 | B2I5 | A11 | 11 | B2VI6 | C17 | Contact resistance on pin 6 on I-100R component |
|  | 12 | B2I6 | D16 | 12 | B2V6 | C11 |  |
| 19 | 13 | BI3 | A15 | 13 | BV3 | A13 | Daisy chain resistance between pin no 3 on I-100 and pin 4 on I-100R. |
|  | 14 | B2I4 | C10 | 14 | B2V4 | C4 |  |
| 20 | 15 | BRI1 | D12 | 15 | BRV1 | D6 | Daisy-chain resistance of the 4 resistances of the back side of the board |
|  | 16 | BRI2 | B4 | 16 | BRV2 | B3 |  |

*Table A.3 Relationship between channel number for the Keithly 3706 instrument, measured resistance and test pin number*

### A.4 Overview of the experimental setup using the Remi firing board

The following tables give an overview of the experimental setup using the Remi firing board. These tables were used as “living” documents during the experimental phase, which lasted for about two months.

| Board no | No of test dev. | Adhesive | Function | Mounted | No. of temp cycles | Comments | Mounting in projectile | Status |
|---|---|---|---|---|---|---|---|---|
| I-1 | 2 | ICA-30S | Firing board | X | 100 | The R chip has been underfilled | Projectile no 1. Mounted vertically in the bottom. Placed in the center | |
| I-2 | 2 | ICA-30S | Firing board | X | 10 | The upper chip has been underfilled | Projectile no 2. Placed vertically in the bottom. Placed in center (as good as it gets) | R chip cracked (no underfill) |
| I-3 | 2 | ICA-4G | Firing board | X | 100 | The upper chip has been underfilled | Projectile 2. Placed vertically in the middle | |
| I-4 | 2 | ICA-4G | Firing board | X | 10 | The R chip has been underfilled | Projectile 1. Placed in the middle and vertically | Upper chip cracked (no underfill) |
| I-5 | 1 | ICA-4G | x-section after mounting. | X | | Reference board | | Delivered to Sintef |
| I-6 | 1 | ICA-4G | cross section after temp cycl. | X | 9,5 | | | Delivered to Sintef |
| I-7 | 1 | ICA-30S | cross section after temp cycl | X | 10 | Possible to do vibration test, red board | | |
| I-8 | 1 | ICA-30S | cross section after temp cycl | X | 10 | Red board | | Delivered to Sintef |

*Table A.4 Experimental setup for the I1-I8 boards.*

| Board no | No of test dev. | Adhesive | Function | Mounted | No of temp cyc | Comments | Mounting in projectile | Status |
|---|---|---|---|---|---|---|---|---|
| U-1 | 2 | ICA-30S | Firing board | No | | | | |
| U-2 | 2 | ICA-30S | Firing board | No | | | | |
| U-3 | 2 | ICA-4G | Firing board. Just to check if the components are on the PCB after firing | X | 100 | 4 resistances broken in temp test. Large changes in the other values, more than 60% | In projectile. To be rotated 90 deg | |
| U-4 | 2 | ICA-4G | Firing board. Not firing board after temp test | X | 10 | Most resistances broken in temp test. Daisy-chain and resistor network OK | | Delivered to Sintef for x section |
| U-5 | 1 | ICA-4G | cross section after temperature test | X | 10,5 | No resistances broken in temp test. Max change is -39% | | |
| U-6 | 1 | ICA-4G | x-section after temp test | X | | Destroyed. Test device fell off during sawing! Use spare board e.g. U-12 | | |
| U-7 | 1 | ICA-30S | x-section after mounting | No | | | | |
| U-8 | 1 | ICA-30S | x-section after temp test (may also be reference board) | No | | | | |
| U-9 | 1 | ICA-30S | Spare board | No | | | | |
| U-10 | 2 | ICA-4G | Cross section after temp test. Firing board after temp test | X | 10 | 1 broken resistor and one changed much. Upper chip is underfilled (easy to inspect) | Projectile no 2. One chip fell off. Rotated 90 deg. Almost at top (placed beside board S-6-2) | |
| U-11 | 2 | ICA-4G | Cross section after temperature test | X | 10 | Possible to do vibration test. 3 broken resistors during temp test | | |
| U-12 | 1 | ICA-4G | Cross section after temperature test | X | 10 cycles | Red board. No resistances broken in temp test. Max change is -21% | | Delivered to Sintef |
| U-13 | 1 | ICA-4G | Cross section after mounting. | X | | Reference board, red board | | Sent by post to Sintef |

*Table A.5 Experimental setup for the U1-U13 boards.*

| Board no | No of test dev | Adhesive | Function | Mounted | No of temp cyc | Comments | Mounting in projectile | Status |
|---|---|---|---|---|---|---|---|---|
| S-1 | 5 | ICA-30S | Shear test after mounting | X | | Ref board | | At Sintef |
| S-2 | 5 | ICA-30S | Shear test after temperature cycling. | X | 100 | | | At Sintef |
| S-3 | 5 | ICA-30S | Shear test after temp test and firing. Not firing board. Used for measuring any differences between 10 and 100 cycles (ref S2 board). | X | 10 | | | At Sintef |
| S-4 | 5 | ICA-4G | Shear test after temperature cycling. | X | 10 + 100 | | | At Sintef |
| S-5 | 5 | ICA-4G | Shear test after temperature cycling. | X | 10 | | | At Sintef |
| S-6 | 5 | ICA-4G | Shear test after temp cycling and firing. | X | 10 | | S-6-1 2 chip. Placed on top in projectile 1. Rotated 90 deg. S-2-2 with 3 chips placed in projectile 2. Same placement as U-10 (almost at top) | |
| S-7 | 5 | ICA-4G | Shear test after mounting | X | | Ref board | | At Sintef |
| S-8 | 5 | ICA-30S | Spare board. Test after temperature cycling. | X | 100 | | | |

*Table A.6 Experimental setup for the S1-S5 boards.*

# Appendix B Paper presented at Pan Pacific Microelectronic Symposium, 2009, Big Island of Hawaii

# DEVELOPMENT OF LOW MODULUS CONDUCTIVE ADHESIVES FOR MEMS INTERCONNECTS


Helge Kristiansen
Conpart AS
2013 Skjetten, Norway

Maaike M. V. Taklo, Thor Bakke
Department of Microsystems and Nanotechnology
SINTEF ICT, NO-0314 Oslo, Norway

Jakob Gakkestad, Per Dalsjø
Norwegian Defence Research Establishment (FFI)
NO-2027 Kjeller, Norway

Rolf Johannessen, Frøydis Oldervoll
Department of Instrumentation
SINTEF ICT, NO-0314 Oslo, Norway

Vu Hoang Nguyen
Vestfold University College
Post Box 2243, NO-3103 Tønsberg, Norway


## BACKGROUND

Isotropic conductive adhesives (ICA) have been used for electronics application for more than 40 years. Traditionally, these adhesives have been made using silver particles or flakes, but also other conductor elements have been used like carbon, copper and nickel. Designing an ICA requires optimisation of a number of factors including final conductivity, rheological properties, total metal content (a cost issue in the case of noble metals) and thermo-mechanical properties [1]. The different implications will be discussed in this paper.

### Conductivity

To make an isotropic conductive adhesive using a non-conductive matrix, the volume fraction of conductive

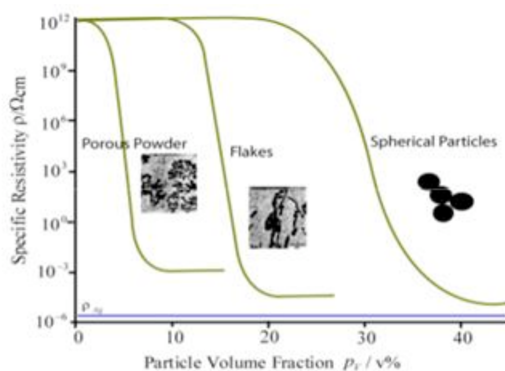


Figure 1. Specific resistance of a system comprising conductive (metal) particles and a non-conductive matrix, illustrating the percolation threshold

particles needs to reach and exceed a certain level, called the percolation threshold. That is, the amount of particles must be sufficient to create at least one path of conduction through the adhesive. This threshold is dependent on the shape of the particles. Given a complete random distribution and orientation of the particles, the percolation threshold is illustrated in Figure 1.

As shown in Figure 1, the volume fraction depends strongly on the shape of the particles. This is evident when studying the difference between for instance spheres and flakes. Additionally, the figure clearly illustrates that replacing a massive metal particle with a particle constructed of two or more phases will dramatically reduce the needed volume fraction. This is exemplified by the porous powder.

An additional comment regarding percolation threshold for flakes is that it requires a random distribution of the flake orientation. This is not the case in a typical microelectronics application where both the application of the adhesive and the shear applied during placement of the component causes a significant orientation of the flakes [2], as illustrated in Figure 2. For practical applications, this means that a significantly higher concentration of flakes is needed to obtain reliable contacts than indicated in Figure 1, which is based on theoretical models.

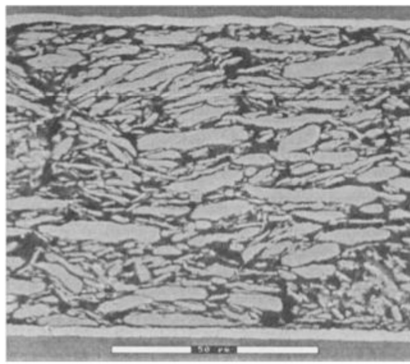

Figure 2. Illustration of the tendency for metal flakes (in this case silver) to align themselves in parallel with the die and substrate

**Rheology**

In practical use, the rheology of the adhesive is a critical parameter, which determines the applicability of the material. As the filler content is increased, the viscosity of the two-phase material increases. This limits the amount of filler that can be applied without using solvents to reduce the viscosity. However, the shape of the particles has a very strong influence on the rheology, as is illustrated in Figure 3 [3].

This means that for some optimal shapes you can add a much larger volume fraction of filler particles without increasing the viscosity beyond optimum values.

**Mechanical Properties**

A typical problem with ICA materials is brittleness. This is caused by adding a large fraction of metal particles with very different thermo mechanical properties than the adhesive matrix. Thermal expansion mismatch between filler and matrix causes high local strain, and typically creates nucleation centres for cracks in the material. To reduce brittleness, flexible molecules can be added to the adhesive matrix. This can improve thermal cycling behaviour, but a reduced glass transition temperature and increased moisture uptake are unfavourable side effects.

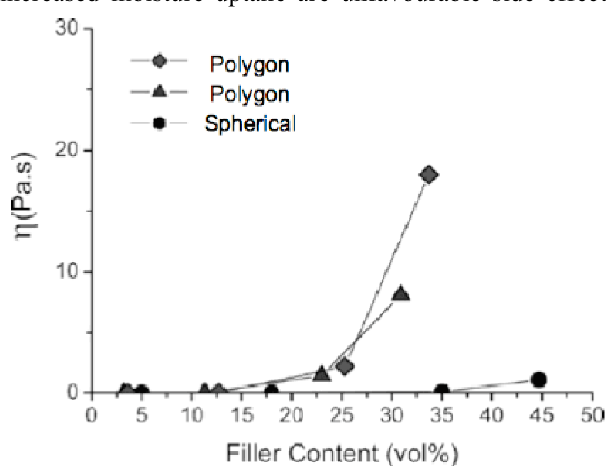


Figure 3. The viscosity of a particle –adhesive system as a function of filler content and filler shape

**Metallized Polymer Core Particles**

A novel idea for how to improve the properties of the ICA material is to replace the solid metal flakes by highly uniformly shaped metal-coated polymer core particles. The drawback of a higher percolation threshold is more than overcome by the fact that much less than 10 % of the particle is actual metal. This introduces the possibility of using noble metals like gold at a reasonable cost. As the viscosity increase due to the addition of such particles compared to added flake like fillers is very modest, there is no need for solvents to optimise viscosity. Instead, viscosity can be optimised by choosing oligomers with suitable molecular weight. Both the spherical shape, and the fact that the thermo mechanical properties are very similar to the adhesive matrix, reduce the local stress in the filler–matrix interface.

Several opportunities arise in terms of optimising the conductive filler properties. A highly controlled size distribution of particles can be made with one or more particle sizes to optimise the filler fraction. Different core materials can be designed with different mechanical properties and glass temperature (Tg). This means that the conductive fillers can be used as the component for mechanical energy absorption needed in e.g. a shock environment. By tuning the Tg of a range of polymer cores, energy absorption can be optimised over a range of temperatures.

## EXPERIMENTAL

**Chip “Design” and Manufacturing**

The background for the test structures that were designed for this work was to find an optimal process for mounting a glass encapsulated MEMS device onto a PCB card. Contact pads on the MEMS device must be electrically and mechanically contacted to corresponding pads on the PCB. The MEMS is realized in a silicon–on-insulator (SOI) wafer. The device layer is etched both to define the mechanical structure of the device and to separate individual contact pads (trench insulation). The buried oxide (BOX) layer is used as a sacrificial layer that is removed between contact pads and below the parts of the device that become movable. To protect the movable parts, a glass wafer with cavities was bonded to the MEMS wafer on wafer scale. The glass wafer was removed from the contact pad areas during dicing, whereas a glass lid remained above the delicate mechanically parts. A cavity must be defined in the PCB substrate to allow the presence of the glass lid as illustrated in Figure 4.

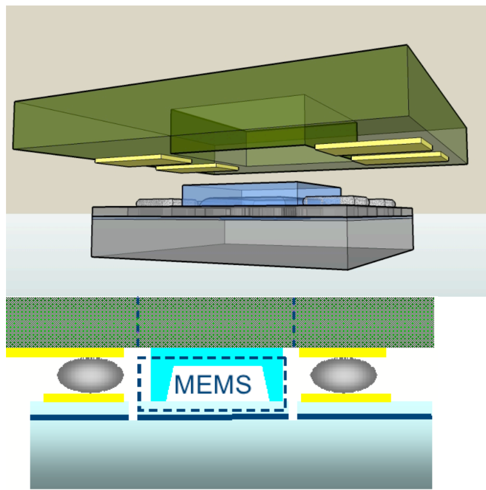


Figure 4. Sketches of a glass encapsulated MEMS device that is mounted on a PCB substrate with a cavity. The optimisation of the mounting process is presented in this work.

In the work presented here however a simple planar chip was used as a substitute for the MEMS device. These test structures, shown in Figure 5, are fabricated using the same fabrication process as the MEMS device but without a glass lid. As a result, an PCB substrate without cavities was also implemented. Four different test structures were included in the wafer layout as illustrated in Figure 5. The test structure nomenclature describes the layout and the width of the trench separating the individual pads. The die size was 3.5 x 3.5 mm$^2$, the same as for the MEMS devices. The MEMS and the test structures were manufactured on 100 mm SOI wafers having a device layer thickness of 43 µm and a BOX layer of 2 µm. The device layer was dry etched using a modified Bosch process in an Alcatel AMS-200 I-Speeder.

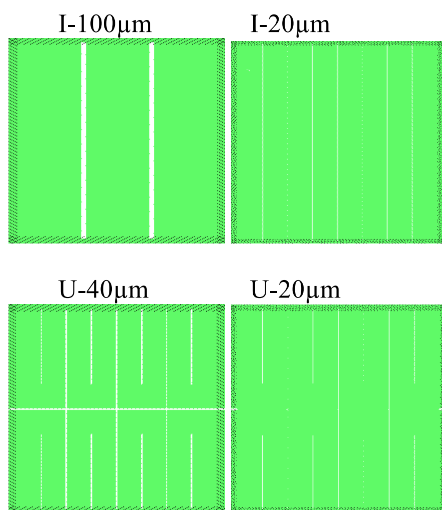


Figure 5. The four different test structures included in the wafer layout: I-100µm, I-20µm, U-40µm, and U-20µm

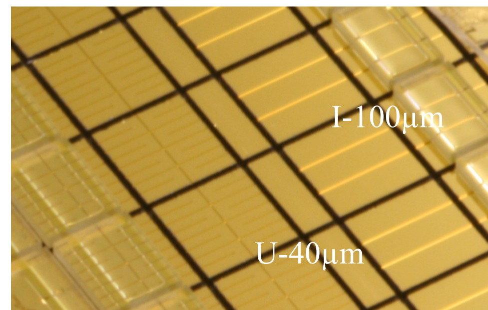


Figure 6. Image of gold sputtered test structures (I-100µm and U-40µm). The image shows components both with and without glass lid. Only components without glass lids were used in this work (Photo: SINTEF/Thor Bakke).

The BOX layer was release etched in a vapour HF tool from Idonus. Gold was sputtered onto the wafers as a final metallization layer before wafer bonding and dicing as can be seen in Figure 6.

**PCB Design and Layout**

A PCB was designed in order to test the conductive adhesives with the test structures mounted on the board. Figure 7 shows the PCB with the mounted test structures. The defined pads on the PCB are 250x350 µm$^2$ for I-100µm test structure and 100x350 µm$^2$ for the other test structures. The pad pitch is 400 µm for the I-100µm test structures and 200 µm for the other test structures.

On the board, there were three locations for doing Kelvin measurement of contact resistance. Kelvin measurements were performed using the I-100µm and I-20µm test structures. Since the pad sizes for these test structures were unequal, a comparison of contact resistance vs pad size is possible. In addition there are three daisy-chain structures, two with four circuits in each, and one chain connecting eight circuits. There were also two structures for short circuit testing. The PCB was a standard four layer FR4 laminate with $T_g$=170 ˚C and four layer s. The conductors and pads consisted of a ~45 µm thick layer of copper and ~5µm layer of nickel. The pads also had an additional~0.1 µm thick layer of chemically deposited gold.

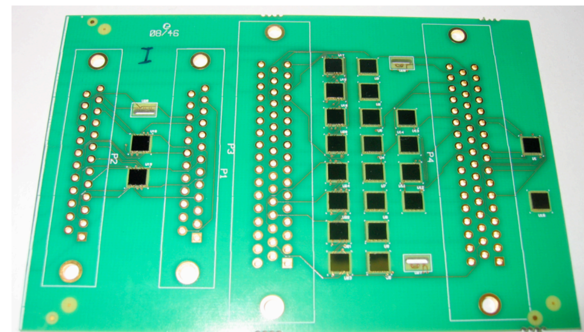

Figure 7. PCB with mounted test components (Photo: FFI/Per Dalsjø)

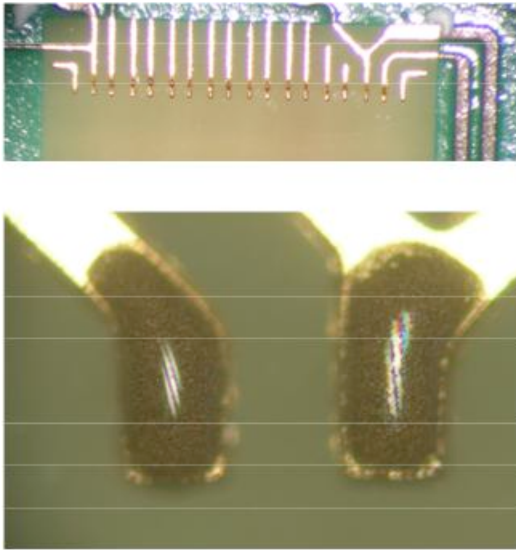

Figur 8. Result from the printing of the adhesive using a stencile printer. a) Evenly spaced stencil openings of 100 um printed using standard settings. b) Close-up shows some minor bleedings of the adhesive. (Photo: FFI/Per Dalsjø)

### Adhesive Manufacturing

The adhesive was manufactured by mixing uniformly shaped metal-coated polymer core particles with a commercially available epoxy resin. A filler fraction of more than 50% was easily obtained.

### Mounting

The adhesive was printed onto the PCBs using a screen printer with a standard steel stencil. Stencil openings with a minimum width of 100 µm and a pitch of 300 µm were printed using standard printer settings. Despite the high filler content, the adhesive had good printing properties. The result from the printing is shown in Figure 8a and b. The close up reveals some bleeding of the adhesive matrix, caused by the high surface tension of the gold plated conductors. In the picture, the individual filler particles are barely visible due to the high filler fraction. The spherical form of the particles means that the migration of particles is impeded, as the thickness of the adhesive layer needs to be at least as thick as the particle diameter.

The silicon test structures were mounted using a My 9 Pick & Place machine from MyData. Various values for the force were applied to the components for process optimisation.

## TESTING AND RESULTS

### Shear Testing

After bonding, ten components were sheared off one of the PCBs and analysed to determine the bonding strength and the appearance of the bond area. The total bond area of the chip is defined by the number of pads and the stencil opening. The stencil opening was reduced compared to the pad size, thus the adhesive coverage of the pads was approximately 75%. The total number of pads was 16, so the total bond area was estimated to 1.05 $mm^2$ for the chips

with a pad size of 250x350 $\mu m^2$. According to MIL-STD-883G, Method 2019.7, this bond area is expected to withstand a shear force of 1.3 kg. The minimum observed bond strength, 2.10 kg, was thus more than 100% higher than the requirements in the MIL-STD.

By studying a fracture surface after shear testing, see Figure 9, we observed that a small area of the ball metallization was sheared off the particle. This indicates that the bonding between the adhesive and the metal is slightly better than that between the polymer core and the metal. The light microscope image illustrates the fact that the density of contact area between particles and the pad on the chip side is high, typically exceeding 20%.

### Cross Sectioning

A few components were cross sectioned to study the contacts. For these components, a bonding force of 15 N had been used, corresponding to a contact pressure of around 1.2 MPa. Figure 10 shows a typical cross section of a contact. The gap between the chip metallization and the PCB pad is approximately 15 µm, which corresponds to 1.5 particle diameter. The metallization on a few of the spheres have cracked. Comparing this picture with mechanical measurements of gold plated particles [4] indicates that the contact force on these particular particles have been higher than 100 MPa.

Table 1. Result from shear test, showing the bond strength.

| Average | 2.36 kg |
|---|---|
| Min | 2.10 kg |
| Max | 2.76 kg |
| Delta | 0.66 kg |
| Median | 2.35 kg |
| Standard deviation | 0.1837 kg |

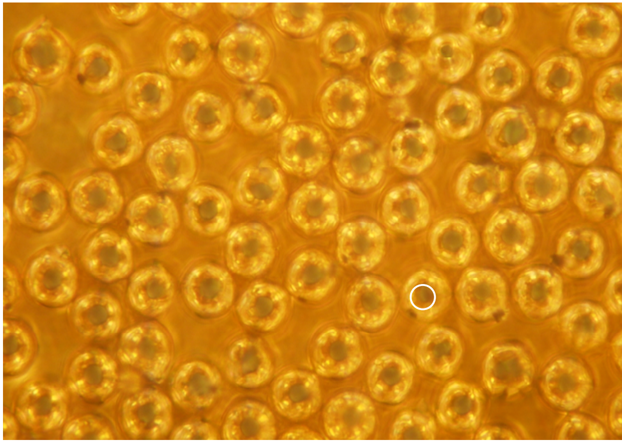

Figure 9. Light microscope image showing the surface of the adhesive after shear testing. The red circle shows an example of contact area between a particle and the pad on the chip side. Note the high density of contact points that have been connected to the pad on the chip side. (Photo SINTEF/Rolf Johannessen)

### Electrical Testing

Initial electrical testing indicated a contact resistance in the order of 1 Ohm which was not satisfactory for the thought application. An effort was launched to find the cause of the high resistance. A bulk sample of the adhesive was cured and connected with two leads. This sample was compared to a similar sample where the gold plated particles were replaced by silver particles. The resistance changed from >10 MOhm for the gold-plated particles, to approximately 3 Ohm with the silver-plated particles. A plausible explanation was that the gold plated polymer particles used for this experiment were originally made for Anisotropic Conductive Film (ACF) applications. A surfactant is added to the balls when manufactured for ACF to aid a uniform distribution in the adhesive matrix. During the ACF mounting process, the particle is highly compressed and this surfactant layer is locally destroyed giving a metal-metal contact. However, in the present experiment the deformation of the particles turned out to be too small to break this steric surfactant layer, preventing metal-to-metal contact.

## CONCLUSION

We have made an Isotropic Conductive Adhesive by dispersing more than 50% by volume of gold plated polymer particles in an epoxy matrix. The resulting paste had a propitious consistence and was easy to apply by screen-printing, even through screen openings of 100 µm. Shear testing of the bonded components revealed that the adhesive gave a minimum bonding strength that was 50% higher than required by the MIL-STD-833. Subsequent characterisation showed a more than satisfactory density of particle-to-pad contacts, indicating that a low contact resistance is possible.

Follow-up tests where the gold plated particles are replaced by silver plated particles are ongoing and these results will be discussed at the conference. Additionally, a new batch of gold plated particles is under preparation and new surfactants will be tested (if needed at all). Further optimisation of filler fraction will be done in addition to tests of a mixture of different particle diameters

## ACKNOWLEDGEMENTS

This work is part of two research projects called “BGA”, sponsored by the NANOMAT program and “ReMi”, sponsored by the BIA program of The Norwegian Research Council. The authors would like to thank Thorkild Kasa, Tone Somme and Atle Skaugen at FFI for helping us with PCB layout, mounting of components and preparing the test setup.

## REFERENCES

[1] Conductive Adhesives For Electronics Packaging, J. Liu (ed), Electrochemical Publications LTD, 1999, ISBN 0 901150 37 1

[2] A. Bjørneklett, L. Halbo, H. Kristiansen, “Thermal conductivity of epoxy adhesives filled with silver particles”, International Journal of Adhesion and Adhesives, Butterworth and Heinemann Ltd, 12 nb. 2, 1992, p 99-104

[3] W.S. Lee, I.Y. Han, Jin Yu, S.J. Kim, K.Y. Byun, “Thermal characterization of thermally conductive underfill for a flip-chip package using novel temperature sensing technique”, Thermochimica Acta 455, 2007, 148–155

[4] T. Helland, “Experimental and numerical study of the nanomechanical properties of polymer particles”, Master Thesis at NTNU, June 2008

# Appendix C Paper presented at the ESTC conference 2010

# Spherical Polymer Particles in Isotropic Conductive Adhesives
# A Study on Rheology and Mechanical Aspects

Hoang-Vu Nguyen[1*], Helge Kristiansen[2], Jakob Gakkestad[3], Rolf Johannessen[4], Nils Hoivik[1], and Knut E Aasmundtveit[1]
[1]Institute of Micro and Nano Systems Technology, HiVe-Vestfold University College, 3184 Borre, Norway
[2]Conpart AS, 2013 Skjetten, Norway
[3]Norwegian Defence Research Establishment, 2027 Kjeller, Norway
[4]GE Vingmed Ultrasound AS, 3191 Horten, Norway
[*]Email Address: hoang.v.nguyen@hive.no, Phone: +47-33037924

**Abstract**

Isotropic conductive adhesive (ICA) filled with metal coated polymer spheres has been studied as a novel approach to increase the flexibility, and hence the reliability of the adhesive compared to traditional metal filled ICAs. In this paper, we have investigated the rheological properties of the novel ICA to evaluate its applicability in practical use. The current work also involves the investigation of the mechanical properties including shear strength of the novel ICA. Spherical polymer particles (SPP) of sizes Ø6 µm and Ø30 µm were investigated in the present study. The results show minor differences in the rheological properties and the adhesion strength for adhesives filled with particles in different sizes. Filling SPP into the adhesive matrix increases the viscosity of the system monotonically and continuously, in excellent accordance with model systems previously reported in the literature. Furthermore, the novel ICA exhibits high mechanical shear strength, being comparable to the traditional solder joint technology and twice higher than the traditional metal filled ICA.

**Introduction**

Isotropic conductive adhesive (ICA) has been commercially available as an alternative to solder interconnects for more than 40 years. ICA consists of a non-conductive adhesive matrix filled with conductive particles. The mechanical strength of the ICA joint comes from the adhesive matrix, while the conductive fillers (typically silver flakes or particles) provide electrical conductivity.

Traditionally ICAs have been heavily loaded with silver (Ag) particles (typically 25 – 30% volume fraction) to ensure electrical conductivity [1]. Such a high metal loading causes significant changes in the mechanical properties of the adhesives, including a highly increased bulk modulus and a reduced flexibility. A novel idea for improvement of the flexibility and hence the reliability of the adhesive is to replace the solid metal particles with metal coated polymer spheres (MPS). The polymer core will provide a high and also controllable degree of flexibility by formulating suitable polymer compositions with various mechanical properties. In addition, the polymer sphere coated with thin metal layer compared to its core radius will have the mechanical properties dominated by the polymer material. In particular, the CTE of the polymer particles can be better matched to that of the epoxy resin in contrast to what is possible when loading the adhesive with the metal fillers. Our recent studies [2, 3] have strengthened the proposal of using MPS in ICA by the achievement of similar or better contact resistance and improved adhesion strength compared to that of traditional Ag epoxies.

One challenge when loading the adhesive with spherical particles is that the percolation threshold will increase compared to ICAs loaded with traditional flake-like fillers [4]. Higher filler concentration in the adhesive matrix may have critical impact on the viscosity of the system, limiting the printing and dispensing capabilities of the novel ICA. In addition, the reduction of volumetric fraction of the adhesive matrix due to high particle concentration can reduce the adhesion strength of the system.

In this study, we have investigated the rheological properties and the mechanical shear strength of a standard epoxy based adhesive filled with spherical polymer particles. Two different particle sizes (Ø6 µm and Ø30 µm) were tested to evaluate the influence of particle size on the process properties of the novel ICA. The mechanical shear strength of the novel ICA has been compared with a conventional metal filled ICA, the traditional solders and the lead-fee solders.

**Materials and Experimental Details**

***Materials***

**Table 1: Specifications of EPO-TEK 353ND [5] and EPO-TEK H20E [6] from technical data sheets**

| Specification | EPO-TEK 353ND | EPO-TEK H20E |
|---|---|---|
| Components and Density | * Part A (resin): 1.20 g/cm$^3$<br>* Part B (curing agent): 1.02 g/cm$^3$ | * Part A: 2.03 g/cm$^3$<br>* Part B: 3.07 g/cm$^3$ |
| Mixing ratio by weight | 10:1 (Part A:Part B) | 1:1 (Part A:Part B) |
| Curing condition | T = 100 °C<br>t = 10 minutes | T = 100 °C<br>t = 2 hours |
| Shear strength at 23 °C | > 36 MPa | > 12 MPa |

Standard epoxy based adhesive, EPO-TEK 353ND, was used in this study as the adhesive matrix for the novel ICA. The adhesive has two components with details specified in Table 1. Spherical polymer particles (SPP) in highly uniform shape of Ø6 µm and Ø30 µm were manufactured by Conpart AS and employed as fillers. The

particles were made from polyacrylics with polymer density 1.20 g/cm$^3$. The polymer particles used in this study were not metal coated as the focus of interest was on the rheological and the mechanical (not the electrical) properties of the novel ICA. The results are thus also representative for the adhesive filled with metal coated SPP. No solvents or surface additives were added to the adhesive.

The Ag epoxy EPO-TEK H20E was used in this study to compare with the novel ICA. The properties of EPO-TEK H20E are described in Table 1.

***Rheological Properties***

In the rheology study, samples were prepared by manually mixing part A (resin) of the adhesive EPO-TEK 353ND with SPP (Ø6 µm or Ø30 µm) at different volume fractions. Thus, no curing agent was added, facilitating the experiments. Part B (curing agent) is only a small part of the final adhesive (mixing ratio by weight of Part A:Part B is 10:1), implying that this simplification has negligible effect on the viscosity of the adhesive within its pot life. The viscosity measurement was conducted using a flat plate rheometer, Paar Physica UDS-200. The gap between two plates was set to 0.5 mm. The complex viscosity of the mixed samples was measured at room temperature under oscillation mode with fixed frequency of 1 Hz.

The applicability of the novel ICA was initially evaluated by conducting stencil printing. Part A of the adhesive EPO-TEK 353ND mixed with SPP at 45, 50 and 55 volume% was printed onto blank substrates by using a Dima HS-100 stencil printer. The stencil is covered with Nickel/Teflon to reduce the adhesion of the adhesives to the bottom surface of the stencil. The thickness of this stencil is approximately 50 µm. No additives were used to improve the rheology of the adhesive with respect to printing.

The samples manufactured for the rheology study are denoted as ICA-6R and ICA-30R. The constituent for each type of the samples is presented in Table 2.

***Mechanical shear strength***

The specimens of the novel ICA and the Ag epoxy EPO-TEK H20E were manufactured for shear strength testing. The adhesive pastes of the novel ICA were prepared by manually mixing both part A (resin) and part B (curing agent) of the adhesive EPO-TEK 353ND with SPP. Mixing ratio by weight of part A to part B is 10:1 as specified in Table 1. Particles of either Ø6 µm or Ø30 µm were loaded into the adhesive matrix to produce samples with different volume fractions of SPP. The Ag epoxy was also mixed manually with weight ratio of part A to part B is 1:1, as defined by the manufacturer (Table 1).

The mechanical shear strength of each testing sample was obtained following the same process. Two strips of adhesive tape (100 µm thick) were applied onto cleaned Ceramic substrate. A sufficient amount of the mixed adhesive paste was then dispensed manually within the space between the two strips of tape. Cleaned Si chip was assembled onto the adhesive deposited on the substrate. The sample was cured at curing temperature of 100 $^{o}$C, but with curing time longer than the values defined in data sheet (Table 1) to ensure complete curing of the adhesive. Curing time for the adhesives filled with SPP, and the Ag epoxy was 1 hour and 3 hours, respectively. Prior to shear test, the adhesive tapes were removed mostly in the areas close to assembled chip to minimize the contribution of tape's adhesion on the measured shear force. An F&K DELVOTEC Bond Tester 5600 was used to conduct the destructive die shear test. Die shear strength was determined from the measured shear force and from the bond area defined by the chip's length and the distance between two strips of tape.

The shear strength testing samples corresponding to the novel ICA loaded with Ø6 µm and Ø30 µm SPP are denoted as ICA-6M and ICA-30M, respectively. The specimens manufactured from the Ag epoxy EPO-TEK H20E are called ICA-Ag. The specifications of test samples used to investigate the mechanical shear strength are summarized Table 2.

**Table 2: Specifications of test samples used to study the rheological properties and the mechanical shear strength. Mixing ratio specified in the table is the ratio by weight of part A to part B of the adhesive.**

| Study purpose | Label of sample | Description |
|---|---|---|
| Samples to study rheological properties | ICA-6R | Part A (EPO-TEK 353ND) filled with Ø6 µm polymer spheres |
| | ICA-30R | Part A (EPO-TEK 353ND) filled with Ø30 µm polymer spheres |
| Samples to study mechanical shear strength | ICA-6M | Part A and part B (EPO-TEK 353ND, mixing ratio is 10:1) filled with Ø6 µm polymer spheres |
| | ICA-30M | Part A and part B (EPO-TEK 353ND, mixing ratio is 10:1) filled with Ø30 µm polymer spheres |
| | ICA-Ag | Part A and part B (EPO-TEK H20E, mixing ratio is 1:1) |

## Results

**Figure 1: Non-uniform suspension of adhesive filled with 60 volume% of SPP**

Uniform suspensions of SPP in adhesive (EPO-TEK 353ND) were obtained with volume fractions ranging from 0 to 55 %. For a volume fraction of 60 %, the resulting suspension was not uniform. The phenomenon is

illustrated in Figure 1. Therefore, the focus in the present study of the rheological properties and the mechanical shear strength was in the range 0 – 55 volume% of SPP.

***Rheological Properties***

Figure 2 shows the complex viscosity (η* = η' - iη'') of ICA-6R and ICA-30R at different volume fractions. The complex viscosity is a measure of viscoelasticity of the system at particular frequency. The real part (η') of the complex viscosity, which links to loss modulus, represents the viscous behavior. The imaginary part (η''), which relates to storage modulus, represents the elastic behavior [7]. As can be seen from Figure 2, the viscous behavior dominates the elastic behavior of ICA-6R and ICA-30R, as expected. In addition, the viscosity increases monotonically and continuously with increasing concentration of particles.

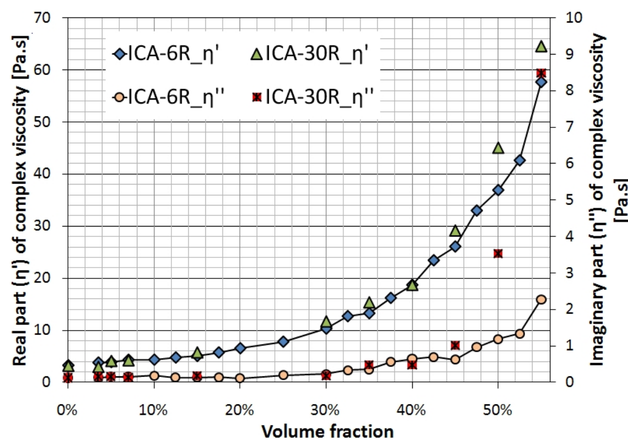


**Figure 2: Complex viscosity of ICA-6R and ICA-30R at different volume fractions of SPP**

| Particles' concentration | ICA-6R | ICA-30R |
|---|---|---|
| 45 volume% | Larger pattern size: 250 x 350 µm². Pattern pitch: 400 µm | |
| 50 volume% | | Narrower pattern size: 100 x 350 µm². Pattern pitch: 200 µm |
| 55 volume% | | |

**Figure 3: Stencil printing images of ICA-6R and ICA-30R at different volume fractions of SPP. There are two types of test patterns. Pattern size and pitch are presented in text as seen in the figure.**

Stencil printing images of ICA-6R and ICA-30R at 45, 50 and 55 volume% are presented in Figure 3. The 45 and 50 volume% versions displayed sufficient printing for both types of adhesives with reasonable repeatability for the pattern of 250 x 350 µm$^2$. Printing the narrower pattern of 100 x 350 µm$^2$ showed poor quality and repeatability, especially ICA-30R. At 55 volume%, both ICA-6R and ICA-30R showed poor printing results even with the larger pattern.

***Mechanical shear strength***

Figure 4 illustrates the impact of the particle concentration on the mechanical shear strength of ICA-6M and ICA-30M joints. In addition, the shear strength of ICA-Ag joints is presented. From Figure 4, the shear strength of ICA-6M joints is remarkably stable with particle loading ranging from 0 volume% up to 40 volume%. For higher particle loading, up to 55 volume%, only a slight decrease in shear strength is observed. For ICA-30M, the mechanical strength of the specimens with 40 and 50 volume% of SPP were obtained. The obtained shear strength is comparable to that of ICA-6M, although the ICA-30M samples with 40 volume% of SPP show somewhat lower shear strength than the corresponding ICA-6M samples. Most importantly, the shear strength of both ICA-6M and ICA-30M joints is considerably higher than that of ICA-Ag joints, even with high concentration of SPP.

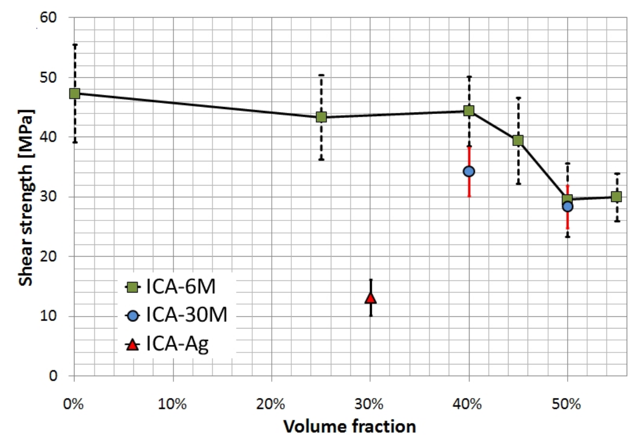


**Figure 4: Mechanical shear strength of ICA-6M and ICA-30M joints in comparison with ICA-Ag joints. (Each data point is average value for at least 5 samples)**

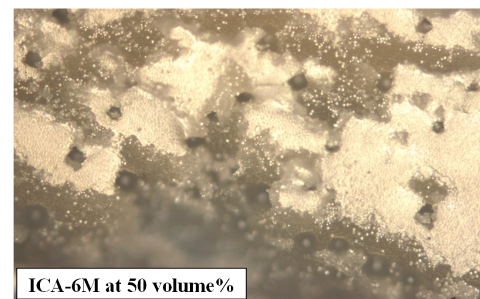


**Figure 5: Typical fracture mechanism of the novel ICA at high concentration of SPP. The image focused on top surface of the adhesive while the substrate was out of focus. Fracture could be observed at bulk of ICA.**

Visual inspection using optical microscope showed that the fracture of EPO-TEK 353ND joints (without particles) was at the interface between the adhesive and the Ceramic substrate, while ICA-Ag joints fractured at bulk of the adhesive. Besides that, ICA-6M and ICA-30M joints at high concentration of SPP had fractures at either

bulk of the adhesive or at adhesive's layers close to chip's interface. Figure 5 illustrates the typical fracture mechanism of the novel ICA filled with SPP.

**Discussion**

The maximum volume concentration ($\Phi_m$) of particles filled into a suspension is important in a rheological study. Dependent on geometric arrangements of monomodal spheres, the theoretical limit of dense sphere packing is in range of 52.4% - 74%. The lower value of the mixing fraction limit can be estimated by assuming that each sphere needs an available volume given by a cube with dimensions equal to the particle diameter to be able to flow freely. This corresponds to a volume fraction of π/6 (52,4%). On the other hand, the maximum packing possible for identical spheres, π/(3√2) = 74%, is calculated based on the crystallographic volume fraction of the closest-packing structures (face-centered cubic/hexagonal close-packing) as presented in [8]. Such close packing would, however, not allow the spheres to flow. Hence, the maximum volume concentration for a fluid system must be below the theoretical maximum limit. Normally, suspensions form the random close-packed arrangement, which depends on the specific system [9]. Previous studies reported the maximum volume concentration for the suspension of monodisperse spheres in the range of 60-65 volume% [9-11]. In our study, non-uniform suspension was obtained at 60 volume% of SPP. It was striking how close these experimentally observed values are to the theoretical limit.

According to the viscosity measurement results (Figure 2), ICA-6R and ICA-30R exhibit dominant viscous behavior over elastic behavior ($\eta' \gg \eta''$), even with high concentration of SPP. The change in elastic behavior of ICA-30R at high concentration of SPP over 45 volume% could be because the viscosity measurement gap of 0.5 mm may not be high enough for measuring highly concentrated ICA-30R. As the ratio of particle diameter to plate gap is increased, the particles are more likely to absorb and release elastic energy during collisions, than dissipating viscous energy in the adhesive resin. This would influence measurement results of $\eta''$. Apart from the imaginary part of the viscosity, which is a relatively small part of the total viscosity, there were no significant differences between ICA-6R and ICA-30R in the rheological properties.

Two empirical models that satisfy both high and low concentration of spherical particles were considered to compare with our viscosity measurement results. Eilers [12] (Ferrini et al. [11]) reported a model (Equation 1) which has been known to be capable of fitting data of viscosity of suspensions loaded with spherical particles. In addition, Krieger and Dougherty [13] presented their model (Equation 2) with explicit notice of the interactions between neighboring spherical particles by means of rotation behavior in the flow of the suspension. However, their model was finally derived with assumption of independent rotation for most of the neighboring spheres.

**Equation 1: Eilers model [12]**

$$\frac{\eta}{\eta_0} = \left(1 + \frac{0.5[\eta]\Phi}{1 - \Phi/\Phi_m}\right)^2$$

**Equation 2: Krieger and Dougherty model [13]**

$$\frac{\eta}{\eta_0} = \left(1 - \frac{\Phi}{\Phi_m}\right)^{-[\eta]\Phi_m}$$

With $\eta$ is the viscosity of suspension at the concentration $\Phi$. $\eta_0$ is the viscosity of the suspending medium without particles. $\Phi_m$ is the maximum volume concentration of particles. $[\eta]$ is the intrinsic viscosity, which is a measure of particle's contribution to the viscosity of a solution. The intrinsic viscosity value depends on the shape of particles and is defined as shown in Equation 3. For uncharged rigid spheres, $[\eta]$ equals 2.5 as obtained by Einstein [14].

**Equation 3: Definition of the intrinsic viscosity [η]**

$$[\eta] = \lim_{\Phi \to 0} \left(\frac{\eta - \eta_0}{\Phi \eta_0}\right)$$

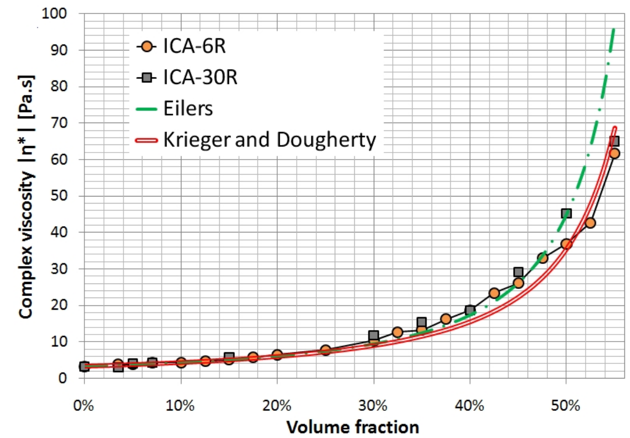


**Figure 6: Total (complex) viscosity as a function of volume fraction. The line graphs correspond to models presented in the text, with [η]=2.5 and $\Phi_m$=0.65. The symbols correspond to total viscosity obtained in this study, which was calculated as $|\eta^*|^2=(\eta')^2+(\eta'')^2$.**

Figure 6 shows the total viscosity, which involves both the real and the imaginary parts of the complex viscosity, obtained in our study. The obtained results were compared with the two models of Eilers and Krieger-Dougherty. The value of $\Phi_m$ (0.65) was selected following an approach suggested by Ferrini et al. [11], in which $\Phi_m$ could be obtained based on best fitting of model's curves (e.g. Eiler's model) to all experimental data. The intrinsic viscosity of 2.5 was used for SPP since the behaviors of SPP and rigid spheres in the extremely dilute solution are expected to be similar. As can be seen from Figure 6, it is clear that both models fit our measured data very well, in the entire range of volume fractions, particularly the Krieger-Dougherty model. This shows that our system behaves comparably to previously

studied model systems. We can therefore state that our system does not exhibit any significant long range interactions between the SPP (e.g. electrostatic forces, electroviscous effect, etc.), even at high fractions of particles. Such non-contact interactions would have implied a higher viscosity than suggested by the model. This observation definitely strengthens the applicability of the novel ICA we have proposed, as it opens up the possibility of processing adhesives with high volume fractions of SPP. It should be noted that the experiments were carried out with non-metalized SPP. Note that the effect of metallization on the rheological properties, if any, would be to eliminate possible electrostatic forces. Therefore, the observations on the rheological properties of the adhesive loaded with non-metalized SPP are claimed to be relevant for a real system, where the adhesive matrix is loaded with metal coated polymer spheres.

The stencil printing results of ICA-6R and ICA-30R have demonstrated the applicability of the novel ICA. Poor printing results for the smaller pattern (100 x 350 $\mu m^2$) might be due to smearing or bleeding of the adhesive pastes. The correlation between particle size and dimension of stencil openings should also be taken into account. However, printing properties of the novel ICA could be improved by adding rheology modifiers to the adhesive, as presented in [3].

**Table 3: Mechanical shear strength of joints manufactured by using different bonding materials**

| Type of joints | Shear strength |
|---|---|
| Novel ICA at 50 volume% of SPP (ICA-6M and ICA-30M) | 29 MPa (Data from Figure 4) |
| ICA-Ag (EPO-TEK H20E) | 13 MPa (Data from Figure 4) |
| Traditional solders (60Sn-40Pb and 63Sn-37Pb) | 28-40 MPa (Data from [15, 16]) |
| Common lead-free solders (Sn-Ag-Cu) | 30-65 MPa (Data from [16-18]) |

Table 3 illustrates the shear strength of the novel ICA at high concentration of SPP in comparison with ICA-Ag, the traditional solders (60Sn-40Pb; 63Sn-37Pb) and the common lead-free solders (Sn-Ag-Cu). The joining strength of the lead-free solders was reported in a wide range since the effect of different reflow conditions on different types of lead-free solders is expected to differ to a high extent.

From Table 3, the mechanical shear strength of the novel ICA is twice higher than that of ICA-Ag. Furthermore, the novel ICA exhibit comparable shear strength to the traditional solders (60Sn-40Pb and 63Sn-37Pb). The sufficiently high shear strength of ICA-6M and ICA-30M, even with particle concentration as high as 50 volume%, indicates the compatibility between SPP and the adhesive. Such compatibility is strengthened by the homogeneous dispersion of SPP in the adhesive as illustrated in Figure 7. On the other hand, the thermo-mechanical properties of the polymer particles are very similar to the adhesive matrix compared to that of metal fillers in the traditional ICA. Thus, the thermo-mechanical properties of the polymer particles, together with the spherical shape, reduce the local stress induced in the filler-matrix interface during curing process. High shear strength of the novel ICA can therefore be expected.

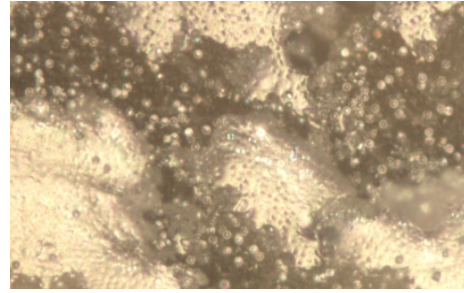

**Figure 7: Optical microscope image showing the surface after shear testing of the novel ICA at high particle concentration. The image shows well dispersion of SPP into the adhesive.**

Table 3 shows that the shear strength of the novel ICA, in general, is somewhat lower than that of the common lead-free solders. However, the high reflow temperature for the lead-free solders (over 200 °C) reduces the integrity, reliability and functionality of printed wiring boards, components and other attachment [15, 17, 19]. The lower curing temperature (100 °C) for the novel ICA is thus an important advantage over the lead-free solders.

**Conclusions**

The current study indicates minor differences in rheological properties between the adhesives filled with Ø6 µm and Ø30 µm SPP. Two empirical models of Eilers [12] and Krieger-Dougherty [13] show very well fitness to the viscosity data measured in our system, in the entire range of volume fractions of SPP. These results indicate that there are negligible inter-particle interactions in the novel ICA, even at high particle concentration. The rheological properties definitely strengthen the applicability of the novel ICA we proposed, where high concentration of SPP is required.

The novel ICA exhibits high mechanical shear strength, which attains 29 MPa even at high concentration of SPP. Such high shear strength is comparable to the traditional solders (60Sn-40Pb and 63Sn-37Pb) and twice higher than ICA-Ag. Compared with the common lead-free solders (Sn-Ag-Cu), the sufficiently high shear strength and the low curing temperature make the novel ICA a strong candidate for alternatives to the lead-containing solders.

The rheological properties and the high mechanical shear strength obtained for our system are strongly promising for the use of metal coated polymer spheres in isotropic conductive adhesives.

**Acknowledgments**

This work has been funded by the Research Council of Norway (RCN) through ReMi project (BIA project number: 187971).

The authors gratefully acknowledge Thorkid Kaasa and Tone Somme at Norwegian Defence Research Establishment for helping us in the evaluation of stencil printing.

**References**

[1] J. H. Lau, C. P. Wong, N. C. Lee, and S. W. R. Lee, "Chapter 17. Introduction to Conductive Adhesives," in *Electronics Manufacturing with Lead-free, Halogen-free and Conductive Adhesive Materials* New York: McGraw-Hill, 2002.

[2] H. Kristiansen, M. M. V. Taklo, T. Bakke, J. Gakkestad, P. Dalsjo, R. Johannessen, F. Oldervoll, and H.-V. Nguyen, "Development of Low Modulus Conductive Adhesives for MEMS Interconnects," in *Pan Pacific Microelectronics Symposium*, Hawaii, United States, 2009, pp. 306-310.

[3] J. Gakkestad, P. Dalsjo, H. Kristiansen, R. Johannessen, and M. M. V. Taklo, "Use of Conductive Adhesive for MEMS Interconnection in Military Fuze Applications," in *SPIE Photonics West*, San Francisco, California United States, 2010, pp. 7592-17.

[4] M. Mundlein and J. Nicolics, "Modeling of Particle Arrangement in an Isotropically Conductive Adhesive Joint," *IEEE Transactions on Components And Packaging Technologies,* vol. 28, no. 4, pp. 765-770, 2005.

[5] http://www.epotek.com/, "EPO-TEK® 353ND Technical Data Sheet," Apr. 2010 ed: Epoxy Technology, Inc., 2010.

[6] http://www.epotek.com/, "EPO-TEK® H20E Technical Data Sheet," Feb. 2010 ed: Epoxy Technology, Inc., 2010.

[7] T. G. Mezger, *The Rheology Handbook*, 2nd ed. Hannover, Germany: Vincentz Network GmbH & Co. KG, 2006.

[8] J. William D. Callister, "Chapter 3. Structures of Metals and Ceramics," in *Fundamentals of Materials Science and Engineering* 5th ed: John Wiley & Sons, Inc., 2001, pp. 31-37.

[9] J. J. Stickel and R. L. Powell, "Fluid Mechanics and Rheology of Dense Suspensions," *Annual Review of Fluid Mechanics,* vol. 37, pp. 129-149, 2005.

[10] J. S. Chong, E. B. Christiansen, and A. D. Baer, "Rheology of Concentrated Suspensions," *Journal of Applied Polymer Science,* vol. 15, pp. 2007-2021, 1971.

[11] F. Ferrini, D. Ercolani, B. d. Cindio, L. Nicodemo, L. Nicolais, and S. Ranaudo, "Shear Viscosity of Settling Suspensions," *Rheologica Acta,* vol. 18, no. 2, pp. 289-296, 1979.

[12] V. H. Eilers, "Die Viskosität von Emulsionen hochviskoser Stoffe als Funktion der Konzentration," *Colloid & Polymer Science,* vol. 97, no. 3, pp. 313-321, 1941.

[13] I. M. Krieger and T. J. Dougherty, "A Mechanism for Non-Newtonian Flow in Suspensions of Rigid Spheres," *Journal of Rheology,* vol. 3, pp. 137-152, 1959.

[14] A. Einstein, "A New Determination of The Molecular Dimensions," *Annalen der Physik,* vol. 19, no. 2, pp. 289-306, 1906.

[15] S. K. Kang, "Development of Lead (Pb)-free Interconnection Materials for Microelectronics," *Metals and Materials International,* vol. 5, no. 6, pp. 545-549, 1999.

[16] T. Siewert, S. Liu, D. R. Smith, and J. C. Madeni, "Properties of Lead-Free Solders," February 11, 2002 ed: National Institute of Standards & Technology and Colorado School of Mines, 2002.

[17] Y. Tian, C. Wang, S. Yang, P. Lin, and L. Liang, "Shear Fracture Behavior of Sn3.0Ag0.5Cu Solder joints on Cu Pads with Different Solder Volumes," in *International Conference on Electronic Packaging Technology & High Density Packaging (ICEPT-HDP)* Shanghai, China, 2008, pp. 1-4.

[18] Y. A. Su, L. B. Tan, V. B. C. Tan, and T. Y. Tee, "Rate-Dependent Properties of Sn-Ag-Cu Based Lead Free Solder Joints," in *11th Electronics Packaging Technology Conference* Singapore, 2009, pp. 283 - 291.

[19] Y. Li and C. P. Wong, "Recent Advances of Conductive Adhesives as a Lead-free Alternative in Electronic Packaging: Materials, Processing, Reliability and Applications," *Materials Science and Engineering R,* vol. 51, pp. 1-35, 2006.

# Appendix D Spie newsroom publication

10.1117/2.1200912.002521

# Conductive adhesives increase microchip packaging density

**Jakob Gakkestad, Per Dalsjo, Helge Kristiansen, Rolf Johannessen, and Maaike M.V. Taklo**

*Interconnecting microelectromechanical systems directly to printed circuit boards can improve reliability and reduce costs of medium-caliber fuzes.*

Cost-effective assembly of custom-designed microelectromechanical systems (MEMS) for medium-caliber fuzes is challenging. In particular, the environment must have a setback acceleration exceeding 60,000g and centripetal acceleration of 9000g/mm out of center in a 30mm×173 projectile. In addition, the space available is very limited. The traditional approach is to mount the MEMS chip in a package that is then soldered to the printed circuit board (PCB). However, by mounting the MEMS chip directly to the PCB using conductive adhesive, we can increase the packaging density while reducing manufacturing cost.

One of the challenges when mounting silicon-based MEMS chips on a PCB is the large difference in thermal expansion coefficient between the silicon and the glass-epoxy PCB laminate. Suitable materials for interconnects need good electrical conductivity combined with sufficient compliance to accommodate the strains that occur during thermal cycling (without causing fatigue).

Isotropic conductive adhesive (ICA) has been used for interconnection of electronic devices for several decades.[1] Traditionally, such adhesives have been made using silver particles mixed with a non-conductive adhesive typically based on epoxy. Other metal particles for creating conductivity have also been used, such as copper and nickel. A typical problem with such ICAs is brittleness caused by thermomechanical and elastic mismatches between the metal particles and the adhesive matrix. Since these traditional ICAs do not have the necessary compliance for our application, we used a novel type of conductive adhesive with better thermal and mechanical properties.

Our approach is to use metal-coated polymer spheres to achieve adhesive conductivity (see Figure 1). The size distribution of the spheres is narrow, with a typical variation of less than 3%. The metal layer of the spheres is about 100nm thick. Noble metals are used to coat the spheres, but the cost of using these metals is limited since less than 10% of the particle volume is metal. The mismatch between the thermal expansion coefficient of the adhesive and the polymer-based spheres is much less than between metal particles and adhesives used in traditional ICAs. In addition, the polymer spheres are flexible, which improves the mechanical properties of the conductive adhesive.

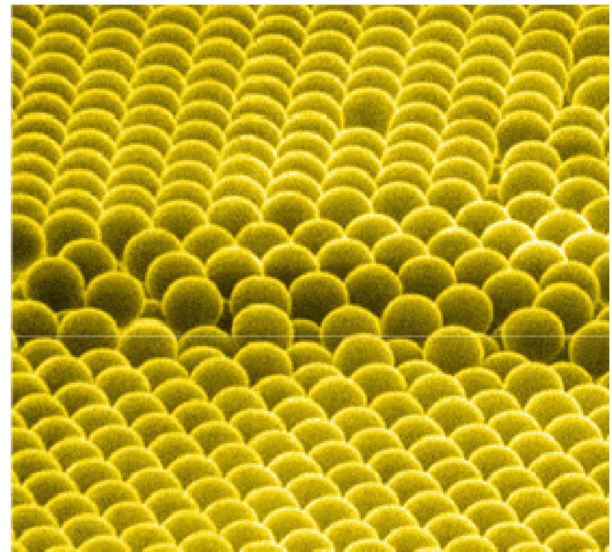

***Figure 1.*** *Scanning electron microscope image of mono-sized polymer balls arranged in a 3D crystal-like structure.*

We have investigated the properties of our ICA in rough environment applications. MEMS test chips with no movable parts have been manufactured and mounted onto a PCB. The size of the MEMS test chips is 3.5mm×3.5mm. We performed accelerated stress tests, including air-to-air thermal shock cycling and realistic firing.

Temperature cycling tests between −46 °C and +70 °C used an adhesive with 30$\mu$m silver coated spheres (see Figure 2). The tested contact resistances, which have a pad size of 250 × 350$\mu$m,

*Continued on next page*

10.1117/2.1200912.002521 Page 2/2

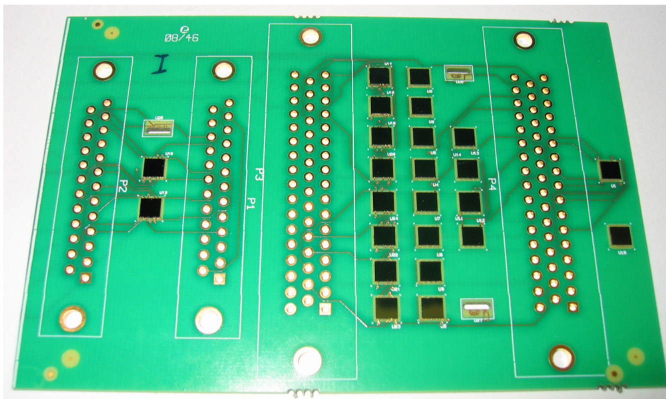


***Figure 2.*** *Printed circuit board with microelectromechanical system test chips. The card is used for measuring contact resistances during temperature cycling tests.*

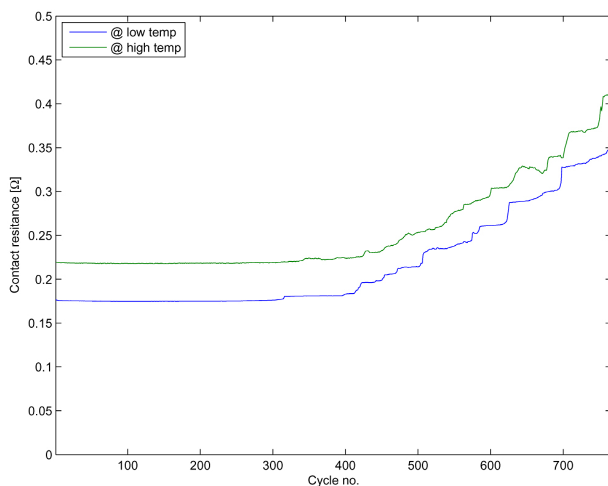


***Figure 3.*** *Contact resistance at high and low temperature as a function of the number of temperature cycles.*

displayed no notable changes after 127 thermal cycles between −46 °C and 70 °C. One PCB was exposed to more than 700 temperature cycles. All contact resistances passed 274 cycles, and one passed more than 750 cycles (see Figure 3).

Shear tests[2] have also been performed on test chips mounted with adhesive containing 10$\mu$m gold spheres. The average bond strength was 24N, which exceeds the requirement in military standard MIL-STD-883G.[3]

Some of the MEMS test chips that had been exposed to temperature cycling were packaged into a 30mm×173 projectile. Recovery firings were performed. The average change in contact resistances after firing was less than 6% compared to values obtained prior to the temperature cycling tests.

The use of conductive adhesives based on uniformly sized polymer spheres for MEMS interconnect in medium-caliber fuzes has so far shown promising results when exposed to temperature cycling and mechanical stress tests. We currently are performing extended temperature and mechanical testing. The results will be presented at the 2010 SPIE Photonic West conference at the end of January in San Francisco.

*Parts of this work have been sponsored by the Norwegian Research Council, grant no 187971/140 and the Norwegian Ministry of Defense.*

## Author Information

**Jakob Gakkestad and Per Dalsjo**
Norwegian Defense Research Establishment
Kjeller, Norway

**Helge Kristiansen**
Conpart AS
Skjetten, Norway

**Rolf Johannessen and Maaike M.V. Taklo**
Sintef Information and Communication Technology
Oslo, Norway

**References**

1. J. Liu, **Conductive Adhesives For Electronics Packaging**, Electrochemical Publications Ltd., Port Erin, 1999. ISBN 0 901150 37 1.
2. H. Kristiansen, M. Taklo, T. Bakke, J. Gakkestad, P. Dalsjø, R. Johannessen, F. Oldervoll, and V. Nguyen, *Development of low modulus conductive adhesive for MEMS interconnects*, **Proc. Pan Pacific Microelectronic Symp.**, pp. 306–310, 2009.
3. Department of Defense, *MIL-STD-883G - Test Method Standard Microcircuits*, 28 February 2006.

© 2009 SPIE

# Appendix E Spie Photonic West conference paper

# Use of Conductive Adhesive for MEMS Interconnection in Military Fuze Applications

Jakob Gakkestad[*a], Per Dalsjo[a], Helge Kristiansen[b], Rolf Johannessen[c] and Maaike M Visser Taklo[c]
[a]Norwegian Defence Research Establishment, 2027 Kjeller, Norway
[b]Conpart AS, 2013 Skjetten, Norway
[c]SINTEF ICT, 0314 Oslo, Norway

## ABSTRACT

A novel conductive adhesive has been used to interconnect MEMS test structures with different pad sizes directly to a PCB in a medium caliber ammunition fuze. The fuze environment is very demanding with a setback acceleration exceeding 60 000 g and a centripetal acceleration increasing radially with 9000 g/mm. The adhesive shows excellent mechanical and thermal properties. The mounted MEMS test structures have been subjected to rapid temperature cycling according to MIL-STD 883G method 1010.8 test condition B and performed well. The test structures with the largest pad sizes passed 100 temperature cycles and firing test where the test structures have been exposed to an acceleration of more than 60 000 g.

**Keywords:** Conductive adhesive, fuze, MEMS, packaging, reliability, polymer spheres

## 1. INTRODUCTION

### 1.1 Conductive adhesives

Isotropic conductive adhesives (ICA) have been used in electronic applications for more than 40 years. Traditionally, ICA has been made by mixing a non-conductive adhesive typically of epoxy type, with silver particles or flakes. However, to reduce cost, also other conductive particles have been used like carbon, copper and nickel. Designing an ICA requires optimization of a number of factors including final electrical conductivity, rheological properties during application, total metal content (a cost issue in the case of noble metals) and thermo-mechanical properties[1].

To make an ICA using a non-conductive matrix, the volume fraction of conductive filler particles needs to reach and exceed a certain level, called the percolation threshold. That is, the amount of particles must be sufficient to create at least one path of particle – particle contacts, and hence conduction through the entire adhesive. This threshold is dependent on the shape of the particles. Given the traditional flake like conductive particles, the percolation threshold will also depend on the orientation of the flakes. In a typical microelectronic application, both the application of the adhesive and the shear applied during placement of the component cause a significant orientation of the flakes[2], as illustrated in Figure 1.

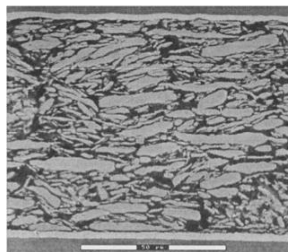

Figure 1. Illustration of the tendency for metal flakes (in this case silver) to align themselves in parallel with the die and substrate

[*] Jakob.Gakkestad@ffi.no, phone + 47 63 80 76 80, www.ffi.no

Reliability, Packaging, Testing, and Characterization of MEMS/MOEMS and Nanodevices IX,
edited by Richard C. Kullberg, Rajeshuni Ramesham, Proc. of SPIE Vol. 7592, 75920I
© 2010 SPIE · CCC code: 0277-786X/10/$18 · doi: 10.1117/12.840890

In practical use, the rheology of the adhesive is a critical parameter, which determines the applicability of the material. As the filler content is increased, the viscosity of the two-phase material increases. This limits the amount of filler that can be applied without using solvents to reduce the viscosity. However, also the shape of the particles has a very strong influence on the rheology[3]. This means that for some optimal shapes you can add a much larger volume fraction of filler particles without increasing the viscosity beyond practical values.

Traditionally ICA materials have suffered from brittleness, caused by the large fraction of metal particles with very different thermo mechanical properties than the adhesive matrix. Thermal expansion mismatch as well as the large difference in compression modulus between filler and matrix causes high local strain, and typically creates nucleation centers for cracks in the material. Adding flexible molecules to the adhesive matrix can reduce brittleness and improve thermal cycling behavior. However, a reduced glass transition temperature and increased moisture uptake are unfavorable side effects.

Metallized Polymer Spheres

A novel idea for improvements of the ICA material properties is to replace the solid metal flakes by highly uniformly shaped metal-coated polymer spheres. A drawback of using spheres is a higher percolation threshold. This is however more than overcome by the fact that much less than one tenth of the particle volume is actual metal. This introduces the possibility of using noble metals like gold at a reasonable cost. As the viscosity increase due to the addition of sphere fillers is very modest compared to adding flake like particles, there is no need for solvents to optimize viscosity. Instead, viscosity can be optimized by choosing oligomers with suitable molecular weight. Both the spherical shape, and the fact that the thermo mechanical properties are very similar to the adhesive matrix, reduce the local stress in the filler–matrix interface. A SEM photograph of metalized polymer spheres is shown in Figure 2.

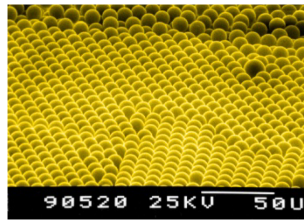


Figure 2. SEM photograph of metalized polymer spheres.

Several opportunities arise in terms of optimizing the conductive filler properties. A highly controlled size distribution of particles can be made with one or more particle sizes to optimize the filler fraction. Different core materials can be designed with different mechanical properties and glass temperature (Tg). This means that the conductive fillers can be used as the component for mechanical energy absorption needed in e.g. a shock environment.

### 1.2 Harsh environments and reliability demands

The electronics in ammunition fuzes are subjected to a number of demanding environmental conditions. When fired, a medium caliber ammunitions such as 30 mm x 173 is subjected to a setback acceleration pulse with an amplitude exceeding 60000 g. As the projectile travels through the barrel, the rifling imparts a spin on the projectile resulting in a centripetal acceleration, which increases radially by 9000 g/mm. The metal to metal contact between the projectile and barrel may also result in severe shocks and vibrations. After 4 ms the projectile exits the barrel. At this point the pressure propelling the projectile is abruptly removed, which may result in mechanical oscillations in different structures such as the packaged electronics. In some cases, the fuze electronics must also operate after the projectile has penetrated a hard target.

In addition, the fuze and its electronics must be capable of remaining safe and operable in severe climatic conditions where temperatures may range from -54° to 71°C.

### 1.3 Packaging concept

Direct chip-on-board packaging concept, where the MEMS device is mounted directly to the PCB, is highly favorable for medium caliber fuze applications, due to the limited space available. This packaging concept provides high integration density at a low manufacturing cost compared to the traditional packaging concept where encapsulated MEMS devices are mounted onto a PCB by e.g. soldering. Electrical and mechanical interconnect technology is however challenging for chip-on-board packaging concepts. Patterned ICA is one technology that can be used for interconnection in a chip-on-board packaging concept. Figure 3 illustrates the proposed ICA based packaging concept that was investigated in this work.

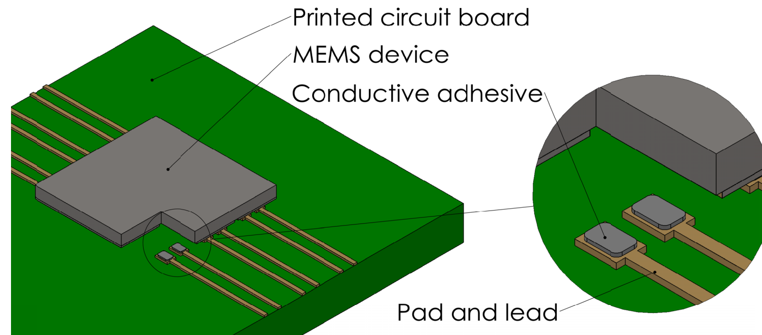


Figure 3 A three dimensional view of the packaging concept investigated in this work. One corner of the MEMS device is cut away to reveal the the patterned conductive adhesive implemented for interconnection

## 2. EXPERIMENTAL

### 2.1 Preparation of adhesives

The isotropic conductive adhesives were based on EPO-TEK®353ND epoxy adhesive manufactured by Epoxy Technology. Two different conductive particles have been used in the present study, both based on metallized polymer spheres to make two different ICAs, denoted ICA-A and ICA-B respectively. For ICA-A 30 micron polymer spheres with a thin silver coating were mixed together with the epoxy, whereas ICA-B contains 4 micron polymer spheres coated with nickel and gold. The adhesion between the polymer sphere and the silver was known to be pore for this specific sample. The volume fraction of metal coated spheres in the adhesive was about 50%. A small adjustment of the particle content was made to improve the printing properties. No solvents or surface additives were added to the adhesive. However, to increase the shear thinning and hence improve printing properties, 353ND-T was used for ICA B. This adhesive includes a small volume fraction of bentonite premixed from the supplier.

The metallized polymer spheres were mixed into the adhesive manually, by gradually adding the particles until the wanted concentration was achieved.

### 2.2 Manufacturing and design of test structures and test board

In order to characterize the properties between the PCB and the MEMS interconnect, we designed “dummy” MEMS ICA test structures with no movable parts. These were fabricated on the same wafers a MEMS device. The MEMS test structures were fabricated using an SOI substrate with 43 µm thick device layer and a 2 µm thick buried oxide layer (BOX). The device layer was dry etched down to the BOX layer in order to define the mechanical structures and to achieve electrical isolation between the contact pads. The dry etching was performed by a modified Bosch process in an Alcatel AMS-200 I-Speeder. Release etching of the BOX layer was achieved using a vapour HF tool from Idonus. A 300-500nm thick layer consisting of chrome, nickel and gold was sputtered onto the wafers to provide a conductive layer. Four different MEMS test structures were fabricated. The layout of these chips is shown in Figure 4. The nomenclature of the test structures denotes the shape of the conducting area, and the width of the trench between these

areas. The size of each test structure is 3.5x3.5 $mm^2$. The pad size for the I-100 chip is 250 X 350 $\mu m^2$ and 100 X 350 $\mu m^2$ for the other test structures. The I-100 test structure has 12 pads, while the other test structures have 32 pads each.

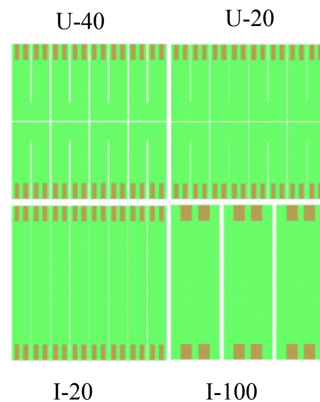


Figure 4. Layout of the four MEMS test structures used in our investigations. The pads are also shown in this layout.

A PCB suitable for both recovery firing test as well as other environmental testes was designed. A photograph of this board is shown to the left in Figure 5. The board is made of FR4 laminate with $T_g$ = 125 °C. On one side of the board two I-100 test structures and four 0402 resistors were mounted. On the other side, two U-40/U-20 test structures as well as four 0402 sized resistors were mounted. The pads and conductors have a thickness of approximately 50 µm, ~45 µm copper and ~5 µm nickel. In addition a ~100nm thick layer of gold is chemically deposited on top of the nickel layer. The board includes contact points for Kelvin measurements of the contact resistances prior to firing tests. However, when the test structures are placed inside the 30 mm projectile, the firing board is cut where the notches are shown in Figure 5. The size of the board placed inside the projectile is 9 x 16 $mm^2$. After cutting the board, Kelvin measurement on the test structures can still be done using a probe station. In the following section, this board is denoted firing board. Previously, we had designed a PCB measuring contact resistances for several I-100 test structures as well as resistances on daisy-chain structures4. A photograph of this PCB is shown to the right in Figure 5. This board is denoted temp board in the following sections.

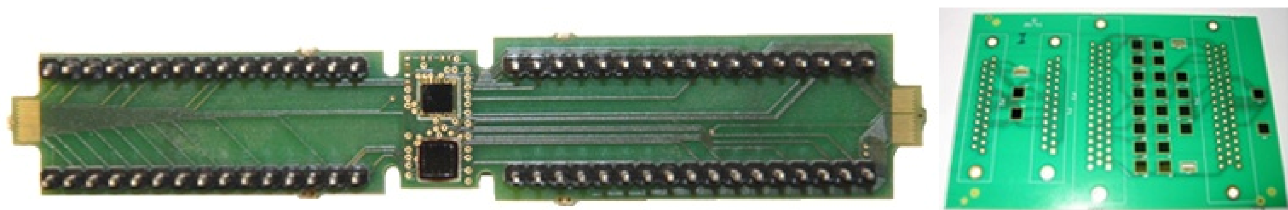

Figure 5. Photograph of the firing board to the left and a previously designed test board to the right.

### 2.3 Mounting of test chips onto test boards

Adhesive was printed onto the firing boards by using a Dima HS-100 stencil printer. The stencil was manufactured by HP Etch[5] and was covered with nickel/teflon. Nickel/teflon has a significantly lower surface energy than the pure metal, and will therefore significantly reduce the adhesion between the adhesive and the edges of the holes and the bottom side of the stencil. The thickness of this stencil is approximately 50 µm over the printing areas.

Eight firing boards were mounted with the I-100 test structure, denoted I1 – I8. Boards I3 – I6 were mounted using ICA-B and boards I1,I2,I7 and I8 with ICA-A. Boards I1-I4 had 2 test structures mounted, while boards I5-I8 had one mounted. Figure 6 shows a picture of the adhesive printed onto the firing boards where the the I-100 test structure will be mounted. The 30 µm polymer spheres are easily visible to the right in the picture. The I-100 test structure has 12 pads, so the total bond area was approximately 1.05 $mm^2$. This represents only approximately 9 % of the chip area which is a very little, and may influence the environmental stressing test results.

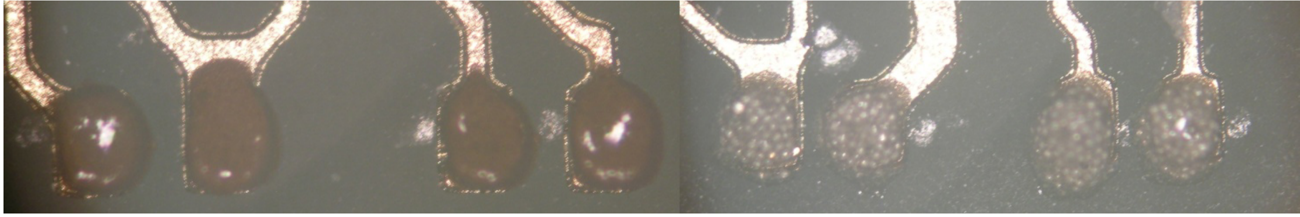

Figure 6. Picture showing stencil printing of ICA-B (left) and ICA-A (right) onto the firing boards (I1-I8).

An important part of the presented work was attributed to development of a sufficient stencil printing process for the fine pitch geometry of the U-40 test structures. Repeatability from pad to pad on individual boards as well as from board to board was not sufficient, as illustrated in Figure 7. As seen from this figure, some pads have adhesive, but some have not. The lack of adhesive will of course result in loss of electrical contact, but also gives reduced shear strength. Due to the difficulty of printing ICA-A though the small pad openings to the U-40 test structures, only ICA-B were used for those test structures.

The boards mounted with the U test structure are denoted U3-U5 and U10 – U13. The U-40 test structure has 32 pads, thus the total bond area will be 1.12 $mm^2$, which is slightly higher than for the I-100 test structures. However, due to challenges encountered with the printing of the adhesive, as shown in Figure 7, the effective contact area is most probably less than for the I-100 structures.

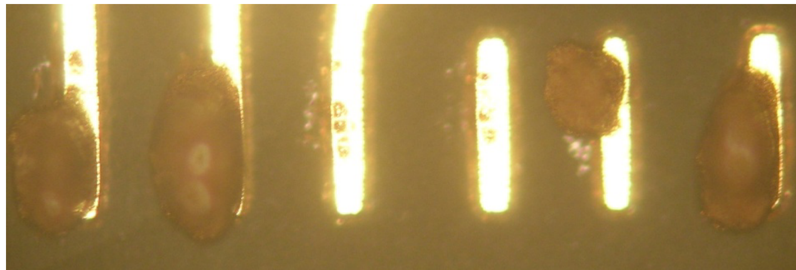

Figure 7. Photograph showing stencil printing of ICA-B on small pads with size 100 x 350 $\mu m^2$.

Test structures were mounted onto the temp board for testing the shear strength of the ICA-A and ICA-B adhesives. Eight boards were mounted, denoted S1 – S8, and each board contained 5 test structures. Boards S4- S7 were mounted with ICA-B and the boards S1 - S3 and S8 with ICA-B. When printing adhesive on these boards, a standard steel stencil was used where the pad openings were made by laser cutting. Figure 8 shows a photograph of printing ICA-A and ICA-B to the boards used for shear tests. The thickness of stencil used was 125 µm.

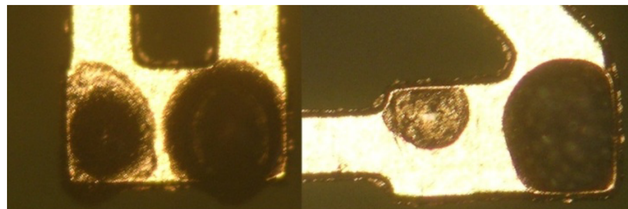

Figure 8. Photograph showing stencil printing of the ICA-B (left) and ICA-A (right) for the boards S1 – S8 used for shear tests.

It should be noted that no underfill has been used when mounting the test structures to the boards.

A My-9 pick and place machine from MyData was used for placing components on the boards. A low mounting pressure was used when placing the test structures to the board. Curing was performed at 150 °C for one minute.

## 2.4 Environmental stressing

Degradation of interconnection points will be accelerated by environmental conditions like static- and dynamic temperature stress as well as mechanical impact in the form of shock and/or vibration. In the current work, thermal cycling and firing test has been performed to investigate impact on the interconnect reliability.

Thermal cycling tests.

Thermal cycling stress test is a simple way to investigate the effect of thermally induced stress on interconnects reliability. For all boards, except for boards used as virgin samples (I5, U13 and S7), rapid thermal cycling stress in the form of air-to-air thermal shock cycling has been performed between -55 and +125°C in a Heraeus HT 7012 S2 thermal cycling chamber. The tests have been performed according to MIL-STD-883 G method 1010.8 test condition B. Test objects has been exposed to 4 cycles per hour, 50 % duty cycle and load transfer time within 60 seconds between temperatures extremes. Selected samples were exposed to 10 and 100 thermal cycles. Electrical resistance was recorded on units after TC stress and compared to values obtained prior to stress.

Recovery firing tests.

After temperature cycle tests, selected boards with test structures were mounted into a 30 mm projectile and recovery firings were performed. These firing tests were carried out at Nammo Test Center at Raufoss. The inner diameter of the projectile is 17.7 mm. The PCBs were mounted inside the projectile, together with a suitable potting material. Figure 9 shows a photograph of the projectile before and after firing. A Bushmaster II cannon was used for firing. Recovery was achieved by firing the projectile into a stack of porous wallboards, about 4 m long. The distance from the cannon to the wallboards was approximately 100 m. When leaving the muzzle, the speed of the projectile is about 1040 m/s. During the flight, the reduction of speed is negligible. Since the stopping distance in the wallboard is approximately the same as the barrel length the resulting negative acceleration is assumed to have the same order of magnitude as the setback acceleration during launch. However, since the projectile tumbles violently inside the wallboards, the direction of the acceleration becomes very random.

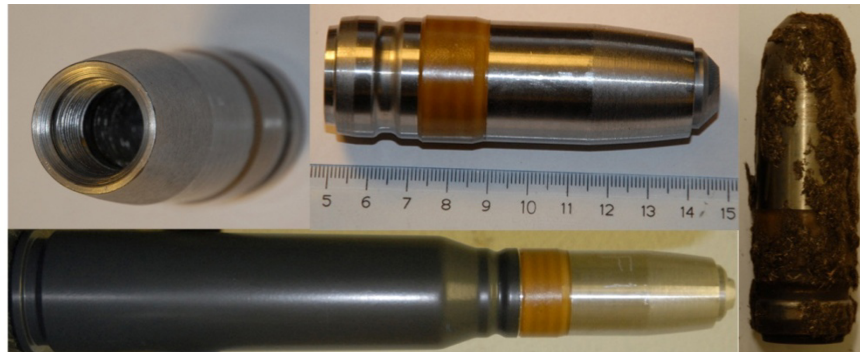


Figure 9. 30 mm projectile used for test firing. Bottom picture shows the projectile ready to be fired. To the right, a recovered projectile is shown.

The I1-I4 boards together with the S6 board were mounted into the 30 mm projectile and recovery firings have been performed. Before firing, but after the temperature tests, underfill was added to one test structure on each I1-I4 board as shown in Figure 10. Hence, it would be possible to determine if this would improve the performance during the firing test.

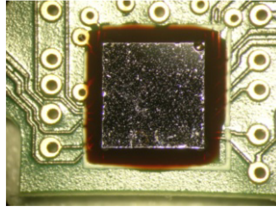

Figure 10. Underfill on one of the test structure used in recovery firing test.

### 2.5 Characterization

Adhesive bond integrity with loss in shear strength and eventually failure can be an issue when the bond is exposed to environmental stress like long term exposure to elevated temperature, thermal excursion and /or mechanical impact

Destructive die shear testing is a simple and fast method to check bump integrity for bonded dies. Test objects were fixed in a bracket socket and a shear head elevated over the substrate surface was forced horizontally to a lateral edge of the MEMS test structures. Shear height should be sufficient to avoid the bonding material and sufficient low to not influence the actual strength of the bond. Furthermore, movement of the shear head should be perpendicular to the side of the chip to avoid chip damage and thereby influence the recorded measurement. Shear strength and failure category were of interest as a reliability monitor of the bonded units. Shear test measurement was performed using a DAGE 2400A shear tester with a D10 kg die shear load cartridge. Shear test was performed at 10 µm/s shear speed at 150 µm shear height. Shear test was performed prior to and after thermal cycling test, and on samples exposed to thermal cycling and firing test.

Samples were cross sectioned and analyzed at each stage of the applied stress test. The devices were embedded in epoxy resin under vacuum (15-20 kPa). They were grinded with SiC paper up to grade 4000 and water lubrication with emphasis on precise cross sectioning through a series of MEMS to PCB interconnection points. Finally, the devices were polished on medium hard cloth with alcohol based lubricant with diamond grade 6 µm and 3 µm. Light microscopy was performed with a NEOPHOT 32 microscope. Selected devices were sputter coated with carbon for subsequent scanning electron microscopy (SEM) analysis.

## 3. RESULTS AND DISCUSSION

### 3.1 Characterization by electrical measurements

Initial contact resistance

A summary of the contact resistances recorded after assembly is presented in Table 1 for the I-100 and U-40 test structures. I-100 test structures mounted with ICA-A display a higher resistance compared to the test structures mounted with ICA-B. This difference can be explained by the thin silver layer coating of the polymer spheres for ICA-A, less than 50 nm thick. This is considerable thinner than the corresponding Au coating on polymer spheres for ICA-B. Beside it was observed incident of silver to delaminate from the core during mixing of spheres and adhesive (see Figure 14). This was caused by low adhesion between silver and polymer sphere. A more superior adhesion can be obtained between polymer sphere and the nickel by actively modifying the surface of the polymer core. This has been shown by compression testing of the metallized spheres[6].

Significantly higher contact resistances were measured for the U-40 test structures compared to the corresponding measurement on the I-100 test structures mounted with ICA-B. This can be explained by smaller contact pads. In addition, printing adhesive on such small areas was challenging, and it was problematic to cover all pads with sufficiently ICA (see Figure 7). This will of course influence the contact resistances. This is the main cause to the relatively high contact resistances we achieved and also the large variation between $R_{max}$ and $R_{min}$.

Table 1 Average contact resistances for I-100 and U-40 test structures mounted with ICA-A and ICA-B.

| ICA type | Test structure | $R_{average}$ (Ω) | $R_{max}$ (Ω) | $R_{min}$ (Ω) | No. of measured resistances |
|---|---|---|---|---|---|
| ICA-A | I-100 | 0.317 | 0.693 | 0.121 | 24 |
| ICA-B | I-100 | 0.103 | 0.161 | 0.062 | 24 |
| ICA-B | U-40 | 0.503 | 1.871 | 0.002 | 39 |

Contact resistance after temperature tests

The average contact resistances for the I-100 and U-40 test structures after the temperature cycle tests are shown in Table 2.

No contact resistances for the I-100 test structures failed during the temperature tests. As can be seen from Table 2, the change in contact resistance is much more pronounced when the samples are exposed to 100 temperature cycles than 10 temperature cycles. For the gold plated spheres, the electrical resistance decreases for the first 10 cycles. This can possibly be explained by tiny mechanical movements between the spheres, causing a more intimate mechanical contact by breaking up tarnish films. This effect has been reported for mechanical cycling of similar metallized polymer spheres[7]. A similar mechanical interaction between the silver coated spheres could likely be the cause of the encountered delamination and cracking of the metal layer due to the bad adhesion of the silver. It is noteworthy that the change in contact resistance after 100 cycles is approximately equal for both types of ICA.

When firing boards containing the U-40 test structure were exposed to 10 temperature cycles, 11 out of 26 contact resistances failed. On one of the boards (U-4) all contact resistances failed.

Table 2 Average contact resistance change as a function of number of temperature cycles for the I-100 and U-40 test structures.

| ICA type | Test structure | No of temperature cycles | $R_{average}$ (Ω) | | % change | No of measured resistances |
|---|---|---|---|---|---|---|
| | | | Initial | After temp cycling | | |
| ICA-A | I-100 | 10 | 0.317 | 0.366 | 15.5 | 8 |
| ICA-B | I-100 | 10 | 0.091 | 0.079 | -13.2 | 8 |
| ICA-A | I-100 | 100 | 0.361 | 0.675 | 87.0 | 8 |
| ICA-B | I-100 | 100 | 0.112 | 0.217 | 93.7 | 8 |
| ICA-B | U-40 | 10 | 1.055 | 1.488 | 41.0 | 15 |

Contact resistance after recovery firing tests

The average contact resistances for the I-100 test structures before and after recovery firing tests are shown in Table 3.

For the I-1- I-4 boards that were fired, 5 out of 32 contact resistances failed. Three contact resistances failed on board, I-2 and two on board I-4. Both boards have been exposed to 10 temperature cycles. The failure is caused by cracking of the silicon test structures and not in the interconnection itself. No underfill was used on the test structures that failed. It should be noted that since only 5 and 6 contact resistances were measured in boards I2 and I4 respectively, the average resistance value for these boards will deviate from the values given in Table 2 where the average values are calculate using eight contact resistances. It should be noted that for the I3-I4 boards, the change after firing is practically identical.

Table 3 Comparison of measured average contact resistance after temperature cycling and after firing tests respectively for I-100 test structures

| ICA type | Board no | No of temp cycles | $R_{average}$ (Ω) after temp cycling | $R_{average}$ (Ω) after firing test | % change | No of measured resistances |
|---|---|---|---|---|---|---|
| ICA-A | I1 | 100 | 0.675 | 0.733 | 8.6 | 8 |
| | I2 | 10 | 0.224 | 0.205 | -8.5 | 5 |
| ICA-B | I3 | 100 | 0.217 | 0.257 | 18.4 | 8 |
| | I4 | 10 | 0.082 | 0.097 | 18.3 | 6 |

### 3.2 Characterization by shear testing

Summary data from shear test measurement performed prior to stress, after thermal cycling and firing test is presented in Table 4 and Table 5 for ICA-A and ICA-B respectively. Measured data is presented in gram force (gf). Test samples mounted with ICA-A displayed lower shear strength and higher standard deviation compared to the corresponding result obtained for samples mounted with ICA-B. Furthermore lower shear strength was recorded for virgin samples compared to samples exposed to thermal cycling for the ICA-A samples. Light microscopy examination of shear tested ICA-A samples revealed distinct difference in the deposited amount of adhesive from sample to sample with less deposited adhesive observed on virgin sample compared to samples exposed to thermal cycling. ICA-B samples displayed high bond strength prior to stress and no notable decrease in bond strength recorded for samples exposed to thermal cycling. Samples exposed to firing test after 10 thermal cycles displayed higher bond strength compared to samples not exposed to firing. The predominant failure mode from shear test was observed to be fracture in the adhesive close to the die interface for all samples except samples after 100 thermal cycles where the predominant failure was observed to be fracture within the Si chip itself.

Table 4. Die shear test result prior to stress and after thermal cycling for ICA-A

| | Sample size | Mean [gf] | Std. dev [gf] |
|---|---|---|---|
| Before stress | 5 | 743 | 458 |
| After 10 TC | 4 | 1884 | 523 |
| After 100 TC | 5 | 2120 | 849 |
| After 10 TC and Firing | | | |

Table 5. Die shear test result prior to stress, after thermal cycling and firing for ICA-B

| | Sample size | Mean [gf] | Std. dev [gf] |
|---|---|---|---|
| Before stress | 5 | 7219 | 1160 |
| After 10 TC | 5 | 7202 | 777 |
| After 100 TC | 5 | 6555 | 1108 |
| After 10 TC and Firing | 5 | 10630 | 345 |

### 3.3 Characterization by cross sectioning

Selected samples were cross sectioned and analyzed by light microscopy and scanning electron microscopy (SEM). Light microscopy images of U-40 ICA-B test samples are presented in Figure 11, Figure 12 and Figure 13, for virgin sample, sample after 10 thermal cycles and after 100 cycles respectively. Samples exposed to 100 thermal cycles displays a gap height between chip and pad on the PCB of ~5 µm, slightly more than one ball height. No visible intimate contact from metal coated spheres was observed to neither the pad on the PCB- nor the chip metallization. Acceptable contact resistances were recorded prior to thermal cycling (see Table 1), and open circuit after. SEM analysis was

performed explore possible void formation with negative result. One plausible explanation is that a void has been formed during thermal cycling, and this void has been filled by potting material prior to cross section analysis. The virgin sample and the sample exposed to 10 thermal cycles display gap height of ~3-4 µm between pad on the PCB and chip with clearly visible metal coated spheres squeezed between the pad and chip metallization. Acceptable contact resistances were recorded for these samples.

I-100 test samples with ICA-B, displays a gap in the order of ~10 µm corresponding to 2 – 3 ball heights, as shown in Figure 14. Intimate contact in the form of well squeezed metal coated spheres is clearly visible. Figure 15 presents image of I-100 test sample mounted with ICA-A. This sample displays a gap of ~30 µm corresponding to one sphere diameter of the 30 µm silver coated sphere. Intimate contact between pad on the PCB and chip metallization is clearly visible, however the extent of ball squeezing can be discussed. This image also shows that patches of the plated silver have been pulled of the spheres.

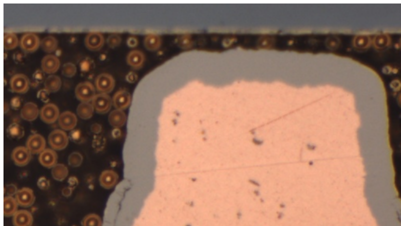

Figure 11. U13: ICA-B virgin sample

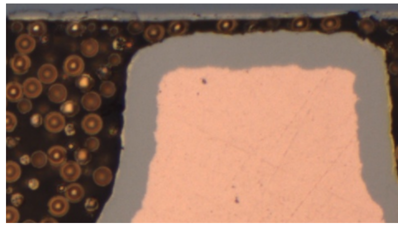

Figure 12. U12: ICA-B after 10 thermal cycles

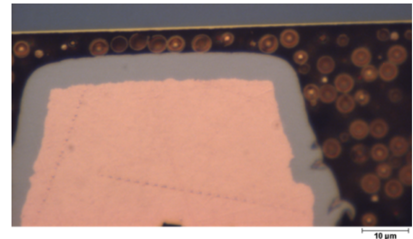

Figure 13. U4:ICA-B after 100 thermal cycles

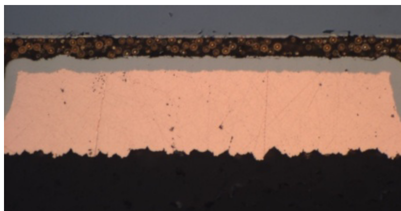

Figure 14. I6: ICA-B after 9.5 thermal cycles

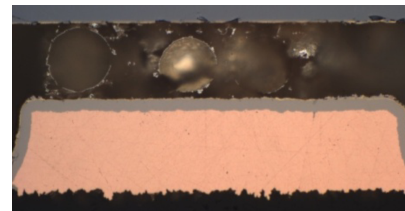

Figure 15. I8: ICA-A after 10 thermal cycles

The cross sections show that the adhesive thickness at the pad area is approximately 30 µm for ICA A and between 4 and 10 µm for adhesive B. For ICA-A, the adhesive thickness seems to be controlled by the ball size, whereas for ICA-B the squeeze film effect defines the minimum thickness for the larger pads, and the ball size represents the minimum adhesive thickness only for the smallest pads.

A rough (but probably conservative) estimate of the maximum strain in the adhesive can be made assuming that the glass temperature of the adhesive represents the zero-stress condition for the mounted test structures. This means that the the maximum strain will occur at the minimum exposure temperature during the temperature cycling. The test structures are 3.5x3.5 mm, which means that the maximum distance to the neutral point of the chip is approximately 2,5 mm.The CTE mismatch is approximately 15 ppm/$^0$C Due to the small area of adhesive we also assume that the adhesive itself absorbs all the strain. This is obviously a very conservative estimate. The shear deformation calculated from these numbers corresponds to approximately 5 µm. In case of the thin interconnections obtained for the ICA-B adhesive the shear deformation is of the same order of magnitude as the interconnect thickness.

Such a thin adhesive interconnection will have negative effects on thermal cycling performance as well as on mechanical shock tests due to the reduced volume for absorption of mechanical energy.

# 4. CONCLUSION

Direct chip-to-board MEMS to PCB interconnect using isotropic conductive adhesive with metal metallized spheres as electrical conductive filler material displayed capability as a viable interconnect technology for rough environment applications such as medium caliber ammunition fuzes.

Using stencil printing, accurate and repeatable adhesive deposition was achieved for ICA-B, with 4 µm gold metallized spheres, for a pad size of 250X350 $\mu m^2$. The highly accelerated thermal cycling stress tests and realistic firing stress tests that were performed showed excellent performance with no notable shear strength degradation and limited changes in electrical contact resistances.

Printing of ICA-A, which was based on the larger 30 µm silver metallized spheres, showed that this printing process needs to be optimized. As a result, the shear shear tests show a significant difference between the ICA-A and ICA-B. The other variations in the results can also largely be contributed to variations in the stencil printing process.

This investigation shows that isotropic conductive adhesive based on metallized polymer spheres can be suitable for direct chip-to-board interconnection of a MEMS device in a fuze application. By implementing such a packaging concept a higher packaging densities and reduced cost can be achieved.

## ACKNOWLEDGEMENTS

Part of this work have been sponsored by the Norwegian Research Council grant no 187971/140 and the Norwegian MoD. The authors want to thank Joachim Moe Graff at Sintef for helping us with cross section of the samples and Thorkild Kaasa, Tone Somme and Atle Skaguen at FFI for helping us with the PCB layout, printing of the adhesive, mounting of components.

## REFERENCES

1. Liu, J. (ed), [Conductive Adhesives For Electronics Packaging], Electrochemical Publications LTD, ISBN 0 901150 37 1, (1999)
2. Bjørneklett, A., Halbo, L., Kristiansen, H., "Thermal conductivity of epoxy adhesives filled with silver particles", International Journal of Adhesion and Adhesives, Butterworth and Heinemann Ltd, 12 nb. 2, 99-104 (1992)
3. Lee, W.S., Han, I.Y., Yu. J., Kim, S.J., Byun, K.Y.,"Thermal characterization of thermally conductive underfill for a flip-chip package using novel temperature sensing technique", Thermochemica Acta 455, 148–155 (2007)
4. Kristiansen, H., Taklo, M.M.V., Bakke, T., Gakkestad, J., Dalsjo, P., Johannessen, R., Oldervoll, F., Nguyen,V.H., "Development of low modulus conductive adhesive for MEMS interconnects", Proc. Pan Pacific Microelectronic symposium, 306-310 (2009).
5. www.hpetch.se
6. He, J. Y., Helland, T., Zhang, Z. L., Kristiansen, H., "Fracture of micrometre-sized Ni/Au coated polymer particles", Journal of Physics D: Applied Physics, 42 (2009)
7. Kristiansen, H. et. al, "Electrical and Mechanical Properties of Metal-coated Polymer Spheres for Anisotropic Conductive Adhesive" PEP 99; 63 – 71(1999)

# Appendix F Publication in Journal of Micro/Nanolithography, MEMS and MOEMS

# Use of conductive adhesive for MEMS interconnection in ammunition fuze applications

**Jakob Gakkestad**
**Per Dalsjo**
Norwegian Defence Research Establishment
Instituttveien 20
NO-2007 Kjeller, Norway
E-mail: Jakob.Gakkestad@ffi.no

**Helge Kristiansen**
Conpart AS
Lahaugmoveien 1
NO-2013 Skjetten, Norway

**Rolf Johannessen**
**Maaike M. Visser Taklo**
SINTEF
Information and Communication Technology
Forskningsveien 1
NO-0314 Oslo, Norway

**Abstract.** A novel conductive adhesive is used to interconnect MEMS test structures with different pad sizes directly to a printed circuit board (PCB) in a medium caliber ammunition fuze. The fuze environment is very demanding, with a setback acceleration exceeding 60,000 g and a centripetal acceleration increasing radially with 9000 g/mm. The adhesive shows excellent mechanical and thermal properties. The mounted MEMS test structures perform well when subjected to rapid temperature cycling according to military-standard 883G method 1010.8 test condition B. The test structures pass 100 temperature cycles, followed by a firing test where the test structures are exposed to an acceleration of more than 60,000 g. © *2010 Society of Photo-Optical Instrumentation Engineers.* [DOI: 10.1117/1.3504691]

Subject terms: conductive adhesive; fuze; microelectromechanical system; packaging; reliability; polymer spheres.

Paper 10006SSPR received Feb. 8, 2010; revised manuscript received Apr. 23, 2010; accepted for publication Sep. 13, 2010; published online Dec. 21, 2010.

## 1 Introduction

### 1.1 *Conductive Adhesives*

Isotropic conductive adhesives (ICAs) have been used in electronic applications for more than 40 years. Traditionally, ICA has been a mix of nonconductive adhesive, typically of epoxy type, with silver particles or flakes. However, to reduce cost, other conductive particles have also been used like carbon, copper, and nickel. Designing an ICA requires optimization of a number of factors including final electrical conductivity, rheological properties during application, total metal content (a cost issue in the case of noble metals), and thermomechanical properties.[1]

To make an ICA using a nonconductive matrix, the volume fraction of conductive filler particles needs to reach and exceed a certain level, called the percolation threshold. That is, the amount of particles must be sufficient to create at least one path of particle–particle contacts, and hence conduction through the entire adhesive. This threshold is dependent on the shape of the particles. Given the traditional flake-like conductive particles, the percolation threshold will also depend on the orientation of the flakes. In a typical microelectronic application, both the application of the adhesive and the shear applied during placement of the component cause a significant orientation of the flakes,[2] as illustrated in Fig. 1.

In practical use, the rheology of the adhesive is a critical parameter that determines the applicability of the material. As the filler content increases, the viscosity of the two-phase material increases. This limits the amount of filler that can be applied without using solvents to reduce the viscosity. However, the shape of the particles also has a very strong influence on the rheology.[3] This means that for some optimal shapes, you can add a much larger volume fraction of filler particles without increasing the viscosity beyond practical values.

Traditionally, ICA materials have suffered from brittleness caused by the large fraction of metal particles with very different thermomechanical properties than the adhesive matrix. Thermal expansion mismatch as well as the large difference in compression modulus between filler and matrix causes high local strain, and typically creates nucleation centers for cracks in the material. Adding flexible molecules to the adhesive matrix can reduce brittleness and improve thermal cycling behavior. However, a reduced glass transition temperature and increased moisture uptake are unfavorable side effects.

#### 1.1.1 *Metallized polymer spheres*

A novel idea for improvements of the ICA material properties is to replace the solid metal flakes by highly uniformly shaped metal-coated polymer spheres. A potential drawback of using spheres in ICAs is the significantly higher percolation threshold. This is, however, more than overcome by the fact that much less than one tenth of the particle volume is actual metal. This introduces the possibility of using noble metals like gold at a reasonable cost. As the viscosity increase due to the addition of sphere fillers is very modest compared to adding flake-like particles, there is no need for solvents to optimize viscosity. Instead, choosing oligomers with suitable molecular weight can optimize viscosity of the resulting ICA. Both the spherical shape, and the fact that the thermomechanical properties are very similar to the adhesive matrix, reduces the local stress in the filler-matrix interface. A scanning electron microscope (SEM) photograph of metalized polymer spheres is shown in Fig. 2.

Several opportunities arise in terms of optimizing the conductive filler properties. A highly controlled size distribution of particles can be made with one or more particle sizes

1932-5150/2010/$25.00 © 2010 SPIE



Downloaded from SPIE Digital Library on 03 Jan 2011 to 193.156.45.118. Terms of Use: http://spiedl.org/terms

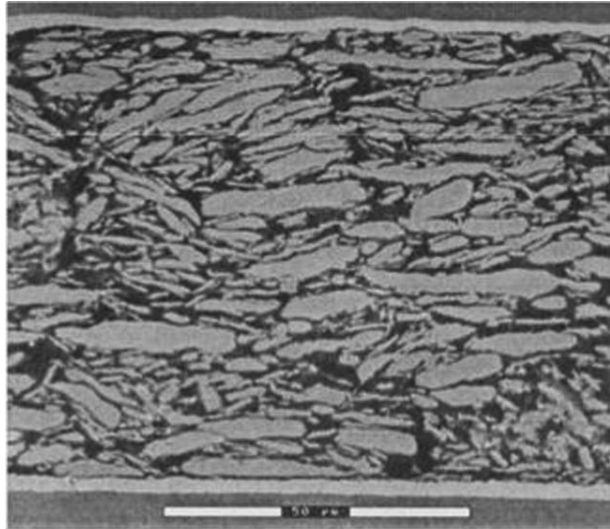

**Fig. 1** Illustration of the tendency for metal flakes (in this case silver) to align themselves in parallel with the die and substrate.

to optimize the filler fraction. Different core materials can be designed with different mechanical properties and glass temperature ($T_g$). This means that the conductive fillers can be used as the component for mechanical energy absorption needed in, e.g., a shock environment.

### 1.2 *Harsh Environments and Reliability Demands*

The electronics in ammunition fuzes are subjected to a number of demanding environmental conditions. When fired, medium caliber ammunitions such as 30 mm × 173 are subjected to a setback acceleration pulse with an amplitude exceeding 60,000 g. As the projectile travels through the barrel, the rifling imparts a spin on the projectile resulting in a centripetal acceleration, which increases radially by 9000 g/mm. The metal-to-metal contact between the projectile and barrel can also result in severe shocks and vibrations. After 4 ms, the projectile exits the barrel. At this point the pressure propelling the projectile is abruptly removed, which can result in mechanical oscillations in different structures such as the packaged electronics. In some cases, the fuze electronics must also operate after the projectile has penetrated a hard target.

In addition, the fuze and its electronics must be capable of remaining safe and operable in severe climatic conditions where temperatures can range from –54° to 71°C.

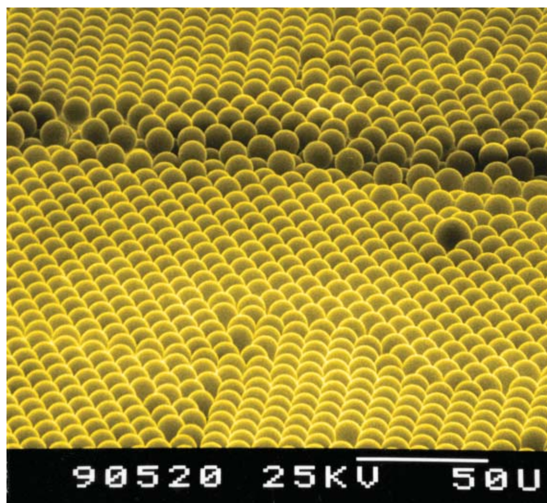


**Fig. 2** SEM photograph of metalized polymer spheres.

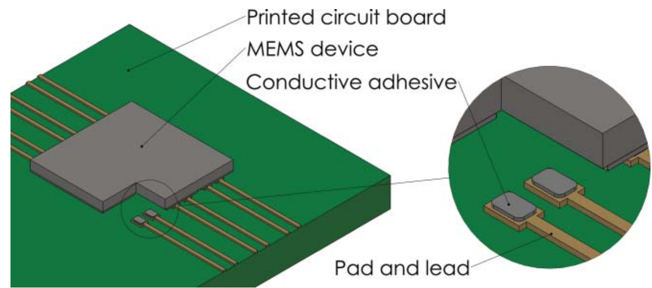


**Fig. 3** A 3-D view of the packaging concept investigating in this work. One corner of the MEMS device is cut away to reveal the patterned conductive adhesive implemented for interconnection.

### 1.3 *Packaging Concept*

Direct chip-on-board packaging concepts, where the MEMS device is mounted directly to the printed circuit board (PCB), is highly favorable for medium caliber fuze applications due to the limited space available. This packaging concept can provide a high integration density at a low manufacturing cost compared to the traditional concept, where numerous process steps are performed to mount the MEMS device in a package, which again is mounted onto a PCB by soldering, for example. Electrical and mechanical interconnect technology is, however, challenging for chip-on-board packaging concepts. Patterned ICA is one technology that can be used for interconnection in a chip-on-board packaging concept. Figure 3 illustrates the proposed ICA-based packaging concept presented in this work.

## 2 Experiment

### 2.1 *Preparation of Adhesives*

The isotropic conductive adhesives were based on EPO-TEK® 353ND epoxy adhesive manufactured by Epoxy Technology (Billerica, Massachusetts). The adhesive is a two-component adhesive, with a glass temperature of approximately 90°C. Two different metallized polymer spheres

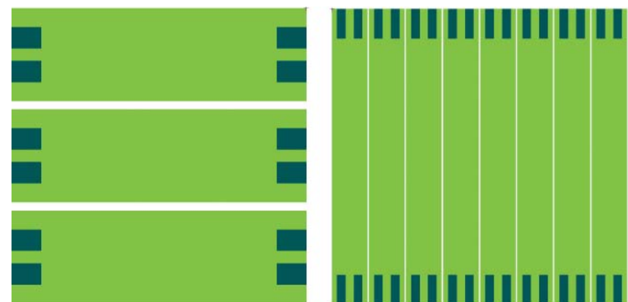

**Fig. 4** Layout of the I-100 (left) and I-20 (right) test structure. The pads are shown in the layout.



Downloaded from SPIE Digital Library on 03 Jan 2011 to 193.156.45.118. Terms of Use: http://spiedl.org/terms

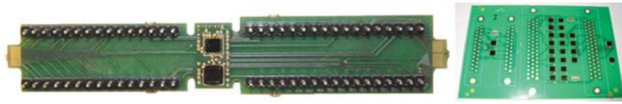

**Fig. 5** Photograph of the firing board to the left and previously designed temp board to the right.

have been used in the present study to make two different ICAs, denoted ICA-A and ICA-B, respectively. For ICA-A, 30-$\mu$m polymer spheres with a thin silver coating were mixed together with the epoxy. The ICA-B contains 4-$\mu$m polymer spheres coated with nickel and gold. The volume fraction of metal-coated spheres in the adhesive was about 50%. A small adjustment of the particle content was made to improve the printing properties. No solvents or surface additives were added to the adhesive.

The metallized polymer spheres were mixed into the adhesive manually by gradually adding the particles until the wanted concentration was achieved.

### 2.2 *Design and Manufacturing of Test Structures and Test Board*

To characterize the properties between the PCB and the MEMS interconnect, we designed "dummy" MEMS test structures with no movable parts. These were fabricated on the same wafers as the real MEMS devices. The MEMS test structures were fabricated using a silicon-on-insulator (SOI) substrate with a 43-$\mu$m-thick device layer and a 2-$\mu$m-thick buried oxide layer (BOX). The layout of the test structures used in this experiment is shown in Fig. 4. The nomenclature of the test structures denotes the shape of the conducting area, and the width of the trench between these areas. The size of the test structure is $3.5 \times 3.5$ mm$^2$. The I-100 test structure has 12 pads with a size of $250 \times 350$ $\mu$m$^2$, while the I-20 test structure has 32 pads with size $100 \times 350$ $\mu$m$^2$.

A PCB suitable for both recovery firing tests as well as other environmental tests was designed. A photograph of this board is shown to the left in Fig. 5. The board is made of FR4 laminate with $T_g = 125°$C. On each side of the board, two test structures as well as four 0402 resistors can be mounted. One side of the board is designed for I-100 test structures, while the other side is designed for test structures with smaller pads and finer pitch.[4] On each side, one test structure is rotated 90 deg with respect to the other test structure. The pads and conductors on the PCB have a thickness of approximately 50 $\mu$m, $\sim$45-$\mu$m-copper, and $\sim$5-$\mu$m-nickel. In addition a $\sim$100-nm-thick layer of gold is chemically deposited on top of the nickel layer. The board includes contact points for Kelvin measurements of the contact resistances prior to firing tests. On each test structure, it is possible to do Kelvin measurements of four contact resistances. When the test structures are placed inside the 30-mm projectile, the firing board is cut where the notches are shown in Fig. 5. The size of the board placed inside the projectile is $9 \times 16$ mm$^2$. After cutting the board, Kelvin measurements on the test structures can still be done using a probe station. In the following section, this board is denoted as the firing board. Previously, we had designed a PCB to measure contact resistances for several I-100 test structures as well as resistances on daisy-chain structures.[5] A photograph of this PCB is shown to the right in Fig. 5. This board is denoted "temp board" in the following sections.

### 2.3 *Stencil Printing of the Adhesive*

The adhesive was printed onto the firing boards by using a Dima (Deurne, The Netherlands) HS-100 stencil printer. The stencil was manufactured by HP Etch (Järfälla, Sweden) and was covered with nickel/teflon. Nickel/teflon has a significantly lower surface energy than the pure metal and therefore significantly reduces the adhesion between the adhesive and the edges of the holes and the bottom side of the stencil. The thickness of this stencil is approximately 50 $\mu$m over the printing areas. Figure 6 shows a picture of the adhesive printed onto the firing boards where the I-100 test structure will be mounted. The 30-$\mu$m polymer spheres used in ICA-A are clearly visible in the right picture in Fig. 6. The total bond area for the test structure was estimated to be approximately 1.05 mm$^2$. This represents only approximately 9% of the chip area, which is very small, and thereby increases stresses in the bonds during the environmental testing.

For shear strength testing of the ICA interconnects, eight temp boards were used. When printing adhesive on these boards, a 125-$\mu$m-thick steel stencil was used where the pad openings were made by laser cutting. The pad size was $250 \times 350$ $\mu$m$^2$. Figure 7 shows a photograph of the varying quality stencil printing results obtained using this steel stencil.

### 2.4 *Mounting of Test Chips onto Test Boards*

Eight boards were mounted, denoted I1 through I8, with I-100 test structures. Table 1 gives the relationship between the boards used, type of ICA, and number of test structures on each board.

**Fig. 6** Picture showing stencil printing of ICA-B (left) and ICA-A (right) onto the firing boards (I1 through I8).



Downloaded from SPIE Digital Library on 03 Jan 2011 to 193.156.45.118. Terms of Use: http://spiedl.org/terms

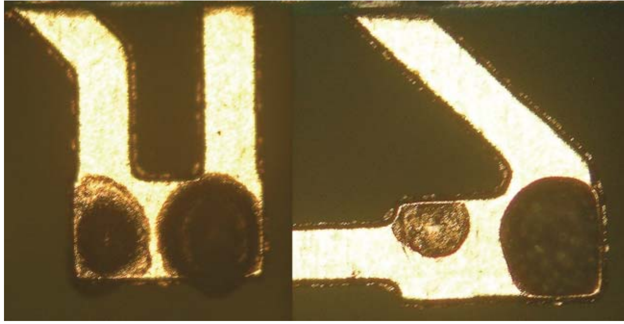

**Fig. 7** Photograph showing stencil printing of the ICA-B (left) and ICA-A (right) for the boards used for shear tests.

For shear strength testing of the ICA interconnects, eight temp boards, denoted S1-S8, were mounted with five test structures each. Table 2 gives an overview of the board numbers, number of components used, and type of ICA used on each board. Since there were not enough I-100 test structures available for the shear testing experiment, I-20 test structures were used instead. The I-20 test structures were rotated 90 deg, so the pads on the temp board are along the conductive path of the I-20 test structure. The width of the conductive paths on the I-20 test structure is 420 $\mu$m, which is larger than the length of the pads (350 $\mu$m). Since no electrical measurement is performed on these boards, it was acceptable to use the I-20 test structure for this purpose.

A My-9 pick-and-place machine from MyData (Täby, Sweden) was used for placing components on the boards. The same low mounting pressure was used when placing all the test structures onto the boards. Curing was performed at 150°C for one minute. It should be noted that no underfill has been used when mounting the test structures to the boards.

### 2.5 *Environmental Testing*

Degradation of interconnection points will be accelerated by environmental conditions like static and dynamic temperature stress, as well as mechanical impact in the form of shock and/or vibration. In the current work, thermal cycling and firing tests have been performed to investigate the impact on the interconnect the reliability.

#### 2.5.1 *Thermal cycling tests*

The thermal cycling stress test is a simple way to investigate the effect of thermally induced stress on the interconnect reliability. We kept one board of each type as virgin samples for reference purposes. For all boards except for boards used as virgin samples, rapid thermal cycling stress in the form of air-to-air thermal shock cycling has been performed between –55 and + 125°C in a Heraeus (Thermo Scientific,Wattham, Massachusetts) HT 7012 S2 thermal cycling chamber. The tests have been performed according to military-standard (MIL-STD)-883 G method 1010.8 test condition B. Test objects were exposed to four cycles per hour, 50% duty cycle, and load transfer time within 60 s between temperature extremes. Selected samples were exposed to 10 and 100 thermal cycles. Electrical resistance was recorded on units after TC stress and compared to values obtained prior to stress.

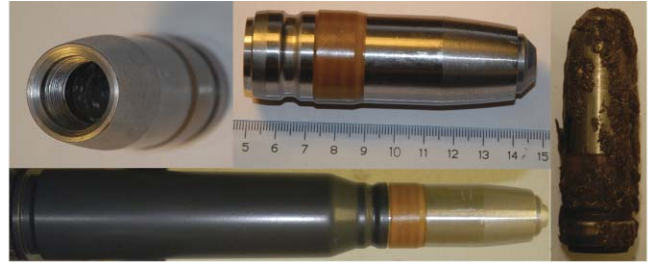


**Fig. 8** 30-mm projectile used for test firing. Bottom picture shows the projectile ready to be fired. To the right, a recovered projectile is shown.

#### 2.5.2 *Recovery firing tests*

After the temperature cycle tests, selected samples were mounted into 30-mm projectiles, and recovery firings were performed. These firing tests were carried out at Nammo Test Center at Raufoss, Norway. The inner diameter of the projectile is 17.7 mm. The PCBs were mounted inside the projectile, together with a suitable potting material. Figure 8 shows a photograph of the projectile before and after firing. A Bushmaster II cannon was used for firing. Recovery was achieved by firing the projectile into a stack of porous wallboards about 4 m long. The distance from the cannon to the wallboards was approximately 100 m. When leaving the muzzle, the speed of the projectile is about 1040 m/s. During the flight, the reduction of speed is negligible. Since the stopping distance in the wallboard is approximately the same as the barrel length, the resulting negative acceleration is assumed to have the same order of magnitude as the setback acceleration during launch. However, since the projectile tumbles violently inside the wallboards, the direction of the acceleration becomes very random.

The I1 to I4 boards, together with the S6 board used for shear test, were mounted into the 30-mm projectile and

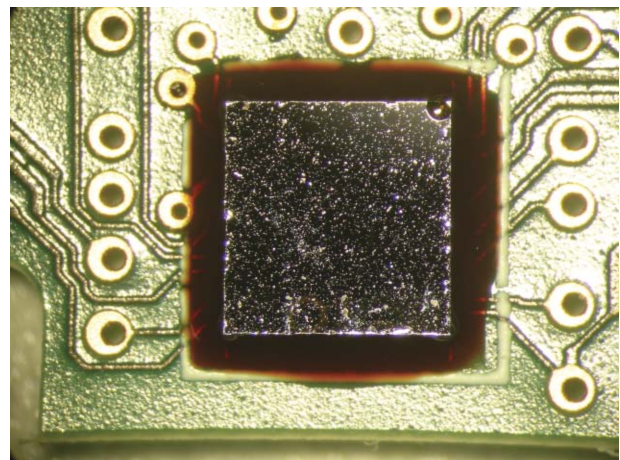

**Fig. 9** Underfill on one of the test structures used in the recovery firing test.



Downloaded from SPIE Digital Library on 03 Jan 2011 to 193.156.45.118. Terms of Use: http://spiedl.org/terms

**Table 1** Relationship between the I1 through I8 boards, number of components mounted on each board, and ICA used for mounting the components. ICA-A uses 30-$\mu$m silver-coated spheres, while ICA-B uses 4-$\mu$m gold-coated spheres. The stencil used when printing adhesive had a thickness of approximately 50 $\mu$m.

| Board number | I1 | I2 | I3 | I4 | I5 | I6 | I7 | I8 |
|---|---|---|---|---|---|---|---|---|
| Type of adhesive | ICA-A | ICA-A | ICA-B | ICA-B | ICA-B | ICA-B | ICA-A | ICA-A |
| Number of I-100 test structures | 2 | 2 | 2 | 2 | 1 | 1 | 1 | 1 |

recovery firings were performed. Before firing, but after the temperature tests, underfill was added to one test structure on each of the I1 to I4 boards, as shown in Fig. 9. Hence, it would be possible to determine if this would improve the performance during the firing test.

### 2.6 *Characterization*

The integrity of the adhesive bonds can be an issue when the bond is exposed to environmental stress, like long-term exposure to elevated temperatures, thermal excursion, and /or mechanical impact.

Destructive die shear testing is a simple and fast method to check bump integrity for bonded dies. Test objects were fixed in a bracket socket, and a shear head elevated over the substrate surface was forced horizontally to a lateral edge of the MEMS test structures. Shear height should be sufficient to avoid the bonding material and sufficiently low enough to not influence the actual strength of the bond. Furthermore, movement of the shear head should be perpendicular to the side of the chip to avoid chip damage and thereby influence the recorded measurement. Shear strength and failure category were of interest as a reliability monitor of the mounted test structures. Shear test measurement was performed using a DAGE (Aylesbury, United Kingdom) 2400A shear tester with a D10-kg die shear load cartridge. Shear test was performed at 10-$\mu$m/s shear speed at 150-$\mu$m shear height. Shear test was performed prior to and after the thermal cycling test, and on samples exposed to thermal cycling and firing tests.

Samples were cross sectioned and analyzed at each stage of the applied stress test. The devices were embedded in epoxy resin under vacuum (15 to 20 kPa). They were grinded with SiC paper up to grade 4000 and water lubrication with emphasis on precise cross sectioning through a series of MEMS to PCB interconnection points. Finally, the devices were polished on medium hard cloth with alcohol-based lubricant with diamond grade 6 and 3 $\mu$m. Light microscopy was performed with a Neophot 32 microscope (Zeiss, Jena, Germany).

## 3 Results and Discussion

### 3.1 *Characterization by Electrical Measurements*

#### 3.1.1 *Initial contact resistance*

A summary of the contact resistances for the I-100 structures prior to the environmental tests is presented in Table 3. The test structures mounted with ICA-A display a higher resistance compared to the test structures mounted with ICA-B. This difference can be explained by the thin silver layer coating of the polymer spheres for ICA-A, which is less than 50 nm thick. This is considerably thinner than the corresponding gold layer coating on the polymer spheres for ICA-B. Another effect contributing to the higher resistance for ICA-A is the partial delamination of the silver from the polymer spheres (see Fig. 10), which may have been caused by the manual mixing of spheres and adhesive. This delamination is caused by low adhesion between silver and polymer spheres. An improved adhesion can be obtained by actively modifying the surface of the polymer spheres. This has been shown by compression testing of the metallized spheres.[6]

#### 3.1.2 *Contact resistance after temperature tests*

The average contact resistances after the temperature cycle tests are shown in Table 4 for the I1 to I4 boards.

None of the contact resistances failed during the temperature tests. As can be seen from Table 5, the change in contact resistance is much more pronounced when the samples are exposed to 100 temperature cycles than ten temperature cycles. For ICA-B, the electrical resistance decreases for the first ten cycles. This can possibly be explained by minute mechanical movements between the spheres, causing a more intimate mechanical contact by breaking up tarnish films. This effect has been reported for mechanical cycling of similar metallized polymer spheres.[7] A similar mechanical interaction between the silver-coated spheres may also be the cause of the encountered delamination and cracking of the silver layer mentioned before. It is noteworthy that the change in contact resistance after 100 cycles is approximately equal for both types of ICA.

**Table 2** Overview of the S1-S8 boards used for shear testing and the type of ICA used. The temp board is used for this experiment, and the stencil is used when the printing adhesive had a thickness of 125 $\mu$m.

| Card number | S1 | S2 | S3 | S4 | S5 | S6 | S7 | S8 |
|---|---|---|---|---|---|---|---|---|
| Type of adhesive | ICA-A | ICA-A | ICA-B | ICA-B | ICA-B | ICA-B | ICA-A | ICA-A |
| Number of I-20 test structures | 5 | 5 | 5 | 5 | 5 | 5 | 5 | 5 |



Downloaded from SPIE Digital Library on 03 Jan 2011 to 193.156.45.118. Terms of Use: http://spiedl.org/terms

**Table 3** Average initial contact resistances and standard deviation for I-100 test structures mounted with ICA-A and ICA-B.

| ICA type | $R_{average}$ (Ω) | Std dev (Ω) | Number of measured |
|---|---|---|---|
| ICA-A | 0.317 | 0.149 | 24 |
| ICA-B | 0.103 | 0.030 | 24 |

### 3.1.3 *Contact resistance after recovery firing tests*

The average contact resistances before and after recovery firing tests are shown in Table 5. 27 out of 32 contact resistances passed the firing test. For the ICA-B-type adhesive, the contact resistance changes are almost identical, regardless of the number of temperature cycles. For the ICA-A adhesive, the samples exposed to 100 temperature cycles show an increase in contact resistance after firing, while the samples exposed to ten temperature cycles show a decrease in contact resistance. However, the number of measured resistances on boards I2 and I4 are five and six respectively. This is due to cracking of components during test firing. Therefore, the average resistance value after temperature cycling for these boards will deviate from the values given in Table 4, where the average values are calculated using eight contact resistances. All the components that cracked were without underfill. On board I2, the $R_{average}$ after firing is calculated from measuring four contact resistances on a structure with underfill, and one resistance on a cracked test structure without underfill.

The most interesting observation is that the contact resistance on the I2 board actually decreased after the firing test. On this board, one contact resistance on the cracked structure was measured. This resistance shows a large decrease in resistance value after firing (–29.9%). The cracking of the component will significantly reduce the mechanical stress in the interconnects and might be a reason for the observed resistance decrease. However, the average change on the four other contact resistances on the structure with underfill is still negative, –3.2%. Resistance measurement was done on some samples during temperature cycling tests. Using the recorded data, the temperature coefficient of resistance during temperature cycling was of the order of 0.0025 $K^{-1}$. When measuring the resistance after temperature cycling and firing tests, the room temperature may have changed a few degrees Celcius, since some days elapsed between the measurements. However, the TC of the resistances is too small to explain the measured resistance change. The effect of having underfill during a firing test is shown in Table 6.

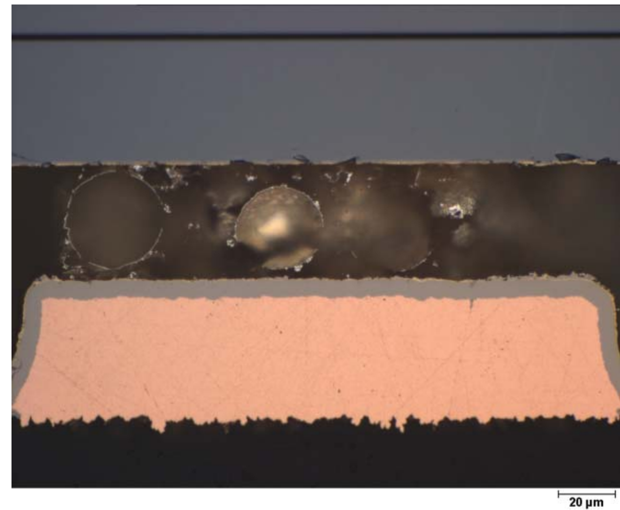


**Fig. 10** Cross section image of ICA-A interconnection after ten thermal cycles.

The results here show clearly that underfill is very favorable with respect to resistance change as a result of firing. It is noteworthy that the ICA-A contact resistance with the test structure with underfill decreases after firing, and that change is almost identical to the change on the I2 board with the test structure having underfill. Adding an underfill will set the ICA interconnects under compression due to curing shrinkage. In addition to reducing the mechanical stress in the interconnects during the firing tests, this can probably explain the small and even negative change in the contact resistance.

## 3.2 *Characterization by Shear Testing*

Summary data from shear test measurement performed on virgin samples and samples exposed to thermal cycling and firing test are presented in Tables 7 and 8 for ICA-A and ICA-B, respectively. Measured data are presented in gram force (gf). Test samples mounted with ICA-A displayed lower shear strength and higher standard deviation compared to the corresponding result obtained for samples mounted with ICA-B. Furthermore, lower shear strength was recorded for virgin samples compared to samples exposed to thermal cycling for the ICA-A samples.

**Table 4** Average contact resistances before and after temperature cycling for I-100 test structures mounted with ICA-A and ICA-B.

| ICA type | Board number | No of temperature cycles | $R_{average}$ (Ω) (std dev) | | Percent change | Number of measured resistances |
|---|---|---|---|---|---|---|
| | | | Initial | After temp cycling | | |
| ICA-A | I1 | 100 | 0.361 | 0.675 (0.246) | 87.0 | 8 |
| | I2 | 10 | 0.317 | 0.366 (0.258) | 15.5 | 8 |
| ICA-B | I3 | 100 | 0.112 | 0.217 (0.084) | 93.7 | 8 |
| | I4 | 10 | 0.091 | 0.079 (0.020) | –13.2 | 8 |



Downloaded from SPIE Digital Library on 03 Jan 2011 to 193.156.45.118. Terms of Use: http://spiedl.org/terms

**Table 5** Comparison of measured average contact resistances after temperature cycling and after firing tests, respectively, for I-100 test structures.

| ICA type | Board number | Number of temp cycles | $R_{average}$ (Ω) after temp cycling (std dev) | $R_{average}$ (Ω) after firing (std dev) | Percent change | Number of measured resistances |
|---|---|---|---|---|---|---|
| ICA-A | I1 | 100 | 0.675 (0.246) | 0.733 (0.326) | 8.6 | 8 |
| | 12 | 10 | 0.224 (0.094) | 0.205 (0.092) | –8.5 | 5 |
| ICA-B | I3 | 100 | 0.217 (0.084) | 0.257 (0.105) | 18.4 | 8 |
| | I4 | 10 | 0.082 (0.022) | 0.097 (0.033) | 18.3 | 6 |

Light microscopy examination of shear tested ICA-A samples revealed distinct differences in the deposited amount of adhesive from sample to sample, with less deposited adhesive observed on virgin samples compared to samples exposed to thermal cycling. The ICA-B samples displayed high bond strength with no notable decrease in bond strength recorded for samples exposed to thermal cycling. Samples exposed to firing tests after ten thermal cycles displayed higher bond strength compared to samples not exposed to firing.

The large standard deviation for ICA-A and the unlikely improved bond strength for ICA-B after firing tests are contributed to variations in contact area caused by the stencil printing process combined with the limited number of samples.

The predominant failure mode from shear test was observed to be fracture in the adhesive close to the die interface for all samples, except samples, after 100 thermal cycles, where the predominant failure was observed to be fracture within the Si chip itself.

No samples with mounted ICA-A were available for testing after ten TC and firings.

### 3.3 *Characterization by Cross Sectioning*

Selected samples were cross sectioned and analyzed by light microscopy and scanning electron microscopy (SEM). Figure 10 presents an image of an I-100 test sample mounted with ICA-A. This sample displays a gap of ~40 $\mu$m, corresponding to approximately 1.3 sphere diameters. This image also shows patches of the plated silver that has delaminated from the polymer spheres. Test samples with ICA-B display a gap in the order of ~10 $\mu$m, corresponding to two to three sphere diameters, as shown in Fig. 11.

The cross sections show that the resulting adhesive thickness at the pad area is approximately 40 $\mu$m for ICA-A and approximately 10 $\mu$m for ICA-B, even though both samples are mounted with the same force.

For ICA-A, the adhesive thickness seems to be controlled by the sphere diameter, whereas for ICA-B, the squeeze film effect defines the minimum thickness. An experiment performed with smaller pads shows that this squeeze film effect is reduced, resulting in an adhesive thickness approaching the sphere diameter.[4]

The cross section on one of the pads on the S8 board is shown in Fig. 12. The test structure is mounted using ICA-A. As previously mentioned, a stencil with thickness ~125 $\mu$m was used when printing the adhesive to the board. As seen from Fig. 12, the adhesive thickness is approximately 50 $\mu$m, which is approximately 10 $\mu$m thicker than for the test structures on the I1 through I8 boards mounted with ICA-A.

### 3.4 *Discussion*

A considerable amount of work was spent on achieving a proper printing of the adhesive. The printing quality is dependent on several factors such as the quality of the stencil, the pressure and speeds of the squeegee, and rheological property of the adhesive such as viscosity and shear thinning properties. As seen from Fig. 7, the quality of the printing is not as good as it should be. This will reflect the variation in the shear test results. This variation in the printing process

**Table 6** Change in resistance during firing tests for test structures with and without underfill. Both boards have been exposed to 100 temperature cycles prior to firing tests. The underfill was added after the temperature cycling. Four resistances are measured in each case.

| ICA type | Board number | Underfill | $R_{average}$ (Ω) after temp cycling | $R_{average}$ (Ω) after firing test | Percent change | Number of measured resistances |
|---|---|---|---|---|---|---|
| ICA-A | I1 | Yes | 0.561 | 0.544 | –3.0 | 4 |
| | I2 | No | 0.788 | 0.923 | 17.1 | 4 |
| ICA-B | I3 | Yes | 0.197 | 0.210 | 6.6 | 4 |
| | I4 | No | 0.236 | 0.305 | 29.2 | 4 |



Downloaded from SPIE Digital Library on 03 Jan 2011 to 193.156.45.118. Terms of Use: http://spiedl.org/terms

**Table 7** Die shear test result for ICA-A.

| | Number of samples | Mean [gf] | Std dev [gf] |
|---|---|---|---|
| Virgin samples | 5 | 743 | 758 |
| After ten TC | 4 | 1884 | 523 |
| After 100 TC | 5 | 2120 | 849 |
| After ten TC and firing test | | | |

**Table 8** Die shear test result for ICA-B.

| | Number of samples | Mean [gf] | Std dev [gf] |
|---|---|---|---|
| Virgin samples | 5 | 7219 | 1160 |
| After ten TC | 5 | 7202 | 777 |
| After 100 TC | 5 | 6555 | 1108 |
| After ten TC and firing test | 5 | 10,630 | 345 |

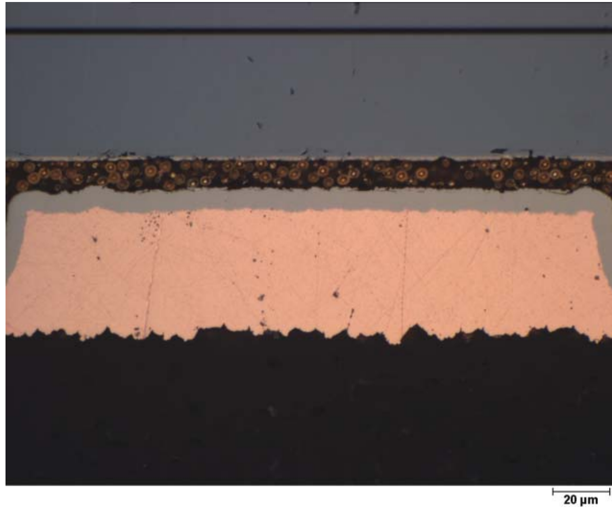


**Fig. 11** Cross section image of ICA-B interconnection after 9.5 thermal cycles.

is probably the main cause of the large standard deviation obtained in the shear test, as well as that the samples exposed to ten TC and firing tests showed a higher shear strength than, e.g., the virgin samples (see Table 8).

Shear force degradation is generally expected to be more severe for thin mechanical joints compared to thicker joints, as there is a reduced volume for absorbing the applied mechanical energy. Increasing adhesive joint thickness from ∼40 to 50 $\mu$m is therefore expected to slightly improve shear force result as well as performance to thermally induced stress and mechanical shock. Hence, the shear properties for the test structures mounted with ICA-A on the I1 to I8 boards is expected to be slightly lower than the results shown in Table 7.

A rough (but probably conservative) estimate of the maximum strain in the adhesive can be made, assuming that the glass temperature of the adhesive represents the zero-stress condition for the mounted test structures. This means that maximum strain will occur at the minimum exposure temperature during the temperature cycling. The test structures are $3.5 \times 3.5$ mm$^2$, which means that the maximum distance to the neutral point of the chip is approximately 2.5 mm.

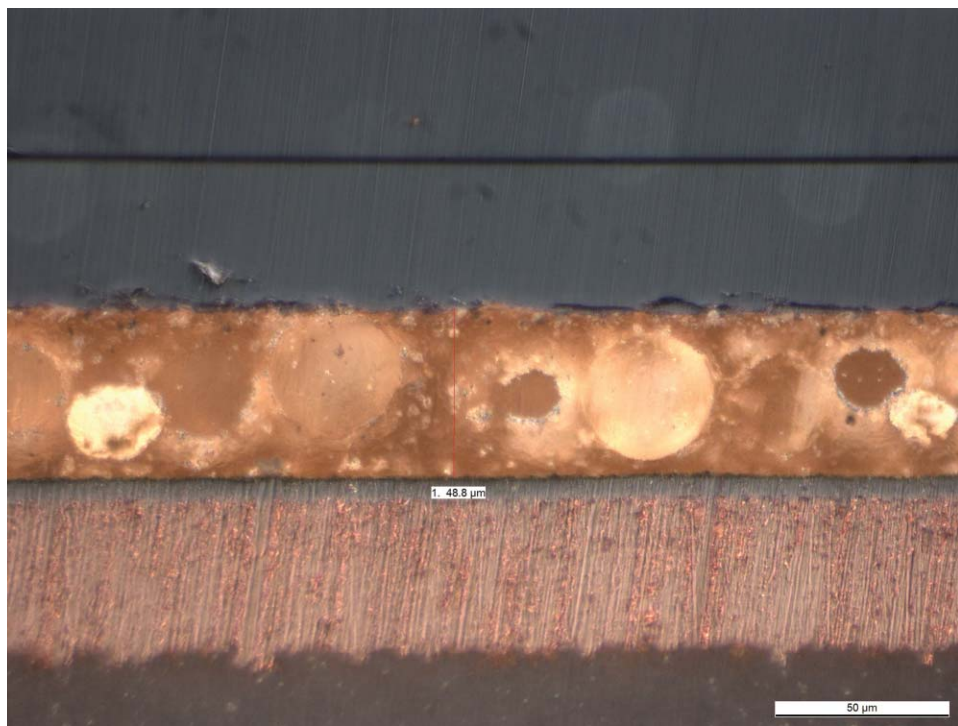


**Fig. 12** Cross section image of one pad on the S8 board. Adhesive thickness is approximately 50 $\mu$m.



Downloaded from SPIE Digital Library on 03 Jan 2011 to 193.156.45.118. Terms of Use: http://spiedl.org/terms

The coefficient of thermal expansion (CTE) mismatch is approximately 15 ppm/°C. Due to the small area of adhesive, we also assume that the adhesive itself absorbs all the strain. This is obviously a very conservative estimate. The shear deformation calculated from these numbers corresponds to approximately 5 $\mu$m. In the case of the thin interconnections obtained for the ICA-B adhesive, the shear deformation is roughly half of the interconnect thickness. Such a thin adhesive interconnection will have negative effects on thermal cycling performance as well as on mechanical shock tests due to the reduced volume for absorption of mechanical energy. It was observed that the large 30-$\mu$m spheres used acted as spacers, increasing the gap between the die and the substrate pads. The result was more than three times an increase in bond thickness, and hence a significant reduction in shear strain.

In the present experiments we have used silver and gold metallization systems. In addition, the tests have been performed without adding humidity. We therefore expect the degradation of the contact resistances to be mainly due to mechanical interaction, either particle—particle or particle—contact pad. Due to the nature of the epoxy matrix, we expect that these interactions are strongest at elevated temperatures, above the $T_g$. Due to nonlinearity, the net effect will be an increased particle separation, increasing the contact resistance. However, during initial temperature cycles this can have more of a rubbing effect, causing a more intimate metallic contact and hence a reduced contact resistance. Also, additional curing of the adhesive can cause an initial reduction in contact resistance.

Adding underfill to some of the test structures before the firing tests gave reduced degradation of the contact resistances. Adding underfill to the test structures before temperature cycling would force the chip and PCB to expand at the same rate, and hence reduce the strain in the interconnect. In addition, the curing shrinkage in the underfill adds a compressive stress in the ICA. This would probably increase the mechanical strength to the structure, providing enhanced performance to temperature cycling, mechanical shock, and vibration.

## 4 Conclusion

Direct chip-to-board MEMS to PCB interconnect using isotropic conductive adhesive with metallized polymer spheres as electrical conductive filler material displays capability as a viable interconnect technology for rough environment applications such as medium caliber ammunition fuzes.

The highly accelerated thermal cycling tests and realistic firing tests that are performed show excellent performance of the ICAs with no notable shear strength degradation and acceptable changes in electrical contact resistances.

The adhesive printing process needs to be refined for both types of adhesives. As a result, the shear tests show a significant difference between the ICA-A and ICA-B. The other variations in the results can also largely be contributed to variations in the stencil printing process.

This investigation shows that isotropic conductive adhesive based on metallized polymer spheres can be suitable for direct chip-to-board interconnection of a MEMS device in a fuze application. By implementing such a packaging concept, a higher packaging density and reduced cost can be achieved.


### Acknowledgments

Part of this work has been sponsored by the Norwegian Research Council grant number 187971/140 and the Norwegian MoD. The authors want to thank Joachim Moe Graff at Sintef and Thorkild Kaasa, Tone Somme, Oyvind Froyland, and Atle Skaugen at FFI for their most valuable assistance during this work.


### References


1. J. e. Liu, *Conductive adhesives for electronics packaging*, *Electrochemical Publications*, Isle of Man (1999).
2. A. Bjorneklett, L. Halbo, and H. Kristiansen, "Thermal conductivity of epoxy adhesives filled with silver particles," *Intl. J. Adhesion Adhesives* **12**, 99–104 (1992).
3. W. S. Lee, I. Y. Han, J. Yu, S. J. Kim, and K. Y. Byun, "Thermal characterization of thermally conductive underfill for a flip-chip package using novel temperature sensing technique," *Thermochimica Acta* **455**, 148–155 (2007).
4. J. Gakkestad, P. Dalsjo, H. Kristiansen, R. Johannessen, and M. M. V. Taklo, "Use of conductive adhesive for MEMS interconnection in military fuze applications," *Proc. SPIE* **7592**, 75920I (2010).
5. H. Kristiansen, M. M. V. Taklo, J. Gakkestad, P. Dalsjo, R. Johannessen, F. Oldervoll, and V. H. Nguyen, "Development of low modulus conductive adhesive for MEMS interconnects," *Proc. Pan Pac. Microelectron. Symp.*, pp. 306–310 (2009).
6. J. Y. He, T. Helland, Z. Zhang, and H. Kristiansen, "Fracture of micrometre-sized Ni/Au coated polymer particles," *J. Phys. D: Appl. Phys.* **42**, 085402 (2009).
7. H. Kristiansen, U. Brudberg, and M. Gulliksen,, "Electrical and mechanical properties of metal-coated polymer spheres for anisotropic conductive adhesive," *PEP 99*, pp. 63–71 (1999).



**Jakob Gakkestad** received his MSc and PhD in electronics from the University of Oslo in 1985 and 1993, respectively. In 1985 he worked as an ASIC designer at Sintef ICT in Oslo, focusing on the design of mixed signal ASICs in BiCMOS and CMOS technology. From 1997 to 2002, he worked at Tandberg Data, where after some time he became manager for the hardware development department. He also worked as a senior analog asic designer at Chipcon (now TI) before he joined the Norwegian Defence Research Establishment (FFI) in 2003. At FFI he is working with electronics and MEMS for gun-launched munitions fuzes.

**Per Dalsjo** received his first MSc degree in mechatronic engineering from the University of New South Wales, Sydney, Australia, in 2001. After working several years as a mechanical engineer, he returned to university, completing a MSc degree in electronic engineering specializing in MEMS at the University of Oslo, Norway, in 2007. Since 2007 he has worked as a research scientist at the Norwegian Defence Research Establishment (FFI) on MEMS systems for gun-launched munitions fuzes and the integration of electronics and mechanics in such fuzes.

**Helge Kristiansen** received his MSc in solid state physics from the University of Oslo (UiO) in 1988. In 1988 he was working at Sintef ICT, previously the Center for Industrial Research with Electronic Packaging. He received his PhD in experimental particle physics from UiO in 1996, and held a part time position at Chalmers from 1999 to 2004. His main field of research was the use of adhesives, thermal management, and instrumentation systems. In 2004 he joined Conpart AS as CTO, where he is involved in the characterization and application of polymer particles for use in electronic applications.

**Rolf Johannessen** received his PhD in physical electronics from the University of Oslo, Norway, in 2008. From 1989 to 2005 he was focusing on materials and processes for harsh environment applications at the Research and Development Department of Getech and the technology department of Alcatel Space Norway, Horten, Norway. He also held a position as educational staff at Horten College of Engineering, Norway. From 2008 to 2010 he was with SINTEF ICT, Oslo, Norway, as a research scientist where he was working on failure mechanisms and packaging technology for harsh environments, fo-




Downloaded from SPIE Digital Library on 03 Jan 2011 to 193.156.45.118. Terms of Use: http://spiedl.org/terms

cusing on high temperature applications. Currently he is on his leave from SINTEFICT in a new position as manufacturing process leader at GE Vingmed Ultrasound, Horten, Norway.

**Maaike M. Visser Taklo** worked for one year with optical sensors as a project engineer at AME AS in Horten, Norway, in 1997. She received her PhD degree in physical electronics from the University of Oslo in 2002. The topic of her thesis was wafer bonding for MEMS. She was employed by the microsystems and nanotechnology department at SINTEF in 1998, where she works today as a senior research scientist and is responsible for their wafer bonding activities. She has several years of experience as a project leader for research projects focused on packaging technologies for MEMS. Through her engagement in the projects e-CUBES and JEMSiP-3D, 3-D integration of MEMS has become one of her main areas of expertise.